STUDY OF ELECTROLYTE ADDITIVES IN LI-ION BATTERIES USING ELECTROCHEMICAL IMPEDANCE SPECTROSCOPY ON SYMMETRIC CELLS

by

Remi Petibon

Submitted in partial fulfilment of the requirements
for the degree of Master of Science
at

Dalhousie University
Halifax, Nova Scotia
August 2013

To my wife and my son,

TABLE OF CONTENTS

LIST OF TABLES

LIST OF FIGURES

ABSTRACT

Electrolyte additives are generally used in commercial Li-ion cells to improve capacity retention and calendar life. Although it is apparent that electrolyte additives play an important role, the details of how they work are poorly understood. In order to be able to distinguish the effect of an additive on the positive or negative electrodes, an experimental method has been developed based on electrochemical impedance spectroscopy of symmetric cells constructed from electrodes of disassembled full cells similar to the method described by previous workers. This technique proved to be useful and showed that the effects of additives on both electrodes depend strongly on their concentration. It also showed that in some cases, when two additives are introduced in the same cell, both additives contribute to the formation of the surface layer of both electrodes. In other cases, each additive controls the formation of the surface layer of only one electrode.

LIST OF ABBREVIATIONS USED

Additive A	Proprietary additive
BMF	Polypropylene blown microfibers
CE	Coulombic efficiency
CIE	Coulombic inefficiency
CPE	Constant Phase Element
DEC	Diethyl Carbonate
DMC	Dimethyl Carbonate
EC	Ethylene Carbonate
EIS	Electrochemical Impedance Spectroscopy
EMC	Ethyl Methyl Carbonate
FEC	Fluoro Ethylene Carbonate
FT-IR	Fourier Transform Infrared
GC-MS	Gas Chromatography-Mass Spectroscopy
HV-LCO	LCO/graphite cell made by Medtronic stored at 4.175 V
IRC	Irreversible capacity loss
LCO	$LiCoO_2$
LFP	$LiFePO_4$
LiBOB	$LiB(C_2O_4)_2$
$LiMO_2$	Lithium transition metal dioxide
LiTFSI	$(LiN(SO_2CF_3)_2)$
LiTFSI	Lithium bis(trifluoromethanesulfonyl) imide
LMO	$Li_{1+x}Mn_{2-x}O_4$
LTO	$Li_{4/3}Ti_{5/4}O_4$
LV-LCO	LCO/graphite cell made by Medtronic stored at 4.075 V
NCA	$Li(Ni_{0.8}Co_{0.15}Al_{0.05})O_2$
NMC	$Li(Ni_{1-x-y}Mn_xCo_y)O_2$
PC	Propylene Carbonate
PS	1,3-Propanesultone
PVDF	Polyvinylidene fluoride
R_{el}	Expression of the impedance of the electrolyte
SCR	Simplified Contact-Randles circuit
SEI	Solid Electrolyte Interphase
SEM	Scanning Electron Microscopy
TMOBX	Trimethoxyboroxine
VC	Vinylene Carbonate
VEC	Vinyl Ethylene Carbonate
XPS	X-ray Photoelectron Spectroscopy
A	Surface of the electrode in m^2
A_D	Warburg coefficient in $\Omega \cdot rad^{1/2} \cdot s^{-1/2}$

c_{sj}	General capacitance in the expression of the impedance of the Warburg type resistance in the SCR model proposed by Atebamba et al. (reference 92)
C	Capacitance in F
CPE_{cc}	Double layer capacitance (constant phase) at the surface of the current collector $\Omega \cdot cm^2$
$CPE_{part..}$	Double layer capacitance (constant phase) at the surface of the active particles $\Omega.cm^2$
D_{chem}	Diffusion coefficient of Li in the active material
e	Charge of an electron in C
e^-	Electron
f	Frequency in Hz
f_{max}	Frequency of the maximum of the negative imaginary part of an RC circuit in Hz
g	Earth's gravitational field in $m \cdot s^{-2}$
$\|I\|$	Amplitude of the AC current in A
$I(\omega, t)$	Frequency and time dependant current (AC current)
j	$\sqrt{-1}$
l	Diffusion length of Li in the active material
L	Distance between the positive and the negative electrodes in m
L	Inductance in H
n^+	Number of cation per m^3
n^-	Number of anion per m^3
p	Arbitrary constant in the expression of the impedance of the Warburg type resistance in the SCR model proposed by Atebamba et al. (reference 92)
Q	Electrical charge in C.
Q	Capacitance in the expression of the constant phase element in F^{α}
r_s	General resistance in the expression of the impedance of the Warburg type resistance in the SCR model proposed by Atebamba et al. (reference 92)
R	Resistance in Ω
R_{cr}	Active particle/current-collector interface resistance $\Omega \cdot cm^2$
R_{ct}	Resistance associated with the transfer of Li^+ from the electrolyte to the active particle, passing through the solid electrolyte interphase in $\Omega \cdot cm^2$
t	Time in s
u^-	Mobility of the anion in $m^2 \cdot V^{-1} \cdot s^{-1}$
u^+	Mobility of the cation in $m^2 \cdot V^{-1} \cdot s^{-1}$
$\|V\|$	Amplitude of the AC voltage in V
$V(\omega, t)$	Frequency and time dependent voltage (AC voltage)
W	Warburg type resistance in the SCR model proposed by Atebamba et al. (reference 92) in $\Omega \cdot cm^2$
z^-	Charge per anion
z^+	Charge per cation

Z	Impedance
$Z_C(\omega)$	Impedance of a capacitor in Ω
$Z_{corr.}$	Total impedance of a Li-ion cell corrected for the contribution of the experimental setup in Ω·cm^2
$Z_{e.s}$	Contribution of the experimental setup to the impedance in Ω
$Z_{Ind}(\omega)$	Impedance of an inductor in Ω
$Z_R(\omega)$	Impedance of a resistor in Ω
Z_{tot}	Total impedance of a full Li-ion cell in Ω·cm^2
Z_W	Expression of the impedance of the Warburg type resistance in the SCR model proposed by Atebamba et al. (reference 92) in Ω·cm^2
$Z_{(-)}$	Contribution of the negative electrode to the impedance in Ω·cm^2
$Z_{(+)}$	Contribution of the positive electrode to the impedance in Ω·cm^2
$Z_{(-/-)}$	Area-specific impedance of a negative electrode in Ω·cm^2
$Z_{(+/+)}$	Area-specific impedance of a positive electrode in Ω·cm^2
$Z_{(+/-)}$	Area-specific impedance of a full Li-ion cell in Ω·cm^2
(-/-)	Negative symmetric cell
(+/+)	Positive symmetric cell
(+/-)	Full cell
α	Exponential factor in the expression of the impedance of a constant phase element
ω	Frequency in rad·s^{-1}
φ	Phase in rad.

ACKNOWLEDGEMENTS

I would like to thank the *Fonds québécois de la recherche sur la nature et les technologies* (FQRNT), for their financial support, along with NSERC and 3M for the partial funding of this work.

I am very grateful to a great number of people for their help and support. Special thanks go to my supervisor Jeff Dahn for his support, enthusiasm and patience. These two years have been a blast mainly because of the challenging, intriguing and motivating atmosphere he provided. I would also like to thank my committee members, Mary Anne White and Mark Obrovac for their help and advice.

Most importantly I would like to give a thousand thanks to my wife for her loving support throughout these two years and for her multiple trips to the University on week-ends. I am infinitely grateful for it.

I would like to thank Connor Aiken for the development of the software for the fitting of the impedance spectra. This saved me a lot of time and effort. Thanks a lot!

I am very grateful to the members of the "chicken coop" for the friendly, energetic and playful (yet very serious!) atmosphere they provided, without forgetting the help and moral support of Eric McCalla, the "mayor of the coop". I would also like to thank Chris Burns and Nupur Sinha for the very interesting discussions we had on our respective projects and their support. I would also like to thank John Camardese for keeping the lab safe and organizing the *Dahn lab* social events along with Kathlyne Nelson. I cannot forget the great help I have received from Robbie Sanderson and David Stevens and for supporting my whining! I would also like to thank Simon Trusler for the help he provided in the design of the tools that rendered this project possible. I am also very grateful for the administrative help and support I have received from Giselle Andrews during the last two years.

CHAPTER 1. INTRODUCTION

1.1 MOTIVATION

Lithium ion batteries are widely used in commercial electronics and are starting to be used in electrified vehicles (plug-in hybrids, fully electric, and hybrid vehicles). However the cost of Li-ion batteries can still be quite high and may prevent a transition from fuel powered to partially or fully electric vehicles. Prud'homme et al.[1] published an analysis on the cost-effectiveness of the electric vehicle in Europe. They concluded that fully electric cars cost an extra 12,000 Euros compared to a fuel powered car over a period of 15 years. This added cost is even worse when the lifetime of present Li-ion batteries is taken into account.

Li-ion batteries normally have a lifetime of a several years. Most fully electric and plug-in hybrid car makers such as Tesla Motors, General Motors and Renault-Nissan provide a battery pack warranty of eight years on their cars. One of the solutions to make electrified vehicles more attractive from a practical and financial point of view is to extend the lifetime of the battery. A longer lasting battery will provide more time to cover the extra cost of the electrified vehicle.

The finite lifetime of Li-ion batteries is due in part to the parasitic reactions between the positive electrode and the electrolyte, the negative electrode and the electrolyte, or due to mechanical failure in some cases. It has been shown by Broussely et al.[2] that the use of additives (compounds added in small quantity to the electrolyte) improves battery performance presumably by slowing down the rate of parasitic reactions imparting a

longer lifetime to the cell. Burns et al. and Sinha et al.[3–6] showed similar results. They showed that some additives reduce the parasitic reactions at the positive electrode and also demonstrated that several additives have the ability to dramatically reduce the impedance of the cell.

Even though these additives are widely used in the battery industry, the details of how they work are not well understood. In order to develop better electrolyte additives and engineer batteries with longer lifetimes it is important to develop a better knowledge of what additives actually do. One must investigate the reaction mechanisms, determine which electrode the additives affect, and how they affect them. Many compounds have been proposed as electrolyte additives[7], principally fully organic compounds, organosilicates, and boron containing compounds. In order to understand how these additives work, it is necessary to test a wide range of compounds and develop testing techniques that provide insights into their mechanisms of action in a rapid manner.

In 2010, Smith et al. developed a high precision coulometry method that allows for a precise and accurate measurement of the amount of charge delivered by the battery and inputted to the battery during discharge and charge respectively. This technique allows, in the majority of cases, one to assess the effect of an additive on the lifetime of the Li-ion cells in a matter of a few weeks.[8,9] In 2011, Sinha et al. developed an automated storage method which measures the open circuit voltage of a cell during storage. This method allows the rate of parasitic reaction at the positive electrode to be measured.[6] In the following years, Burns et al. and Sinha et al. used these two methods along with

electrochemical impedance spectroscopy to assess the effect of several additives in commercial machine-made Li-ion cells.[3,4,6,9]

Figure 1.1 reviews some of the earlier work by Burns et al.,[10] where impedance spectra were collected and then cells were cycled for extended periods at 55ºC. Figure 1.1e shows the normalized capacity versus cycle number of wound prismatic $LiCoO_2$/graphite cells cycled between 4.075 V to 3.4 V at 55ºC and a current density of C/10 with different vinylene carbonate (VC) and trimethoxyboroxine (TMOBX) additive combinations. The current density is expressed in "C rates" where 1C corresponds to a full charge (for example from C_6 to LiC_6 for graphite) in 1 h. A current density of C/10 corresponds to a full charge in 10 h. The normalized capacity represents the number of electrons delivered by the cell during discharge, normalized to the number of electrons delivered during the first discharge. The cycle number refers to the number of charge/discharge sequences (which is equal to one cycle) the cell underwent. Figures 1.1a to 1.1d show the electrochemical impedance spectra of the same cells measured after the high precision cycling but before the 55ºC cycling shown in Figure 1.1e. Figure 1.1e shows that the different VC and TMOBX combinations have a great impact on the cycling performance and that the combination of VC and TMOBX yields better results than VC or TMOBX alone. Figures 1.1a to 1.1d show that the impedance of the cells is greatly reduced by the addition of TMOBX but it is unclear if TMOBX affects the positive electrode side, the negative electrode side or both.

In order to be able to distinguish the effect of an additive on the positive or negative electrode, an experimental method has been developed based on electrochemical

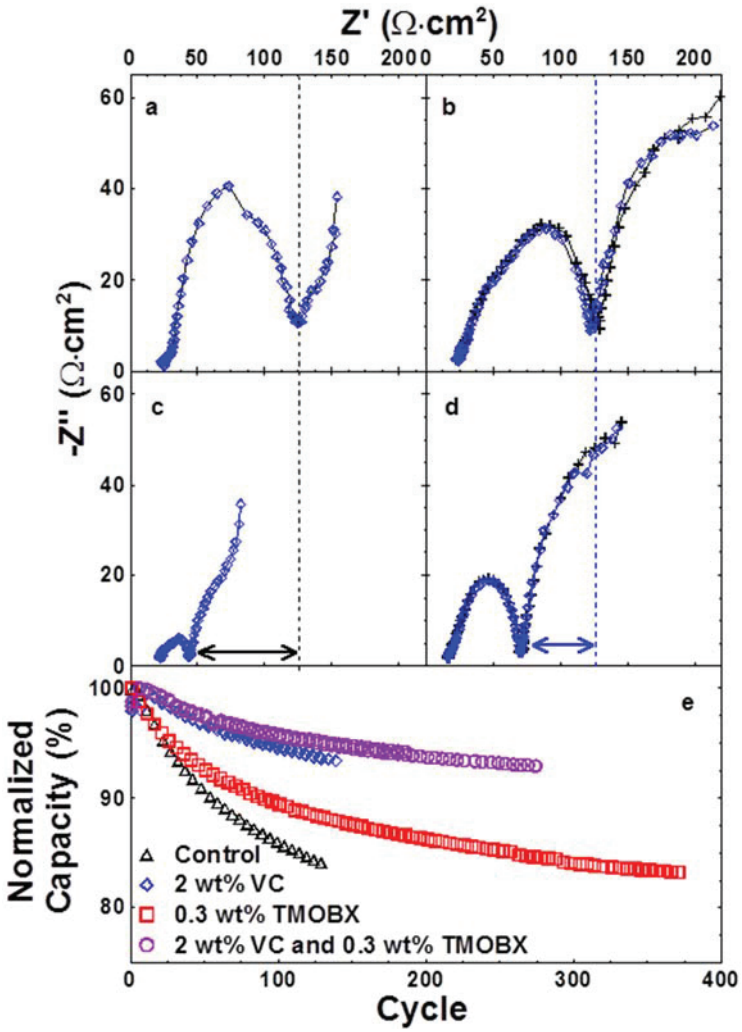

Figure 1.1 The negative imaginary area-specific impedance versus the real area-specific impedance at room temperature for $LiCoO_2$/graphite cells containing: no additive (a); 2 wt.% VC (b); 0.3 wt.% TMOBX (c); and 2 wt.% VC + 0.3 wt.% TMOBX (d). Panel e shows the normalized discharge capacity versus cycle number of these cells during long-term cycling at a C/10 rate at 55.0 ± 0.5°C (e). Reproduced with permission from *J. Electrochem. Soc.*, **160**, A117-A124 (2013). Copyright 2003, The Electrochemical Society.

impedance spectroscopy of symmetric cells constructed from electrodes of disassembled full cells similar to the method developed by Chen et al.[11] This thesis presents the details of this experimental method along with a comparative study of the effect of additives on the positive and negative electrode of Li-ion cells. The next sections of this chapter will

present a brief overview of Li-ion batteries. The present knowledge on surface chemistry in Li-ion electrodes and a brief overview of electrolyte additives are presented in Chapter 2. Chapter 3 deals with the experimental details of the technique developed which is a study of electrolyte additives in Li-ion cells using electrochemical impedance spectroscopy on symmetric cells. Chapter 4 presents a discussion on the experimental method and the interpretation of impedance spectra of Li-ion cells. Chapter 5 deals with the results of studies on electrolyte additives in commercial prismatic wound cells and pouch cells using EIS on symmetric cells and high precision coulometry.

1.2 LI-ION CELLS

1.2.1 GENERAL CONFIGURATION

Typically, a Li-ion cell consists of graphite negative electrode and a lithium transition metal oxide positive material soaked in an organic carbonate based electrolyte containing a lithium salt.[12] Between the two electrodes, an electrically insulating porous polymer membrane (polypropylene/polyethylene) is inserted to prevent any direct electron transfer. Both the positive and negative materials act as hosts for the intercalation and de-intercalation of lithium during charge and discharge. During charge, a current is applied to the cell to force the thermodynamically unfavored reaction. The electrons are forced from the positive electrode to the negative electrode. Upon charging, Li^+ ions intercalate into the negative electrode. Meanwhile Li^+ ions de-intercalate from the positive electrode and go into solution. The two half reactions at the positive electrode and negative electrode respectively during charging a Li-ion cell with a lithium transition metal dioxide positive electrode and a graphite negative electrode is given by:

$$LiMO_2 \rightarrow Li_{1-x}MO_2 + xLi^+ + xe^- \quad (1.1)$$

$$C_6 + xLi^+ + xe^- \rightarrow Li_{\frac{x}{y}}C_6 . \quad (1.2)$$

When a $LiCoO_2$ positive electrode is used, $y \sim 0.5$ and represents the maximum value that x can take.

During discharge, the thermodynamically favorable reaction occurs. The Li ions de-intercalate from the negative electrode and go into solution. Meanwhile, Li ions from the solution intercalate into the positive electrode. The electrons are driven through an external circuit where useful work can be done. The open circuit voltage of both electrodes vs. Li/Li^+ depends on their respective lithiation state (the value of x in $Li_{1-x}MO_2$ and $\frac{x}{y}$ in $Li_{\frac{x}{y}}C_6$). Figure 1.2 shows as schematic of a Li-ion cell with a graphite negative electrode and a $LiCoO_2$ positive electrode.

The lithium-ion battery is always manufactured in the discharged state. The initial amount of active lithium (lithium that can be exchanged back and forth between the positive and negative electrode) is controlled by the active mass of the positive electrode and its specific capacity (capacity per gram of active material, which is proportional to the amount of Li that can be reversibly intercalated and de-intercalated in and out of the positive electrode).

Figure 1.3 shows the galvanostatic charge-discharge curves for a $LiCoO_2$ positive electrode at a current density of C/20. The x-axis represents the cumulative charge passed during the experiment (integration of the current vs. time). If all the current is due to the

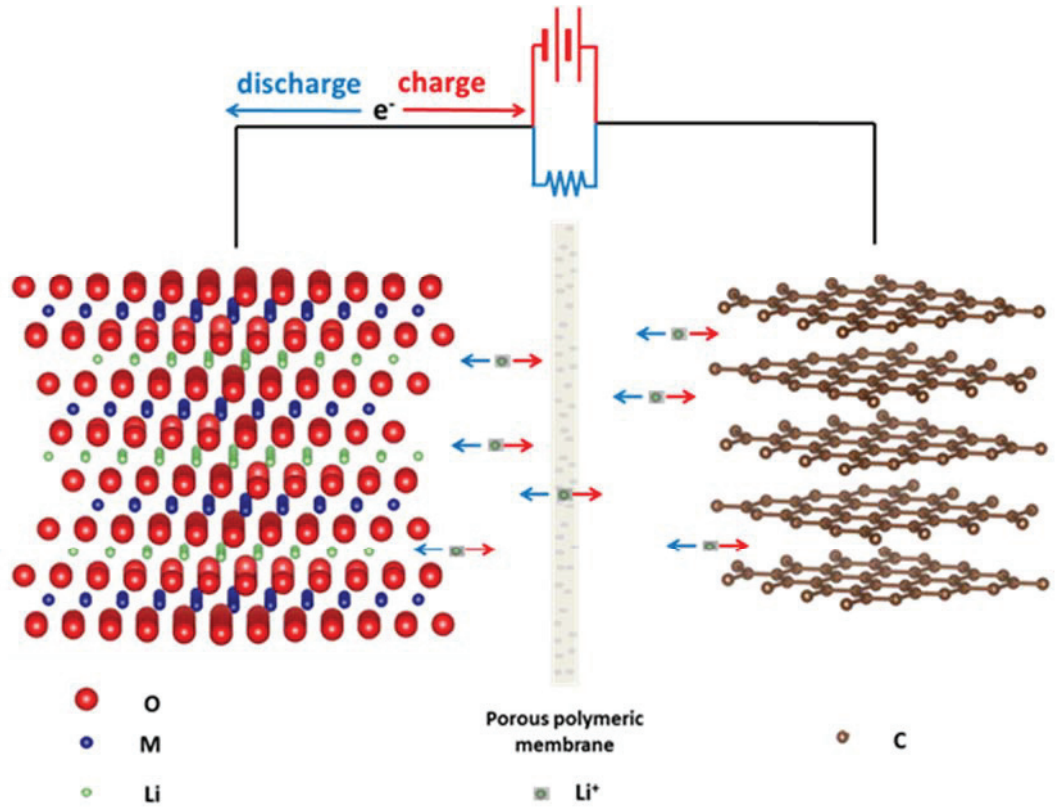

Figure 1.2 Schematic of a Li-ion cell with a graphite negative electrode (right) and $LiCoO_2$positive electrode (left).

intercalation of lithium in the material, the x-axis then represents the amount of lithium in the electrode and is commonly called the capacity axis. In the Li battery field, the capacity axis units used are mAh instead of coulombs (1 mAh = 3.6 C).

1.2.2 ELECTRODES IN LI-ION BATTERIES

Amongst the most common positive electrode materials are lithium cobalt oxide ($LiCoO_2$), commonly called LCO; lithium nickel manganese cobalt oxide ($LiNi_{1-x-y}Mn_xCo_yO_2$), called NMC; lithium manganese oxide ($Li_{1+x}Mn_{2-x}O_4$), called

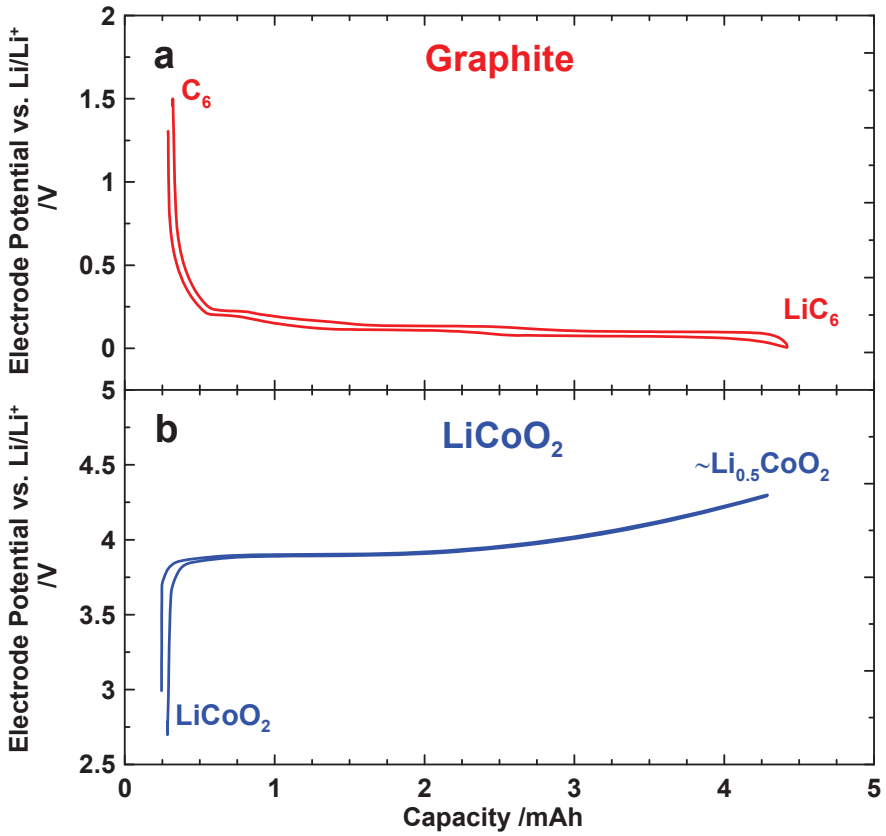

Figure 1.3 Galvanostatic charge-discharge curves for a graphite negative electrode (a) and a $LiCoO_2$ positive electrode (b) cycled vs. Li/Li^+ at a current density of C/20.

LMO; lithium nickel cobalt aluminum oxide ($LiNi_{0.8}Co_{0.15}Al_{0.05}O_2$), called NCA; and lithium iron phosphate ($LiFePO_4$) called LFP. They have average voltages between 3.4 V vs. Li/Li^+ (for LFP) and 4.1 V (for $Li_{1+x}Mn_{2-x}O_4$).[12] Most of these materials are used in battery packs in electric, hybrid vehicles, and portable electronics. For instance, NMC and LMO are used in the Chevrolet Volt, LMO is used in the Nissan Leaf, NCA is used in the cars manufactured by Tesla, and LFP in the Blue car made by Bolloré.

Li metal is generally not used as the negative electrode in commercial cells because of its high reactivity and safety problems. Instead of Li metal, graphite is usually used. Graphite-based materials have been introduced for their improved safety, low reduction potential vs. Li/Li^+, and high gravimetric capacity.[13] As a consequence, the voltage of a cell that uses graphite as the negative electrode is close to that of a cell using Li metal. Several other chemistries for negative electrodes exist but are not as commonly used. Amongst them is lithium titanate oxide ($Li_{4/3}Ti_{5/4}O_4$) called LTO and alloys based on metals that alloy with lithium, including Si or Sn. They all have their advantages and drawbacks. For example LTO has a lower capacity fade during cycling than graphite but has a lower energy density (lower specific capacity and higher potential). Sn and Si have a better energy density than graphite but suffer from high capacity fade upon cycling.[12] For a more in depth description of the history of the Li-ion battery, readers are invited to consult reference 11.

1.2.3 ELECTROLYTE SYSTEMS

The electrolyte typically used in a Li-ion cell is composed of a mixture of organic carbonates and a lithium salt. The most common solvent is made from ethylene carbonate (EC) or propylene carbonate (PC), mixed with either ethyl methyl carbonate (EMC), diethyl carbonate (DEC) or dimethyl carbonate (DMC). Organic carbonates are generally used for their relatively large operating potential window, film forming properties, relatively low viscosity and good Li^+ solubility. The chemical structures of the organic carbonates mentioned are shown in Figure 1.4.

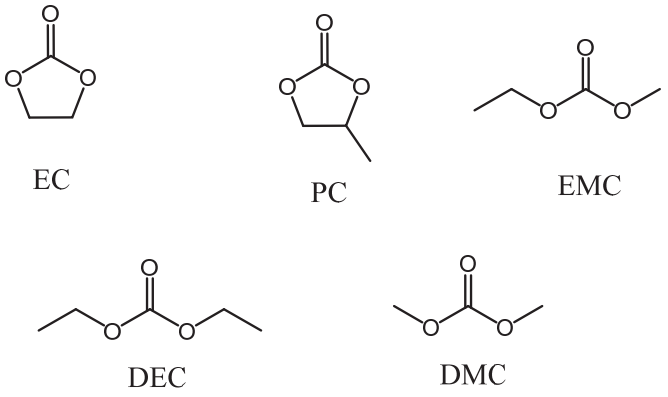

Figure 1.4 Chemical structure of common organic carbonates used in the formulation of electrolytes in Li-ion batteries.

The most common lithium salt used in the electrolyte is lithium hexafluorophosphate ($LiPF_6$). Other salts can be used like lithium tetrafluoroborate ($LiBF_4$); lithium perchlorate ($LiClO_4$); lithium bis-oxalatoborate ($LiB(C_2O_4)_2$), commonly called LiBOB; and lithium bis(trifluoromethylsulfonyl)imide ($LiN(SO_2CF_3)_2$), commonly called LiTFSI. However, these salts might have some drawbacks compared to $LiPF_6$. For example $LiBF_4$ and $LiB(C_2O_4)_2$ have low conductivity at low temperature,[14,15] $LiClO_4$ provides poor safety and $LiN(SO_2CF_3)_2$ is expensive and has poor stability at high voltage.[16] The structures of the lithium salts mentioned are shown in Figure 1.5.

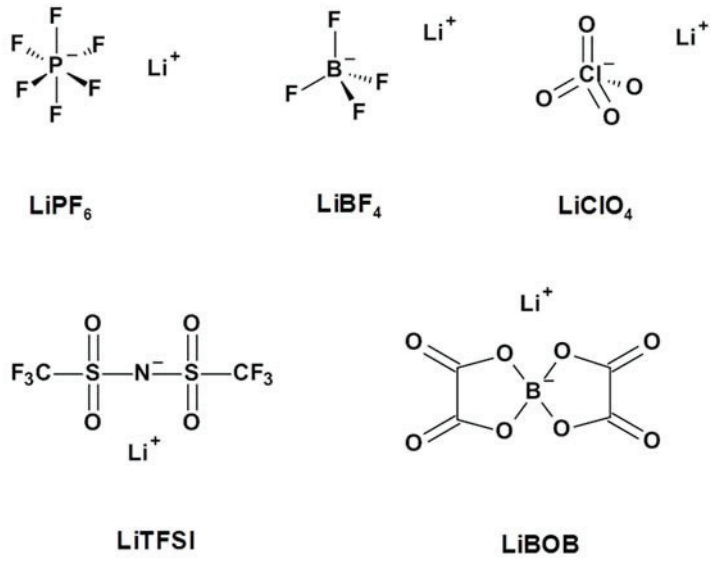

Figure 1.5 Structure of the anion and cation of common salts used in the formulation of electrolytes in Li-ion batteries.

CHAPTER 2. ELECTRODE-ELECTROLYTE INTERPHASE AND ELECTROLYTE ADDITIVES

2.1 ELECTROLYTE REACTIVITY

The characteristics that made the Li-ion cells popular for their use in consumer electronics and good candidates for electric vehicles are their high volumetric energy density, safety, and cost. However, parasitic reactions between the electrolyte and the electrodes shorten the lifetime of the cell. For example Zhang et al.[17] and Egashira et al.[18] showed that the reduction potential of ethylene carbonate is about 1.36 V vs. Li/Li^+ and that an electrolyte composed of 1M $LiPF_6$ EC/DEC shows signs of oxidation around 4.0 V vs. Li/Li^+. Typically, the potential range of the positive electrode in a Li-ion cell during cycling is between 3.5 - 4.3 V vs. Li/Li^+ and between 1.2 - 0.005 V vs. Li/Li^+ for the graphite negative electrodes. This shows that the electrolyte is not thermodynamically stable at either electrode.

In Li-ion cells with a graphite negative electrode and a lithium transition metal dioxide positive electrode, without additive, the negative electrode is more reactive towards the electrolyte than the positive electrode.[19] The lifetime of these cells is then controlled by the rate of reactions at the negative electrode. However, with the use of electrolyte additives the rate of reactions at the negative electrode is greatly reduced and in some cases falls in the same range as the rate of reactions at the positive electrode. The reactivity of the positive electrode towards the electrolyte then becomes more and more important in determining the lifetime of the battery.

2.2 SOLID ELECTROLYTE INTERPHASE (SEI)

Even though the Li-ion cell (electrodes and electrolyte) is not thermodynamically stable, a standard Li-ion cell still has a service life of several years. This indicates that the electrodes are kinetically stable towards the electrolyte. This kinetic stability comes from the formation of a solid layer at the surface of both electrodes during the first few cycles. During the first charge, both electrodes react with the electrolyte. Some of the by-products of these reactions are not soluble in the electrolyte and precipitate at the surface of the electrodes. Fortunately, this layer of precipitated by-products is electronically insulating and ionically conducting and is called the solid electrolyte interphase (SEI) as first introduced by Peled in 1979.[20] The electrolyte oxidation-reduction reactions at both electrodes are slowed down due to the electronically insulating property of the interphase once formed. The battery can still function properly since the interphase allows Li ions to diffuse through it. The creation of such an interphase is crucial for the proper operation of the Li-ion cells and is the reason for the possibility of engineering Li-ion cells that last several years.

2.2.1 SOLID ELECTROLYTE INTERPHASE AT THE NEGATIVE ELECTRODE IN STANDARD ELECTROLYTE

The use of EC allows graphite to be used as a viable replacement for the Li metal electrode. It was proposed that this ability comes from the reduction of EC at the negative electrode as shown by: [21]

$$2EC + 2e^- + 2Li^+ \rightarrow (CH_2OCO_2Li)_{2(s)} + C_2H_{4(g)}. \quad (2.1)$$

The solid product of this reaction (lithium alkyl carbonate) precipitates at the surface of the graphite electrode and forms a physical barrier that is electronically insulating and ionically conducting and prevents the solvent from co-intercalating within the graphite structure[22]. PC also reacts at the negative electrode but does not provide a protective layer at the surface of the electrode.[23] The surface chemistry of negative electrodes in regular electrolytes has been extensively studied over the past two decades. Several surface characterization techniques have been used such as Fourier transform infrared spectroscopy (FT-IR), Raman spectroscopy, in-situ atomic force microscopy (AFM),[23–26] and x-ray photoelectron microscopy (XPS).[27,28] Some electrochemical techniques have also been used to characterize the negative electrode reactivity towards the electrolyte such as chronopotentiometry, EIS, and cyclic voltammetry. Several good reviews on the SEI composition in carbonaceous electrodes are available.[29] Some of the key findings are presented below.

The study of the composition of the SEI revealed that the reactions between the negative electrode and the electrolyte are much more complicated than shown in equation 2.1. The SEI on the negative electrode is comprised of inorganic and organic compounds coming from the reduction of the solvent and salt from the electrolyte. It has been generally proposed that closer to the electrode the SEI is composed of inorganic compounds and that closer to the electrolyte the SEI composition is dominated by organic compounds.[30-33]

Some of the major components detected either by XPS or FT-IR are $(CH_2OCO_2Li)_2$ coming from the reduction of EC,[21,34–37] and ROLi[21,27,38–44] from the reduction of co-

solvents like PC. Evidence of the presence of LiF, resulting from the reduction of the fluorinated salts and their reaction with hydrofluoric acid (which a contaminant present in most electrolytes)[31,45] were found. The presence of polycarbonates from the reaction of the solvent[31] was also demonstrated along with LiOH.[37,46,47] Other compounds have also been detected, but more rarely, such as LiC_2O_4, LiOMe and LiO_2CR.[39,43]

Novak et al. also showed that the SEI formation on graphite depends on both the presence of oxygen on the terminal carbons of the graphene sheets and on the disorder of the graphene sheets.[48,49] Some studies also showed that the composition of the SEI on graphite is different on the edge plane (plane perpendicular to the graphene sheets) than on the basal plane (plane parallel to the graphene sheets).[45]

Aurbach et al. also stressed the importance of the low solubility of the by-products of the reactions of the electrolyte components in obtaining a good SEI.[34] Since the SEI is composed of reaction by-products of the electrolyte, it is highly dependent on the electrolyte formulation (solvent, co-solvent and salt used). That is why the introduction of additives in small quantities can alter the composition of the SEI and slow down the parasitic reactions.

2.2.2 SOLID ELECTROLYTE INTERPHASE AT THE POSITIVE ELECTRODE IN STANDARD ELECTROLYTE

Positive electrode surface chemistry has received less attention. However, some general understanding of this chemistry exists. It has been shown that the impedance of the positive electrode increases significantly upon cycling and during storage[50] which indicates either the presence and growth of a surface film or the modification of the

crystal structure at the surface of the active particles. Generally, the salt in the electrolyte is stable towards the positive electrode.[51] However, some salts inevitably react with impurities from which the products precipitate, such as the precipitation of LiF as shown by:[51]

$$LiPF_6 \rightleftharpoons LiF_{(s)} + PF_{5(g)} \quad (2.2)$$

$$LiPF_6 + H_2O \longrightarrow LiF_{(s)} + POF_3 + 2HF. \quad (2.3)$$

Moshkovich et al.[51] showed that the solvents commonly used in Li-ion cells are not electrochemically stable at potentials higher than 3.5 V and undergo oxidation based on studies on polarized inert electrodes (Pt, Au, Al). However, they did not detect any oxidation of $LiClO_4$, $LiAsF_6$, $LiPF_6$, $LiC(SO_2CF_3)_3$ and $LiN(SO_2CF_3)_2$ even at a potential as high as 5 V. Aurbach et al. saw evidence of the presence of polycarbonates in the positive electrode surface films based on FT-IR measurements.[50,52] The existence of these polycarbonates may be explained by anionic polymerization initiated by ROLi species or by the oxidation of the solvent and subsequent cationic polymerization as shown below .[52]

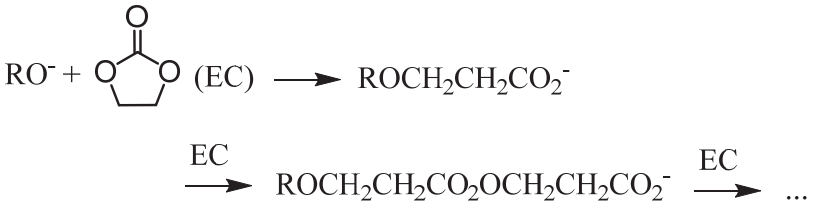

(2.4)

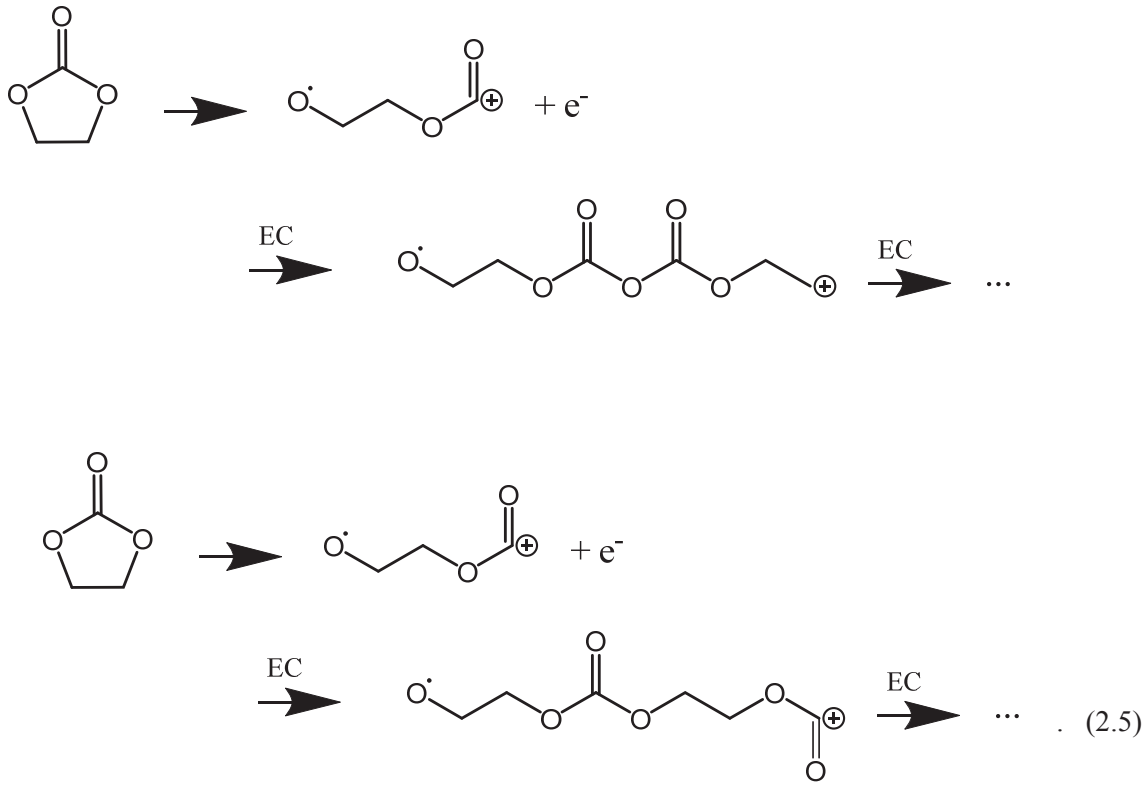

(2.5)

Evidence for the presence of $ROCO_2Li$ and ROLi species, much like the one present at the negative electrode, has been shown.[50,51]

2.3 ELECTROLYTE ADDITIVES

In order for the Li-ion cells to be widely used in electric vehicles and other long-term applications several properties need to be optimized. Amongst them are the energy density, cycle life, impedance, cost and safety.[53] Energy density and cost are intrinsic properties of the active materials[54] and often limited by the positive electrode material used and will not be discussed in this thesis. Cycle life, impedance, and safety of Li-ion cells can be improved through the use of additives in the electrolyte. Additives are chemical compounds added to the electrolyte in small quantities (0 to 10 wt.%).[7] Zhang

made an extensive review of different functions of electrolyte additives in 2006.[7] Mainly, additives are used for four different purposes: improving the cycling performance, improving lifetime, reducing impedance and improving safety. This report will focus on additives that affect the cycle life of batteries, reduce impedance, and improve lifetime.

In 2005, Broussely et al. published the results of the testing of Li-ion cells over the course of several years of cycling.[2] In their report, they indicated that the aging mechanisms responsible for the finite lifetime of the battery were due to parasitic reactions at the negative electrode due to unstable SEI, impedance growth and parasitic reactions at the positive electrode at high state of charge and high temperature. This indicates that even though the SEI imparts some kinetic stability to the cell, it may not stabilize it enough to get the desired cycle life. But most importantly, they also showed that the use of additives (vinylene carbonate in their case) is beneficial and dramatically improves the cycle life of the cell. The aging mechanisms of the Li-ion battery have been generally assigned to several factors:

1) SEI instability at the negative electrode due to either poor surface passivation or SEI deterioration due to the volume expansion of the active material[55]
2) Presence of water or HF contamination especially for $LiMn_2O_4$[56]
3) Material loss and degradation[55]
4) Impedance increase[55]
5) Electrolyte oxidation at the positive electrode[3]

Some of these different factors are dependent on one another, for example, the presence of HF has been proposed to be one of the causes of SEI degradation[56]. As a result, factors

1) and 2) might be linked in some cases. Also, 4) and 5) might be linked as massive electrolyte oxidation at the positive electrode and thick SEI formation at the negative electrode can lead to a large impedance increase. As a consequence, additives improve the cycling performance by affecting one or more of these factors. Ideally, an additive or an additive combination should positively affect all these factors at the same time. That is to say an additive or additive combination should help create an electronically insulating SEI with good passivation at both the positive and negative electrodes with high Li^+ conduction (low impedance SEI) that can withstand the volume changes of the active material.

2.3.1 ADDITIVES FOR IMPROVED CYCLING

Generally the first objective of an additive is to stabilize the SEI of the graphite electrode. Some of these additives are said to be "film forming additives". These additives are organic compounds that can either produce a polymeric film or that produce insoluble by-products that precipitate at the electrode surface.[7] In order for these additives to preferentially react at the carbon electrode their reduction potential is generally higher than that of the solvent components. One of the most well-known film forming additives is vinylene carbonate (VC).[57] A large array of compounds has been **proposed** as film forming additives such as carbonates (*e.g.* fluoroethylene carbonate, vinyl ethylene carbonate, allyl ethyl carbonate),[58] sulfites (*e.g.* ethylene sulfite)[59] and halogenated lactones.[60] However, some new findings by Xiong et al.[61] showed that VC does not reduce the rate of parasitic reactions at the graphite electrode in Li/graphite cells at

temperature below 60°C. This exemplifies the lack of understanding of how these additives work.

Other additives are thought to react with by-products of the electrolyte degradation and give better components for an efficient SEI. Amongst them are Li_2CO_3,[62] sulphur dioxide,[63] aromatic compounds capable of forming stable radicals[64] and organic and inorganic boron compounds.[65–67] Alkali salts (sodium or potassium salts) also have been identified as good additives to improve cycling performances of graphite cycled against Li metal.[68]

Since HF and water are thought to be detrimental to both the SEI and the positive electrode material some additives capable of suppressing them have been developed. Examples of these additives are amines[69] and organic compounds containing N-Si bonds.[70] Other additives were designed to stabilize the Lewis acid, PF_5, formed by the decomposition of $LiPF_6$ when this salt is used in the electrolyte. These additives are mainly Lewis bases containing phosphorus and nitrogen atoms capable of sharing their lone electron pair to the PF_5.[71] The molecular structures of some common electrolyte additives are shown in Figure 2.1.

2.3.2 STUDY OF ELECTROLYTE ADDITIVES

The way electrolyte additives are studied generally does not allow an assessment of what constitutes a good SEI nor of what class of additives imparts a stable and efficient SEI. Generally, in academia, additives are studied individually by XPS, FT-IR and low precision coulometry without comparisons to other efficient additives or specifying the

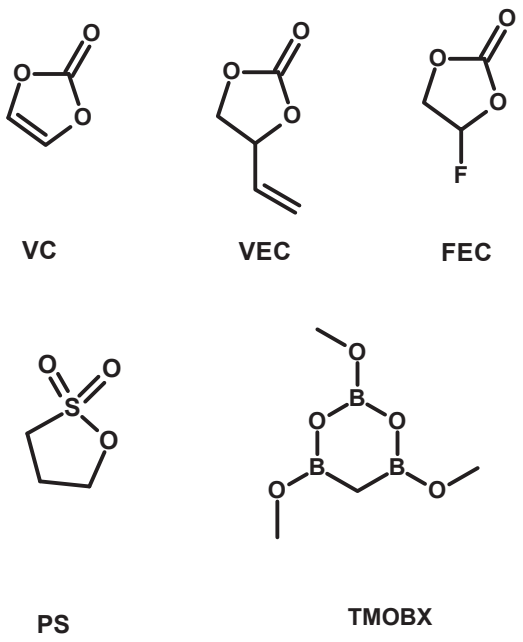

Figure 2.1 Molecular structures of some common electrolyte additives used in Li-ion batteries.

active material to additive ratio used in the study.[72–76] This provides only specific information on one particular additive. Not surprisingly, these studies often reveal that additives decompose to organic species that precipitate at the surface of the electrode. Furthermore, these analyses are often done on cell designs that are very different from the design of commercial cells. Cells used in the research field are usually made up of man-made electrodes with poor reproducibility and a very low active material to conductive additive (carbon black) ratio compared to commercial electrodes. The electrolyte mass to active material mass ratio is often very high such that the cells are "flooded" which is again very far from real Li-ion cells. This implies that the properties of electrolyte additives found in cells commonly used in the academic field are not the same as in commercial cells.

Some researchers have started making studies on electrolyte additives using machine-made cells actually used in commercial application. For instance, Burns et al. and Sinha et al. used commercial machine-made cells to compare the effect of different additives on the cycling performances of the cells.[3–6,77,78] As mentioned in the first chapter, it is often difficult to assess which electrode additives affect in a rapid manner. It is even more challenging to use a cell configuration close to those used by industry. However, EIS performed on symmetric cells as introduced by Chen et al.[11] can be used for this purpose as will be presented in Chapters 3 and 4.

The study of additives is without a doubt very complex. For instance, Smith et al.[9] estimated that parasitic current at the positive electrode of commercial $LiMn_2O_4$/graphite 18650 cells to be in the order of tens of μA. This current is about 2000 times smaller than the current caused by the intercalation of lithium. Unveiling the way additives work is even more difficult when interactions between the positive and negative electrodes exist. For instance, Broussely et al.[2] suggested an interaction between the negative and positive electrode resulting in the production of CO_2. Li et al. showed evidence of interactions between the positive and negative electrodes in LTO/$LiNi_{0.5}Mn_{1.5}O_4$ cells.[79] In their study, they showed evidence of the LTO electrode reacting with the products of the reaction between the positive electrode and the electrolyte. Sloop et al.[80] also proposed a similar mechanism where the products at one electrode migrate to the other electrode and react. This means additive studies that use half cells (negative material/Li, and positive material/Li) cannot be trusted. The use of full cells is therefore essential to get information on the way additives work in real life cells.

CHAPTER 3. ELECTROCHEMICAL IMPEDANCE SPECTROSCOPY ON SYMMETRIC CELLS: EXPERIMENTAL DETAILS

3.1 ELECTROCHEMICAL IMPEDANCE SPECTROSCOPY (EIS)

EIS is an electrochemical technique that is used in multiple research areas such as biology, metallurgy, and electrochemical storage.[81] This technique consists of measuring the current resulting from the alternating voltage bias that the cell is subjected to, as shown in Figure 3.1. The AC potential is inputted in a range of frequencies from mHz to

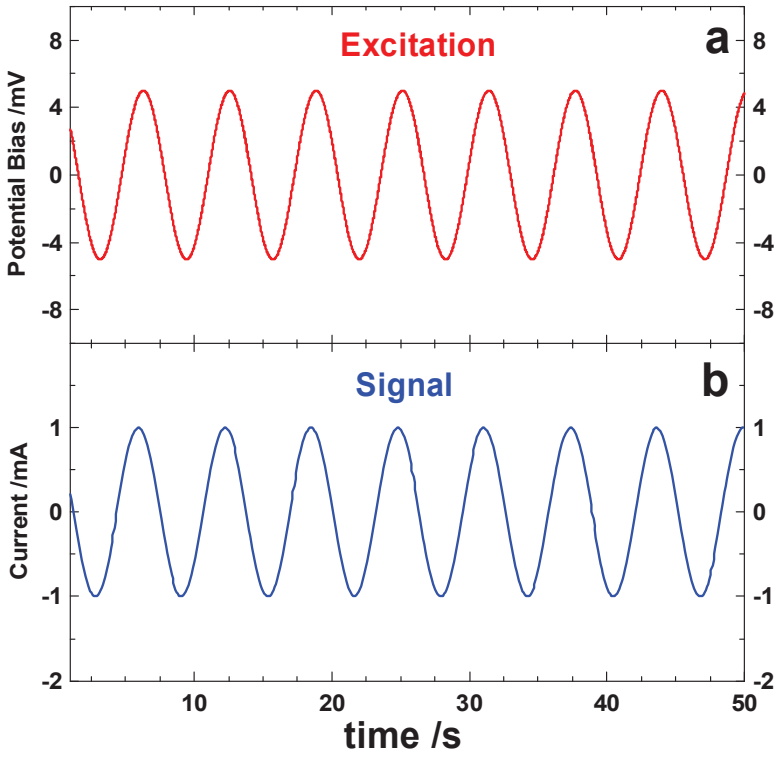

Figure 3.1 AC Potential centered around open circuit potential applied to the cell (a) and resulting current during EIS measurement (b); only one frequency is shown.

MHz. The amplitude of the AC potential applied to the cell is in the mV-range, centered around the open circuit equilibrium potential, usually between +/- 5-10 mV. A small amplitude is applied so that the current response is linear with voltage. The current resulting from the potential bias is then recorded as a function of the frequency. EIS allows the different contributions to the current to be separated. For example, in Li-ion cells the contribution from electrical double layer charging and intercalation processes are apparent at high to medium frequencies, and the slow solid state diffusion phenomena are apparent at low frequencies. The current resulting from the bias has the same frequency as the AC potential applied to the cell. However, depending on the phenomenon impeding the current, there can be a phase shift between the potential and the current.

The impedance, $Z(\omega)$, is calculated as the ratio of the voltage, $V(\omega,t)$, to the current, $I(\omega,t)$, at each frequency, ω, as given by:[81]

$$Z(\omega) = \frac{V(\omega,t)}{I(\omega,t)} = \frac{|V|sin(\omega t)}{|I|sin(\omega t+\varphi)} \quad . \tag{3.1}$$

The symbol φ represents the phase difference between the AC current and the AC voltage. Since it is easier to manipulate imaginary numbers than trigonometric ratios with different phases, and for that reason, the impedance is always expressed in terms of imaginary numbers. The transformation from sines and cosines to imaginary numbers is realized using Euler's rule:

$$e^{j\omega t} = \cos(\omega t) + jsin(\omega t)\ . \tag{3.2}$$

3.1.1 IMPEDANCE OF SIMPLE ELECTRONIC COMPONENTS

Figure 3.2 shows three simple electronic components used to model the impedance of Li-ion cells. These components are a resistor, a capacitor, and an inductor. The development for the expressions of the impedance of a resistor, $Z_R(\omega)$, is given by:[81]

$$Z_R(\omega) = \frac{V(\omega,t)}{I(\omega,t)} = \frac{|V|sin(\omega t)}{|I|\sin(\omega t)} = R \tag{3.3}$$

where R is the resistance in Ω, $I(\omega,t)$ is the AC current in A and $V(\omega,t)$ is the AC potential in V. The development for the expressions of the impedance of a capacitor, $Z_C(\omega)$, is given by:[81]

$$C = \frac{\mathrm{Q}}{V} \tag{3.4}$$

$$I(\omega,t) = \frac{d\mathrm{Q}}{dt} = \frac{d}{dt}CV(\omega,t) = \frac{d}{dt}C|V|sin(\omega t) = CV\omega\cos(\omega t) \tag{3.5}$$

$$Z_C(\omega) = \frac{|V|e^{j\omega t}e^{-j\pi/2}}{C|V|\omega e^{j\omega t}} = \frac{-j}{C\omega} = \frac{1}{j\omega C} \tag{3.6}$$

where C is the capacitance in F, Q is the number of charge in C, V is the potential

Figure 3.2 Symbols of relevant electronic components.

difference in V.

The development for the expression of the impedance of an inductor, $Z_{Ind}(\omega)$, is given by:

$$L = \frac{V(\omega,t)}{dI(\omega,t)/dt} \tag{3.7}$$

$$V(\omega,t) = L\frac{dI(\omega,t)}{dt} = L\frac{d}{dt}|\mathrm{I}|\sin(\omega t) = L\omega\,|\mathrm{I}|\cos(\omega t) \tag{3.8}$$

$$I(\omega,t) = |\mathrm{I}|\sin(\omega t) = \ |I|cos\left(\omega t - \frac{\pi}{2}\right) \tag{3.9}$$

$$Z_{Ind}(\omega) = \frac{V(\omega,t)}{I(\omega,t)} = \frac{L\omega\,|\mathrm{I}|\cos(\omega t)}{|I|cos\left(\omega t - \frac{\pi}{2}\right)} = \frac{L\omega e^{j\omega t}}{e^{j\omega t}e^{-j\pi/2}} = \frac{L\omega}{-j} = jL\omega \tag{3.10}$$

where L is the inductance in H.

Equations 3.3 to 3.10 show that capacitors and inductors induce a phase shift between the voltage and the current, whereas resistors do not. They also show that the impedance of inductors and capacitors depend on the frequency, whereas the impedance of resistors does not. The impedance of circuits comprised of simple electronic components follows the same rules as those for total resistance. Figure 3.3 shows the rules for the calculation of the impedance of two elements connected in series and parallel.

Figure 3.4 shows the impedance of some simple circuits along with the Nyquist representation and Bode representation of their impedance as a function of frequency.[81] The Nyquist representation of the impedance, also called the Cole-Cole representation,[81] presents the negative imaginary part of the impedance as a function of the real part of the

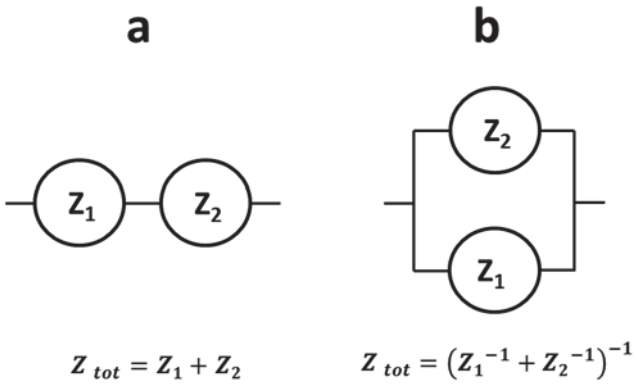

Figure 3.3 Circuit of two components in series (a) and in parallel (b) along with the expression of their total impedance.

impedance. The Bode representation of the impedance presents the real part and negative imaginary part of the impedance as a function of the logarithm of the frequency. Though less used, the Bode representation is more practical as it gives the frequency of each data point.

Figure 3.4a shows that the circuit made from a resistor and capacitor in series has a fixed value of the real part which is equal to the resistance, and a negative imaginary part that has a limit of 0 Ω when the frequency approaches infinity. Figure 3.4b shows that the circuit made of a resistor and an inductor in series also has a constant real part of the impedance which is equal to the value of the resistance. However, its negative imaginary part approaches infinity as the frequency tends to infinity.

Figure 3.4c shows the circuit composed of a resistor and capacitor in parallel. This circuit shows a distinctive semi-circle in the Nyquist representation. The Bode representation of its impedance presents a step-wise decrease from low to high frequency in the real part of

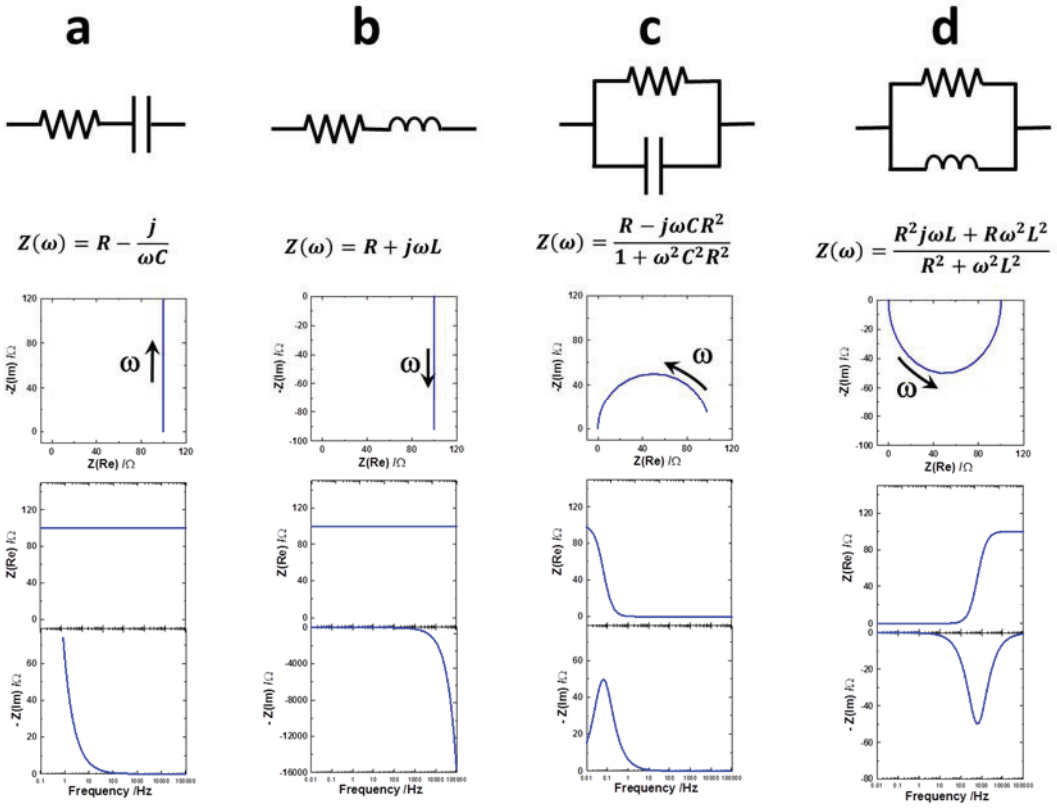

Figure 3.4 Nyquist representation (top graph) along with the direction of increasing frequency, ω, and Bode representation (bottom two graphs) of the impedance of resistor and capacitor in series (a), resistor and inductor in series (b), resistor and capacitor in parallel (c), and resistor and inductor in parallel (d).

the impedance. The step size is equal to the value of the resistance. The negative imaginary part of the impedance shows a bell-shaped curve, where the frequency at its maximum is equal to $f_{max} = 1/2\pi RC$.

Figure 3.4d shows a circuit composed of a resistor and inductor in parallel. This circuit presents an inverted semi-circle with a diameter which is equal to the value of the resistance. The Bode representation of its impedance presents a step-wise increase from low to high frequency in the real part of the impedance. The step size is equal the value

of the resistance. The negative imaginary part of the impedance shows an inversed bell-shape curve.

3.1.2 ACTIVE PARTICLE MODELING

In order to interpret the impedance of a Li-ion cell, the different contributions to the impedance are modeled using simple electronic components. Figure 3.5 shows a simple circuit model for a hypothetical single active particle. This impedance model consists of a resistor modeling the charge transfer resistance for the incorporation of lithium from the electrolyte to the active particle and passing through the SEI, in series with a Warburg

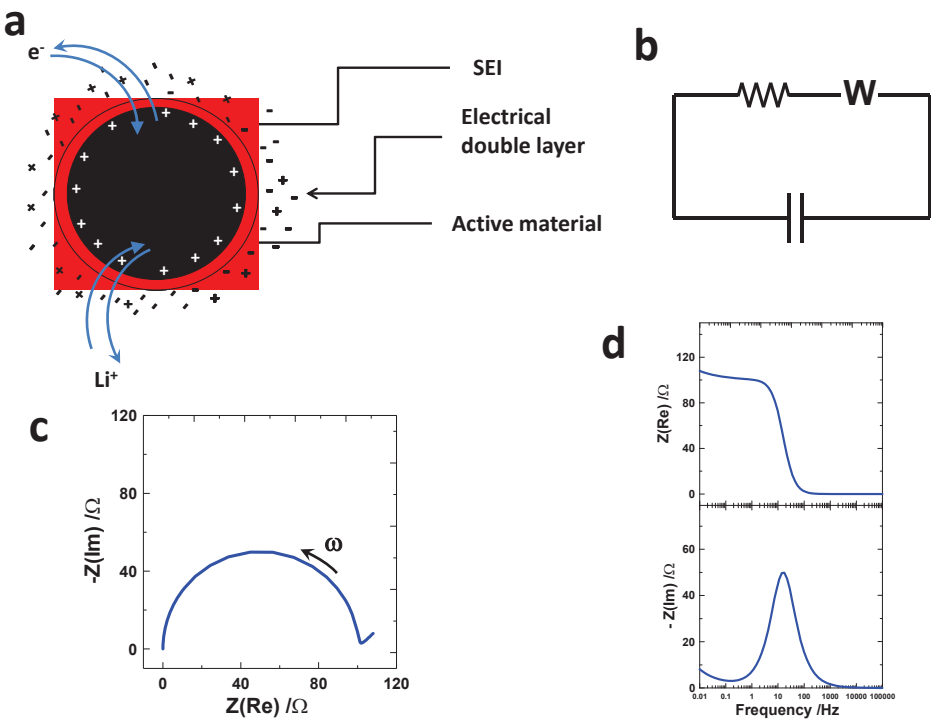

Figure 3.5 Schematization of a single active particle in the electrolyte (a), a simple electronic circuit model (b) along with the Nyquist representation (c), and Bode representation (d) of the circuit model.

resistor modeling the solid state diffusion from the edge of the particle to the center of the particle, which are in parallel with a capacitor modeling the double layer capacitance. The simplest Warburg-type resistor models semi-infinite diffusion at a planar electrode and the expression of its impedance is given by:

$$Z_W(\omega) = \frac{A_D}{\omega^{1/2}} - \frac{jA_D}{\omega^{1/2}} \tag{3.11}$$

where ω is the frequency in rad·s^{-1}, and A_D is the Warburg coefficient in Ω·rad$^{1/2}$·s$^{-1/2}$ which is related to the chemical diffusion of Li in the active particle.

Figure 3.5c shows the Nyquist representation of the impedance of the circuit. The circuit shown in Figure 3.5b is characterized by a distinctive semi-circle in the Nyquist representation with a diameter equal to the value of the resistance, and a 45° tail at low frequency (right part of the x-axis). Figure 3.5d shows the Bode representation of the impedance. This circuit model also gives a distinctive signature in the Bode plot. This signature is a step-wise increase from high to low frequency in the real part of the impedance and a small slope at very low frequency. The step size is equal to the value of the resistor. The negative imaginary part of the impedance shows a bell-shaped curve, where the frequency at its maximum is equal to $f_{max} = 1/2\pi RC$.

3.1.3 ELECTRODE MODELING

The nature of the electrodes in Li-ion batteries makes them difficult to model. Simple models always assume either smooth and flat electrodes, or single smooth spherical or slab-shaped particle. However, electrodes in a Li-ion cells are commonly manufactured

as composites of small active particles (micrometer size or nanometer size in some cases), with 2 - 4 wt.% of carbon black as a conductive additive, and 2 - 4 wt.% of polyvinylidene difluoride (PVDF), or another polymer as binding agent. Figure 3.6 shows a scanning electrode microscopy (SEM) image of a commercial $LiCoO_2$ (LCO) electrode. From this image, the active particles, carbon black and PVDF (both appearing dark) can be clearly seen. This configuration makes the modeling of the impedance of a whole electrode quite complicated. For example, Meyers et al. proposed an impedance model for porous electrodes which involves more than 12 adjustable parameters.[82] This renders the fitting of an impedance spectrum inaccurate as it is easy to get two exact same spectra with different values assigned to the numerous parameters. The model proposed by Meyers et al. used spherical particles with a surface film. The equivalent circuit model for a single particle was derived by solving the Butler-Volmer equation, assuming a resistive film with a capacitance, double layer charging, and solid state diffusion assuming that

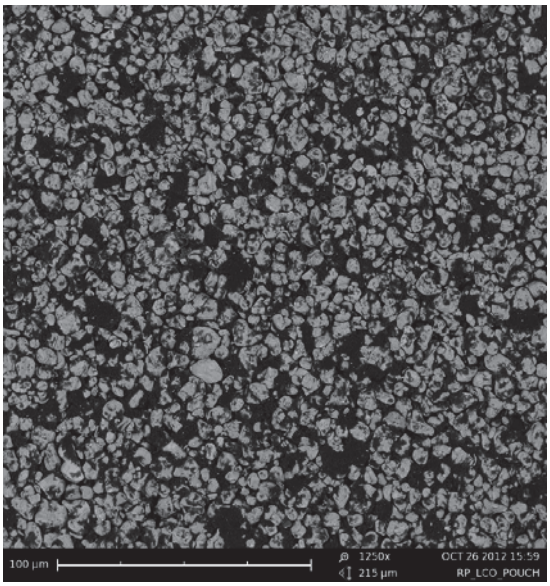

Figure 3.6 Scanning electrode microscopy image of a commercial $LiCoO_2$ electrode.

Fick's law is obeyed[82]. They then modeled the electrode impedance by considering the particles as being electrically connected together along with considering the ionic conductivity of the electrolyte as well as the particle size distribution. Figure 3.7 shows the different circuit models derived by Meyers et al. for a single particle.[82]

EIS spectra are too often modeled without careful verification that the observed features are assigned to the right phenomena. The impedance spectra of typical electrodes show two distinctive features, one in the high frequency range and the other in the medium frequency range. There is no consensus on the originating phenomena of these features. For instance, Levi et al. proposed that the higher frequency feature comes from lithium

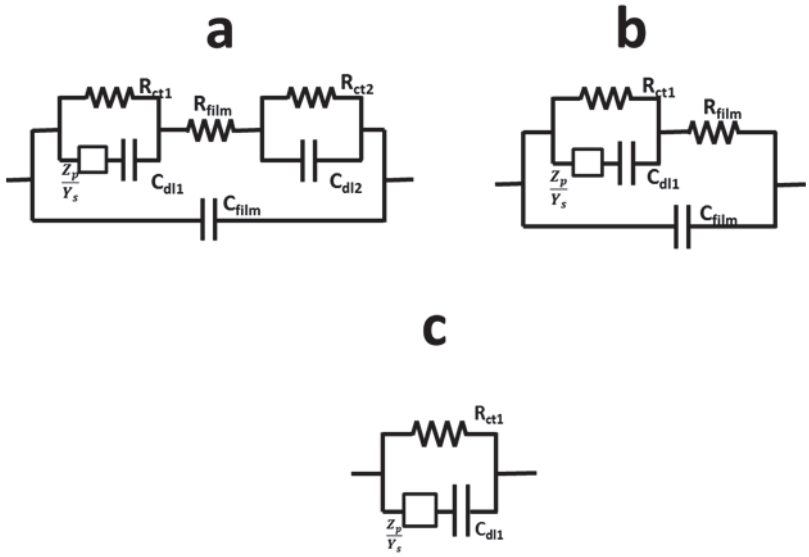

Figure 3.7 Circuit models for a single particle used to derive the impedance of an electrode, proposed by Meyers et al. [82] Model a includes an internal and external interfacial impedance as well as a resistive film, model b considers only an internal interfacial impedance and resistive film, model c considers only an internal interfacial impedance and no resistive film. Adapted from reference 82.

ion migration through the SEI and the related film capacitance, and that the medium frequency feature comes from the transfer of Li^+ through the SEI-active particle interphase.[83] In the same publication the authors showed that different electrode porosities, particle sizes and size distributions may lead to different shapes of the impedance spectra. Hjelm et al. showed experimental evidence that the high frequency feature of positive electrodes comes from the contact resistance between the current collector and the active particles.[84] This was supported by the dependence of the existence and magnitude of the high frequency semi-circle on the nature of the substrate on which the electrode was deposited. This assignment was later supported by Gaberscek et al. [85] in 2008 where they showed that the size of the high frequency semi-circle was highly dependent on the pressure the battery was subjected too when using uncalendared electrodes.

The lack of consensus and the multiple parameters involved in modeling EIS spectra makes the extraction of particular parameters such as particle size, diffusion coefficient, pore size, *etc.* very difficult and shows the lack of care most researchers apply when interpreting EIS spectra. In order to prevent misinterpretation, the only information that will be drawn from the EIS spectra in this thesis is whether the surface of the particle is changed upon the addition of one or more electrolyte additives. Section 4.3 presents the model used to fit the EIS spectra.

3.1.4 BATTERY MODELING

The expression for the impedance of Li-ion cell (negative electrode/electrolyte/positive electrode), Z_{tot} , is given by:

$$Z_{tot} = Z_{e.s} + Z_{(-)} + Z_e + Z_{(+)} \tag{3.12}$$

where $Z_{e.s.}$ is the impedance of the cables and components of the frequency response analyzer and experimental setup, $Z_{(-)}$ is the negative electrode impedance, $Z_{(+)}$ is the positive electrode impedance, and Z_e is the electrolyte impedance. The contribution from the experimental setup which often appears as an inductive component can be corrected by measuring the impedance of a short circuit and subtracting it from the impedance of the cell. The impedance of the short circuit is not identical to the contribution of the experimental setup, however it is very close.

The expression of the impedance of the electrolyte, Z_e, is given by:

$$Z_{el} = \frac{\mathrm{L}}{Ae(n^+z^+u^+ + n^-z^-u^-)} = R_{el} \tag{3.13}$$

where L is the distance between the positive and negative electrode, n^+ and n^- are the number of cations and anions per m^3 respectively, z^+ and z^- are the charge of the cation and anion, respectively, u^+ and u^- are the cation and anion mobility in $m^2 \cdot V^{-1} \cdot s^{-1}$, respectively, e is the charge of an electron in C, and A is the area of the electrodes in m^2.

The resistance of the connections between the frequency response analyzer and the cell is not reproducible and the resistance of the electrolyte is not something of interest in this thesis. Therefore, the impedance of the short circuit is subtracted from the impedance of the cell, and the real impedance of all cells is shifted to the same value at the highest frequency measured. The expression of the corrected impedance, $Z_{corr.}$ is given by:

$$Z_{corr.} = Z_{(-)} + Z_{(+)}. \quad (3.14)$$

The expression for the impedance of the positive and negative electrodes depends on the equivalent circuit model that best represents the electrode system. The contributions of both electrodes to the full cell impedance often overlap and are not distinguishable. The goal being to distinguish which electrode is affected by an additive, the contributions of the negative electrode and of the positive electrode must be unambiguously separated. The solution to this problem is to measure the impedance of both electrodes independently. This can be done using symmetric cells.

3.2 EIS ON SYMMETRIC CELLS

The measurement of the individual impedance of the positive and negative electrodes of a full Li-ion cell can be done in two ways. The first is to introduce a reference electrode in the cell, making a three electrode cell. The reference electrode of choice is usually Li metal. This configuration is difficult to put in place, especially in commercial cells. Moreover, the presence of Li metal, which is more reactive than graphite, can alter the behavior of additives in the cell. The second way to measure the impedance of the two electrodes individually is to use symmetric cells, as introduced by Chen et al.[11] A symmetric cell is a cell composed of two of the same electrodes. A positive symmetric cell is composed of two positive electrodes, *e.g.* two LCO electrodes and a negative symmetric cell is composed of two negative electrodes, *e.g.* two graphite electrodes for example. The impedance of a positive symmetric cell, $Z_{+/+}$, negative symmetric cell, $Z_{-/-}$, and a full cell, $Z_{+/-}$, is then given by:

$$Z_{+/+} = Z_+ + Z_e + Z_+ = 2Z_+ + Z_e \quad (3.15)$$

$$Z_{-/-} = Z_- + Z_e + Z_- = 2Z_- + Z_e \quad (3.16)$$

$$Z_{+/-} = Z_+ + Z_e + Z_- . \quad (3.17)$$

The relation between the sum of the impedance of a positive symmetric cell and a negative symmetric cell and the impedance of a full cell is then:

$$Z_{+/+} + Z_{-/-} = 2Z_+ + 2Z_e + 2Z_- = 2Z_{+/-} . \quad (3.18)$$

Chen et al. demonstrated the validity of Equations 3.15 to 3.18 using symmetric cells reconstructed from a 18650 cell electrodes with a $LiNi_{0.8}Co_{0.2}O_2$ positive electrode and a graphite negative electrode.[11] The 18650 cell format contains large electrodes that can be salvaged and cut in smaller electrodes that can be used to reconstruct symmetric cells. Using commercial machine-made Li-ion cells with long electrodes allows symmetric cells to be reconstructed while inclusion of different additives allows their effects on both electrodes to be assessed.

3.3 STUDY OF ELECTROLYTE ADDITIVES USING EIS ON SYMMETRIC CELLS: EXPERIMENTAL METHOD

The first EIS on symmetric cell experiments were made using commercial machine-made wound prismatic $LiCoO_2$/graphite and $Li[Ni_{0.4}Mn_{0.4}Co_{0.2}]O_2$/graphite cells with 1M $LiPF_6$, EC:EMC (3:7 by weight) manufactured by Medtronic. The cells studied contained 1.5 g of electrolyte per gram of negative active material.

Figure 3.8 shows the history of the cells used in this study. The cells were first subjected to an automated storage test[6]. This test consists of two discharge-charge cycles between the lower and upper voltage cut-offs, followed by an open circuit storage step of 500 h at the top of charge. The two discharge-charge cycles and the open circuit voltage steps were then repeated one more time. The lower and upper voltage cut-offs of the NMC cells were 3.3 V and 4.225 V, respectively. Two groups of $LiCoO_2$/graphite cells were used. The lower and upper voltage cut-offs of the first group, called LV-LCO cells, were 3.4 V and 4.075 V, respectively. The lower and upper voltage cut-offs of the second group, called HV-LCO cells, were 3.4 V and 4.175 V, respectively. All cells contained the same graphite negative electrode and the negative-to-positive active material ratio was balanced according to their voltage cut-offs.

After the automated storage test, the cells were then put away for approximately one year at an open circuit voltage around 3.9 V at room temperature (19°C – 22°C). The cells

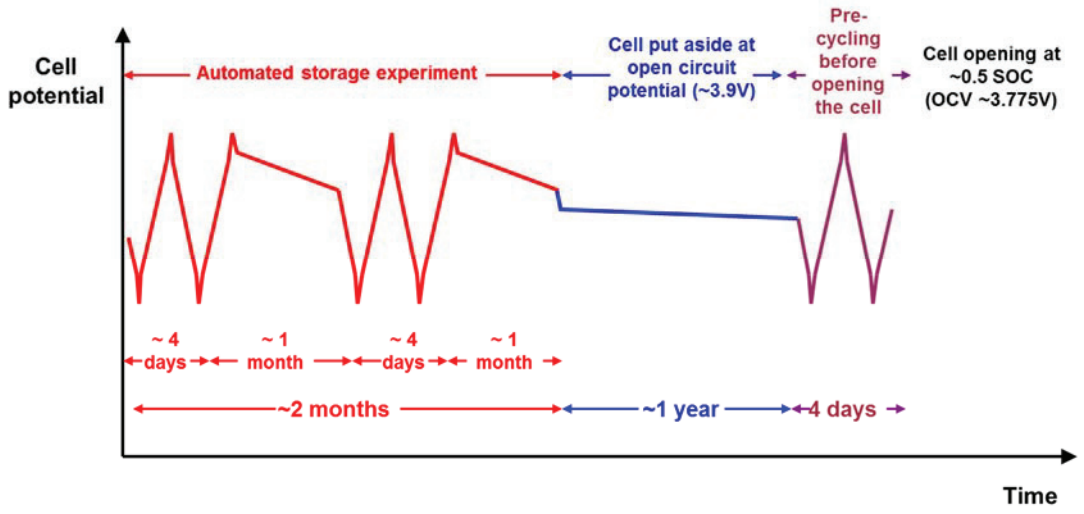

Figure 3.8 History of the Medtronic cells before opening.

were then cycled for a short period (one full cycle) and stopped at an open circuit voltage of 3.775 V, corresponding to approximately 50% state of charge. The electrochemical impedance spectra of the cells were then taken at 10°C, 20°C, 30°C, and 40°C. The cells were then carefully opened in an argon-filled glove box.

Figure 3.9 shows a Medtronic cell along with the device used to open the wound cells. The prismatic wound cells have metal cases so the cell opener consists of a saw blade mounted on a guide (Figure 3.9b) and a cell holder (Figure 3.9c.). Using the cell holder and guide, one can cut off the top of the cell can without shorting the cell or damaging the electrodes. From the long doubled-sided electrodes, 9 coin-cell size (1.54 cm^2) positive electrodes and 9 coin-cell size negative electrodes were cut with a precision punch. The double sided electrodes were directly used; one side was not cleaned off the

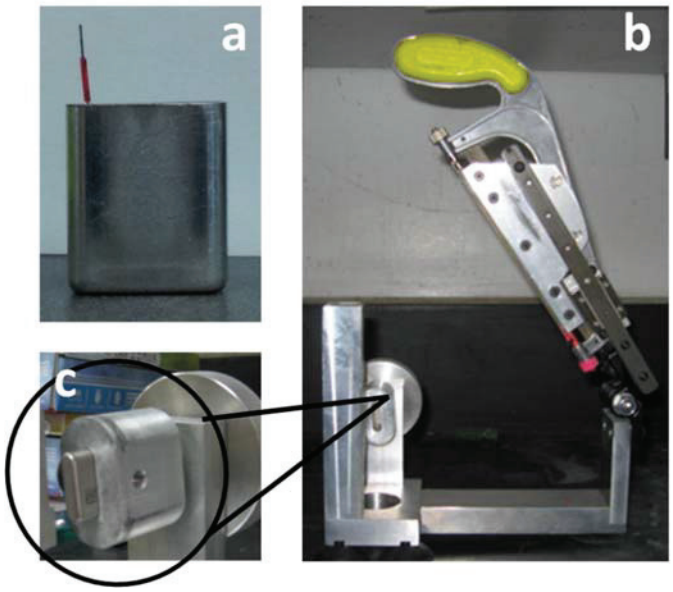

Figure 3.9 Pictures of a Medtronic Li-ion cell (a), the cell opener (b), and a magnification of the cell holder of the cell opener (c).

current collector. From the punched (double sided) electrodes, 3 full coin cells, 3 negative symmetric coin cells and 3 positive symmetric coin cells were reassembled using one polypropylene blown microfiber separator (BMF – available from 3M Co. 0.275 mm thickness, 3.2 mg/cm^2)[86] and the same electrolyte formulation as the parent prismatic wound cells.

As will be shown in the next chapter, the use of double sided electrodes in the coin cells did not affect the cycling or the EIS measurements of the coin cells. Aluminum sputtered cans and aluminum spacers were used for the positive electrode symmetric cell assembly in order to minimize any effect of hardware corrosion.[87]

The EIS spectra of the reassembled coin cells were then recorded at 10°C and 30°C in that order. All EIS spectra were taken using a BioLogic VMP3 equipped with two EIS boards. Many EIS spectra were collected over the course of these experiments and in order to automate the process somewhat, the output of one VMP3 EIS board was connected to a Keithley 705 scanner and the output of the other to a Keithley 706 scanner. Each scanner housed two Keithley 7053 10-channel high current scanner cards. In-house software was designed and written so that each scanner could connect up to 16 cells sequentially to have their EIS spectra measured automatically overnight. All impedance spectra were collected at constant temperature by housing the cells in temperature-controlled boxes at 10.0 and 30.0 ± 0.2°C. Figure 3.10 presents a flowchart of the experimental steps involved in the study of additives by EIS on symmetric cells.

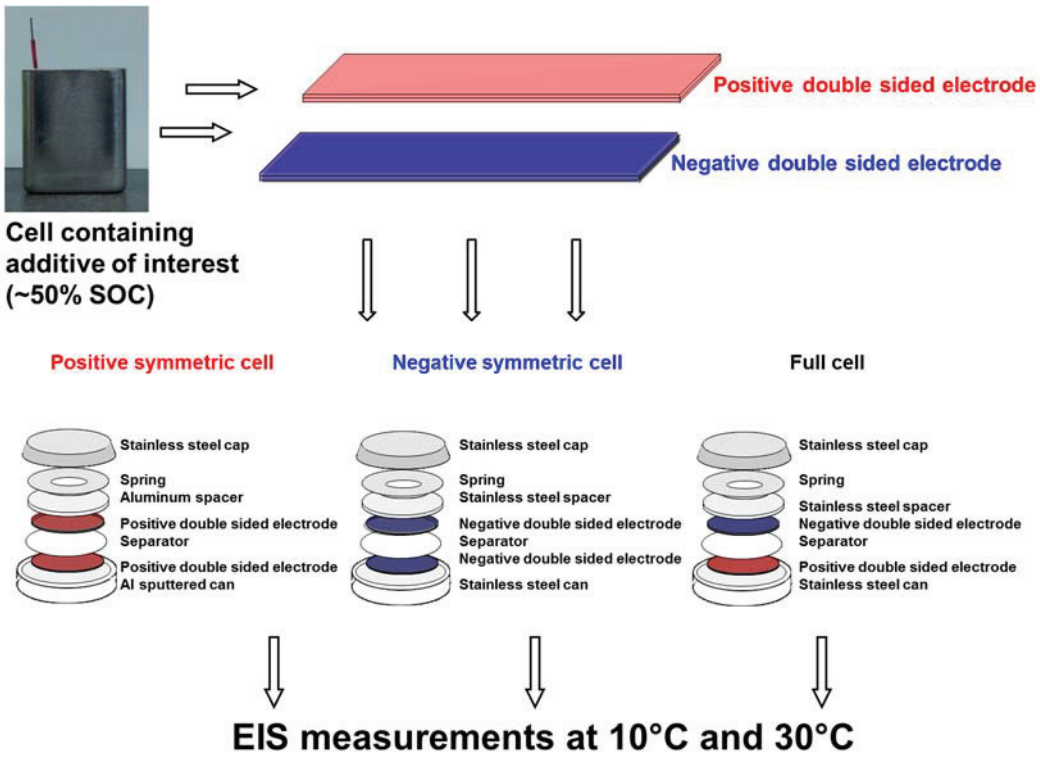

Figure 3.10 Flowchart of the experimental steps for the study of additives using EIS on symmetrical cells.

The second set of experiments was carried out using dry machine-made pouch cells with a nominal capacity of about 225 mAh. The advantage of these cells is that as opposed to the commercial Medtronic cells used in the first experiments, the dry pouch cells allow total control of the composition of the electrolyte studied. The Medtronic cells were supplied by the company and contained additives and additive amounts that were of interest to them. For that reason some combinations and concentration ranges could not be obtained. The dry pouch cells are highly repeatable cells since they are machine-made. The only added step that these cells require is the filling of the cell with the electrolyte.

Machine-made 225 mAh $LiCoO_2$/graphite wound pouch cells were obtained dry from Pred Materials (60 East 42nd Street, Suite 1456 New York, NY 10165). The pouch cells from Pred Materials were filled with 0.75 g of 1 M $LiPF_6$ in ethylene carbonate (EC): ethyl methyl carbonate (EMC) (BASF) in a ratio of 3:7 by weight as control electrolyte and electrolytes containing different additives. After electrolyte filling, cells were vacuum sealed with a compact vacuum sealer (MTI Corp.). All electrolyte filling and vacuum sealing was done in an argon-filled glove box. Centrifugal wetting was used for electrode wetting with an acceleration of 50 *g* for 20 minutes. The cells were then placed in a temperature box at 40°C where they were held at 1.5 V for 24 hours, to allow for the completion of wetting before charging at 2 mA for 10 hours and then at 15 mA to 4.2 V. Cells were then discharged at 15 mA to 3.775 V where they were removed from the charger, transferred into the glove box, cut open to release gas generated during formation and then vacuum sealed again. The formation charge and discharge steps were conducted on a Maccor Series 4000. After degassing, the cells were cycled, and were then taken apart following the steps described previously.

Table 3.1 shows the source and purity (when available) of the chemicals used in the formulation of the electrolytes.

Table 3.1 Source of purity of chemicals used for the formulation of the electrolytes

Chemical	Company	Purity /%
EC	BASF	99.95
EMC	BASF	98
LiPF6	BASF	99.8
VC	BASF	99.5
FEC	BASF	99.5
LiTFSI	3M	NA
TMOBX	BASF	NA
VEC	BASF	NA

CHAPTER 4. ON THE EXPERIMENTAL METHOD

4.1 PROOF OF CONCEPT

Figure 4.1 shows the Bode representation of the reassembled full cell area specific impedance, (+/-), along with the negative symmetric cell area specific impedance divided by two, (-/-)/2, the positive symmetric cell area specific impedance divided by two, (+/+)/2, and half of the sum of the positive and negative symmetric cell area specific

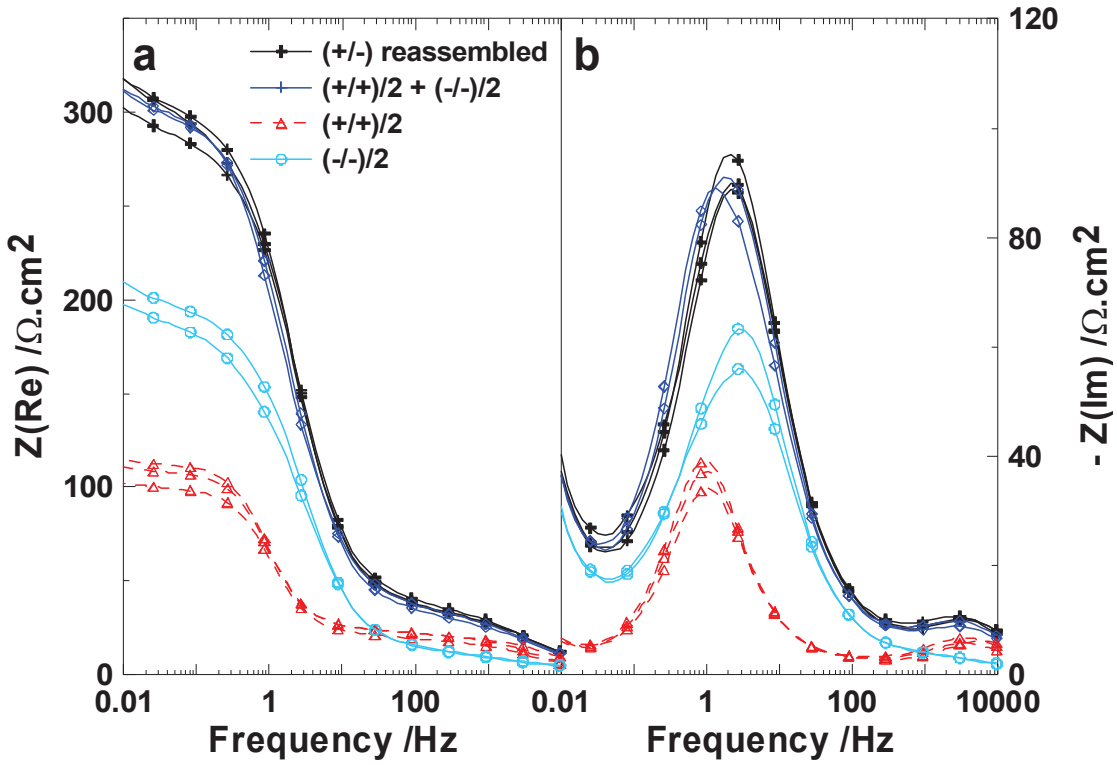

Figure 4.1 Area-specific real impedance (a) and area-specific negative imaginary impedance as a function of the logarithm of the frequency (b) for the reassembled full coin cells, (+/-), half of the positive symmetric coin cells impedance, (+/+)/2, half of the negative symmetric coin cells impedance, (-/-)/2, and the sum of half of the positive and half of the negative symmetric cell impedance. All cells had electrolyte containing 2 wt.% VC + 0.3 wt.% TMOBX with all measurements made at 10°C.

impedances, (-/-)/2 + (+/+)/2. The area specific impedance was calculated as the impedance of the cell multiplied by the geometrical area of the electrode. This allowed the impedance of the untouched cells which have a geometric area of about 73 cm^2 to be compared with the impedance of the full reassembled cells which have an area of about 1.54 cm^2. As shown by Chen et al.,[11] since the full cell configuration was LCO/LCO/BMF/Graphite/Graphite and the symmetric cell configurations were LCO/LCO/BMF/LCO/LCO and graphite/graphite/BMF/graphite/graphite, half the sum of the positive and negative symmetric cell impedances should be equal to the full cell impedance. Figure 4.1 shows the excellent agreement between the impedances of the symmetric cell sum and the reassembled full cell.

Figure 4.2 shows the time dependence of the impedance measurements at 30°C for the full reassembled cells, the negative symmetric cells and the positive symmetric cells containing control electrolyte. Figure 4.2 shows that the impedance of the full cell changed slightly with time, that the impedance of the negative symmetric cell was very stable and that the impedance of the positive symmetric cell changed very rapidly with time. This is a general trend for most electrolytes with or without additives. This indicates that the kinetics of the parasitic reactions at the positive electrode were faster in the positive electrode symmetric cell than in the full cell. This suggests that the positive electrode reacted with electrolyte, creating species that were scavenged at the negative electrode. Without a low potential electrode in the cell, these species accumulated and the impedance of the positive symmetric cell continued to increase with time. The concept of interactions between the positive and negative electrodes has been suggested by several researchers as introduced in section 2.3.2. Considering the previous evidence

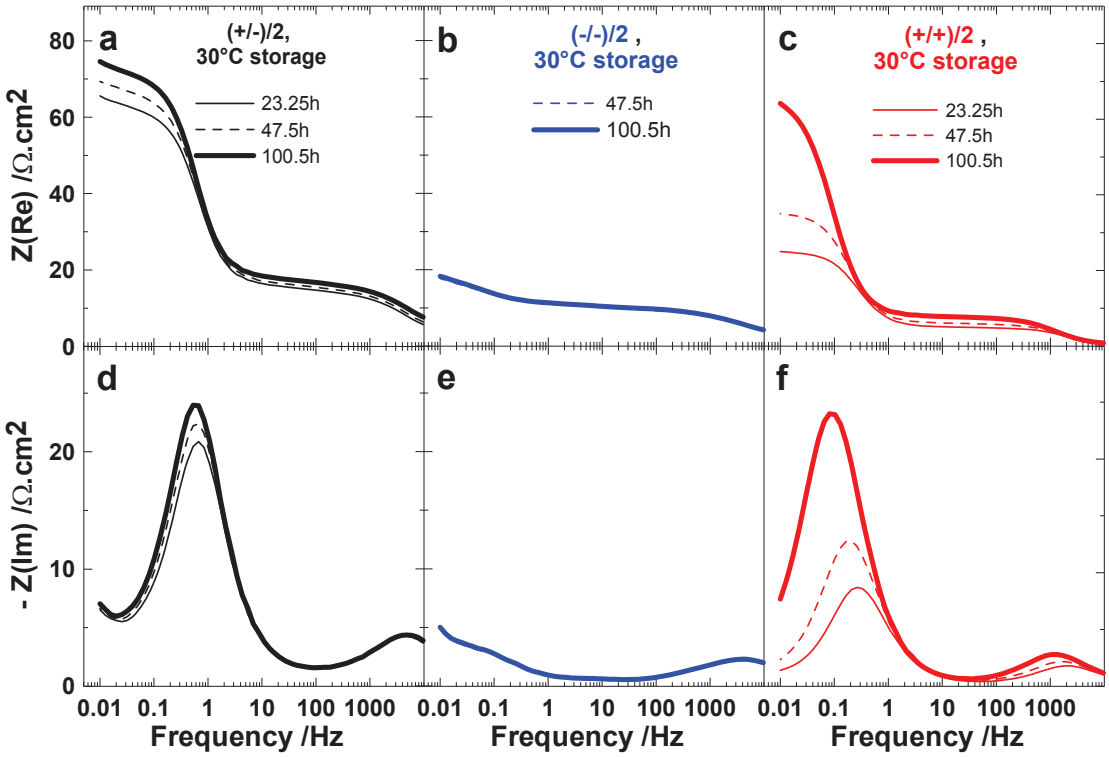

Figure 4.2 Area-specific real impedance (a-c) and area-specific negative imaginary impedance as a function of the logarithm of the frequency (d-f) for the reassembled full cell (a, d), half of the negative symmetric cell impedance (b, e), and half of the positive symmetric cell impedance (c, f). The electrolyte in the cells contained no additives and the measurements were made at 10°C as a function of time, as indicated.

of electrode-electrode interactions (see section 2.3.2) it is not inconceivable that the absence of one electrode, the negative electrode in the case of the positive symmetric cell presented in Figure 4.2, can induce a different behavior in the stability of the other.

It is impossible to measure the impedances of all the positive electrode symmetric cells immediately after assembly because the impedance of each cell is measured at several temperatures and multiple cells are measured sequentially. Therefore it was sometimes necessary to estimate the impedance of the positive/positive symmetric cell from the

difference between the impedances of the full reassembled cell and the negative/negative symmetric cell. The excellent match between the sum and the full cell impedances in Figure 4.1 was caused by the slower rate of change of the positive symmetric cell impedance as a function of time when TMOBX and VC are added to the electrolyte.

4.2 COMMENTS ON THE EXPERIMENTAL METHOD

4.2.1 CHOICE OF STATE OF CHARGE

Figure 4.3 shows the Bode representation of the area specific impedance of a Medtronic LCO/graphite cell containing 2% VC and 2% LiTFSI at different cell potentials. This figure shows that the impedance changes significantly with cell potential. Opening the cells at the same state of charge is then mandatory in order to compare their impedance and to make sure that the changes seen in the impedance are due to surface alteration by the additive and not due to potential differences. The potential of 3.775 V corresponds to a state of charge slightly lower than 50%. This allows symmetric cells that can be cycled to be constructed. Reconstructing symmetric cells from two electrodes salvaged from the same parent cell that is not close to 50% of state of charge would cause Li plating in negative symmetric cells and bring the positive electrodes to too high of a potential in the positive symmetric cells during cycling.

4.2.2 DOUBLE SIDED ELECTRODES

In order to keep the electrodes from the disassembled wound cells as pristine as possible, the double-sided electrodes were used directly in the coin cells. In order to demonstrate that the side of the electrode shielded from the separator by the foil current collector is

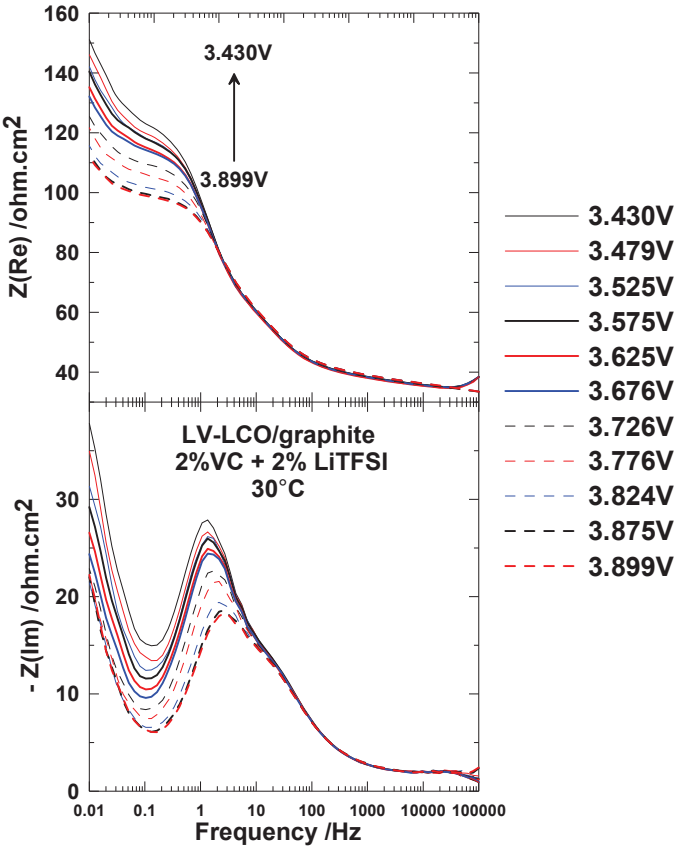

Figure 4.3 Bode representation of the area specific impedance of a LV-LCO/graphite Medtronic cell with 2% VC and 2% LiTFSI at 30°C at different cell potential.

basically electrochemically inactive, single-sided and double-sided graphite half cells were assembled and cycled at 30°C at various current densities.

A commercial graphite double-sided electrode was used for the half cell assembly. From this double-sided electrode, one side was carefully cleaned with a scalpel for the assembly of the single-sided graphite half cells. Figure 4.4 shows the capacity versus current for double-sided and single-sided electrodes. A single-sided electrode has an areal capacity of about 4 mAh/cm^2, leading to a cell capacity of 6 mAh for the 1.54 cm^2 electrodes used here. The C-rates examined in Figure 4.4 ranged from C/15 to C/120.

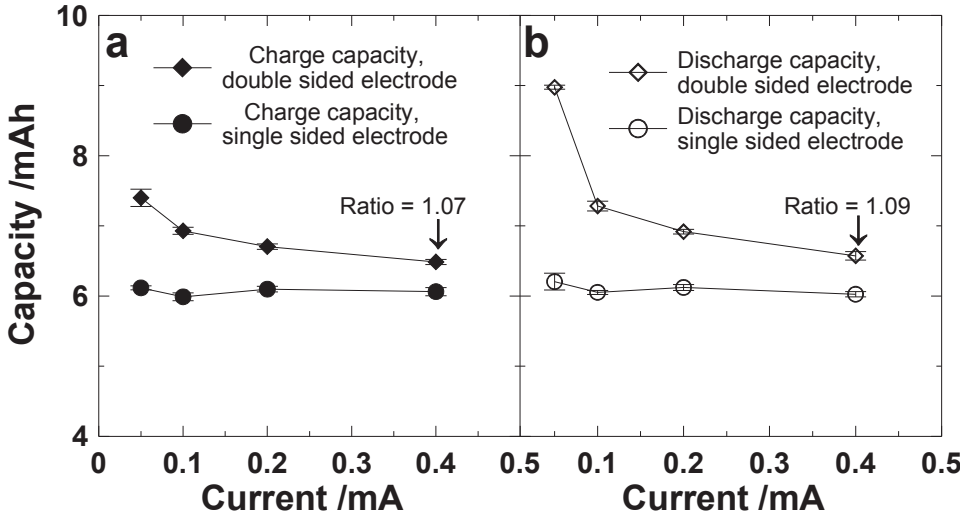

Figure 4.4 Charge capacity (a) and discharge capacity (b) of double-sided and single-sided graphite half cells (Li/graphite).

The single-sided electrodes showed no capacity variation over this range of rates. By contrast, the double-sided electrodes showed an initially larger capacity (by 8%) and an increase in capacity for rates below C/30. This suggests that at very low rates there is some access to the electrode material behind the current collector and that this access increases as the rates decrease.

The lowest frequencies probed with EIS in these experiments were 0.001 Hz which corresponds to a period of 1000 sec or an effective rate of 3C. Additionally, the largest AC current that flowed during the 10 mV excitation was 0.4 mA which is less than C/10. Based on Figure 4.4, significant access of Li to the back side of the double-sided electrode (behind the current collector) under the conditions used in the EIS experiments is not expected. In fact, EIS experiments done on single and double-sided and single sided electrode positive symmetric cells showed no difference in their impedance except

for an increase in a feature at high frequency. This high frequency feature corresponds to the interface between the active material and the current collectors as will be discussed in section 4.3. Using double-sided electrodes greatly simplifies the experimental procedure and allows undamaged (by scraping) electrodes to be studied.

4.2.3 ELECTRODE DAMAGE

Figure 4.5 shows the Bode representation of the area-specific impedance of the wound cells (before opening - called the untouched cells) along with the reassembled full coin cells containing no additive (control electrolyte), 1% VC, 2% VC, 0.3% TMOBX and 2% VC + 0.3% TMOBX. Figure 4.5 shows that the spectra of the untouched cells are nearly identical to the spectra of the reassembled full cells. The minor differences could come from the difference in the electrode configuration. In the wound prismatic cells, an inductive component can be present which is not in the reassembled coin cells. The reassembled cells also have a more pronounced high frequency feature (too small to see on the scales selected in Figure 4.5). As it will be shown in section 4.3, this high frequency feature can be attributed to the interface between the current collector and the active particles.[85]

The growth of this feature in the re-assembled cells is caused by two different phenomena. The first is the difference in the number of current-collector/active particle interfaces at the positive electrode. In the wound cell, one of these interfaces is present (one between the aluminum foil and the LCO particles). On the other hand, since both sides of the double-sided electrode are kept in the reassembled coin cells, the number of interfaces is three. There are two aluminum/active particle interfaces between the

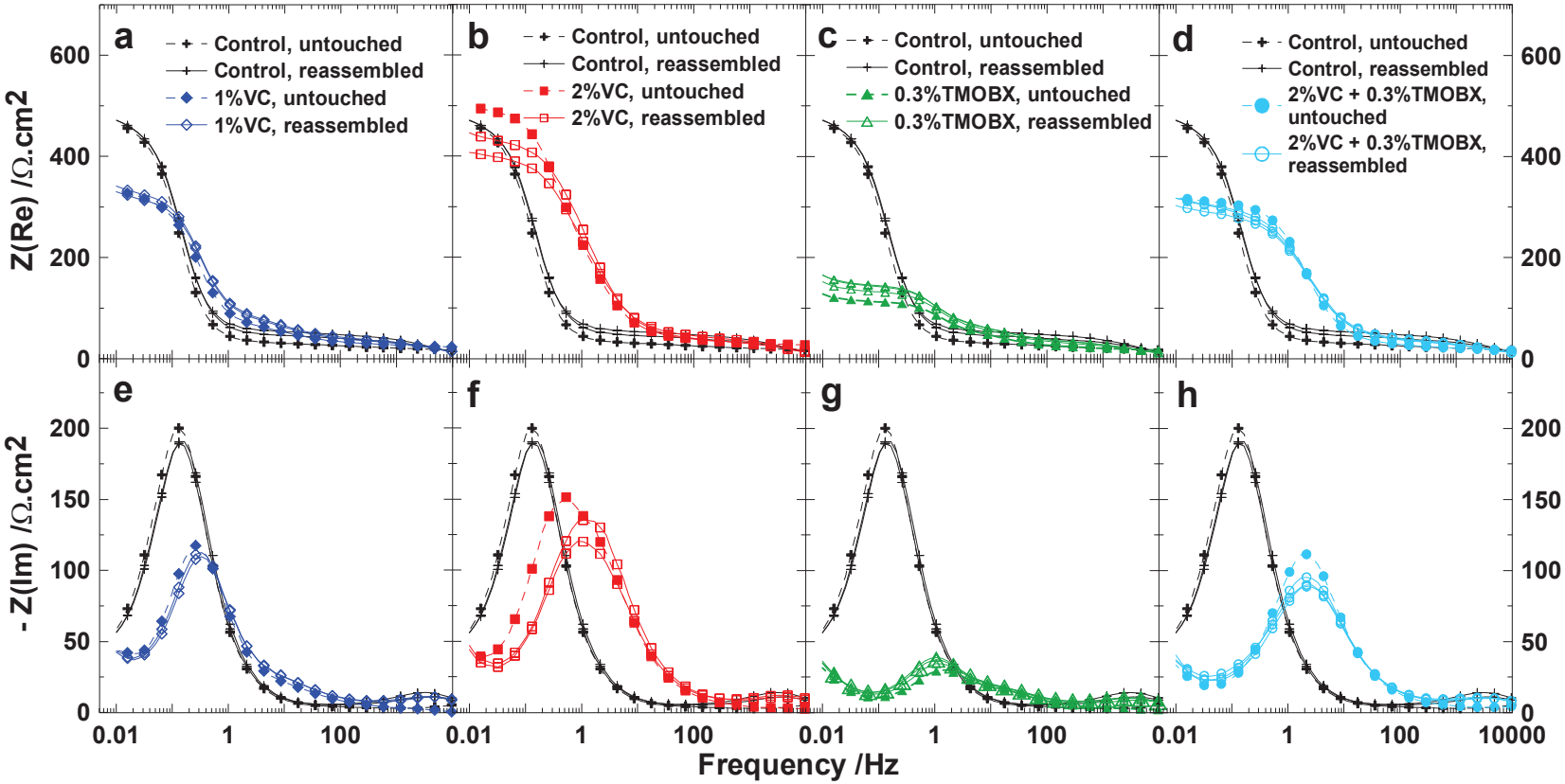

Figure 4.5 Bode representation of the area specific impedance for $LiCoO_2$/graphite wound and re-assembled coin cells with: 1 wt.% VC additive (a, e); 2 wt.% VC additive (b, f); 0.3 wt.% TMOBX additive (c, g); and 2 wt.% VC + 0.3 wt.% TMOBX additives (d, h) at 10°C. The results for cells with control electrolyte are shown in each panel for comparison.

aluminum foil and the LCO particles and one between the LCO particles and the coin cell can. The second phenomenon responsible for the growth of the semi-circle can be the handling of the electrode. Since the electrodes are unfolded (by unwinding the electrodes) and punched, some loss of contact between the current collector and the active particles might occur. This loss of contact would increase the electronic resistivity of the interface.

4.2.4 CELL TO CELL REPRODUCIBILITY

Figure 4.6 shows the Bode representation of the area-specific impedance of duplicate HV-LCO Medtronic cells containing 0.3% TMOBX, the impedance of the reassembled full coin cells impedance, the calculated positive symmetric cell impedance divided by two and the negative symmetric cell impedance divided by two, all measured at 10°C. Figure 4.6a shows that the reproducibility from one wound cell to another is very good.

Figure 4.6b, 4.6c and 4.6d show a perfect match between the impedance of the re-assembled full cell, calculated positive and negative symmetric cell from one duplicate to the other. This demonstrates the excellent reproducibility of the experimental procedure. Interpretation of the impedance spectra of the positive and negative electrodes

In order to interpret the changes in the impedance of the negative electrode and positive electrode an electrolyte additive induces, it is necessary to be able to distinguish the contributions to the impedance and determine how the change in the surface of the electrode affects the impedance spectrum. Since there is no agreement in the literature on the interpretation of the impedance spectra, simple experiments have been performed.

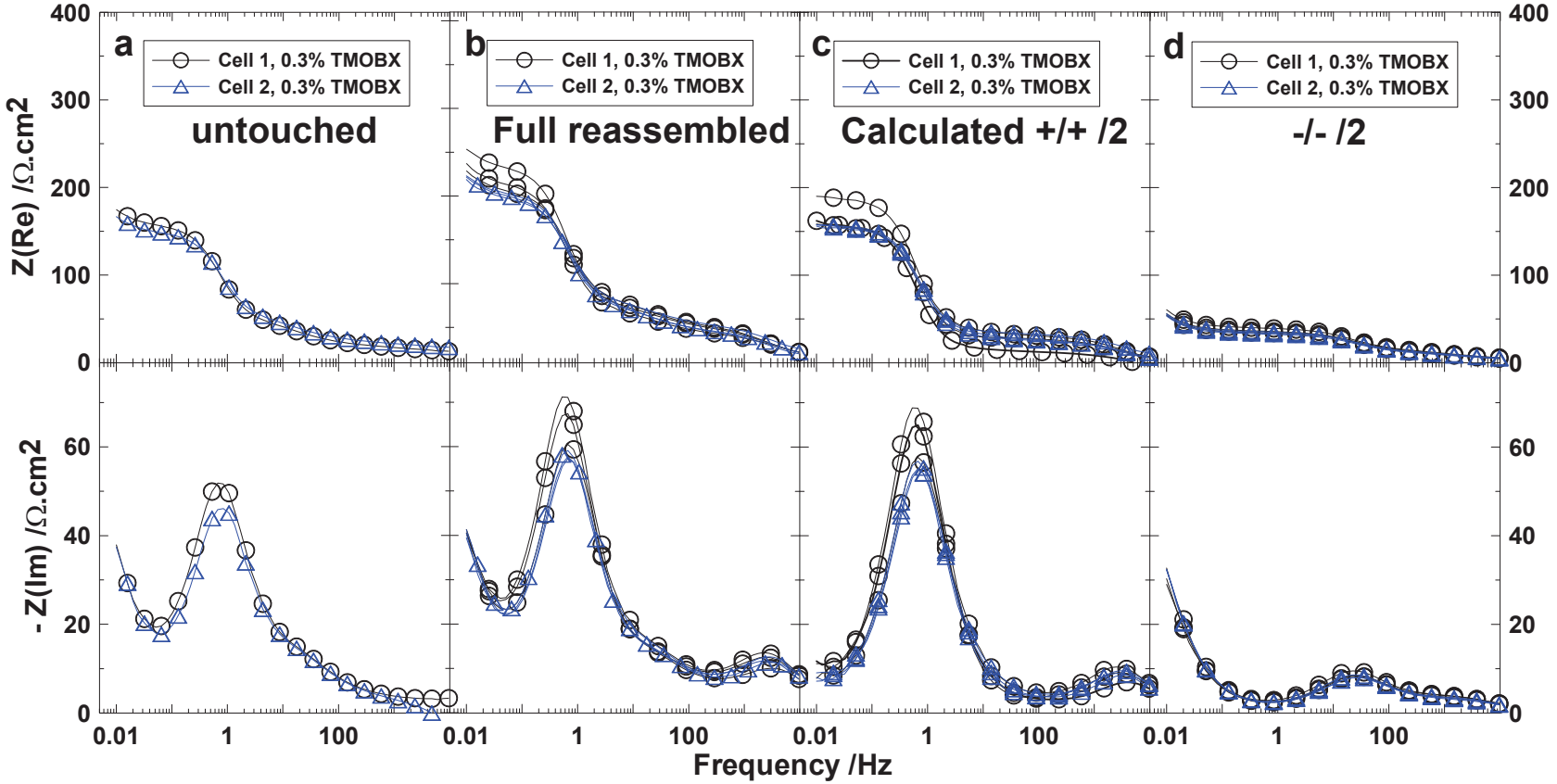

Figure 4.6 Bode representation of the area-specific impedance of duplicate untouched HV-LCO wound cells containing 0.3% TMOBX (a), the impedance of the reassembled full coin cells (b), calculated positive symmetric cell impedance divided by two (c) and measured negative symmetric cell impedance divided by two (d). This figure demonstrates the excellent reproducibility of the method.

Figure 4.7 shows the Bode representation of the area specific impedance of an untouched HV-LCO/graphite Medtronic cell after long-term cycling (a) measured at 10°C, 20°C, 30°C, and 40°C and a zoom-in on the high frequency feature (b). The impedance of the untouched cell shows four different features. There is a feature at high frequency (100 - 10,000 Hz) that does not present a high temperature dependence, two overlapping

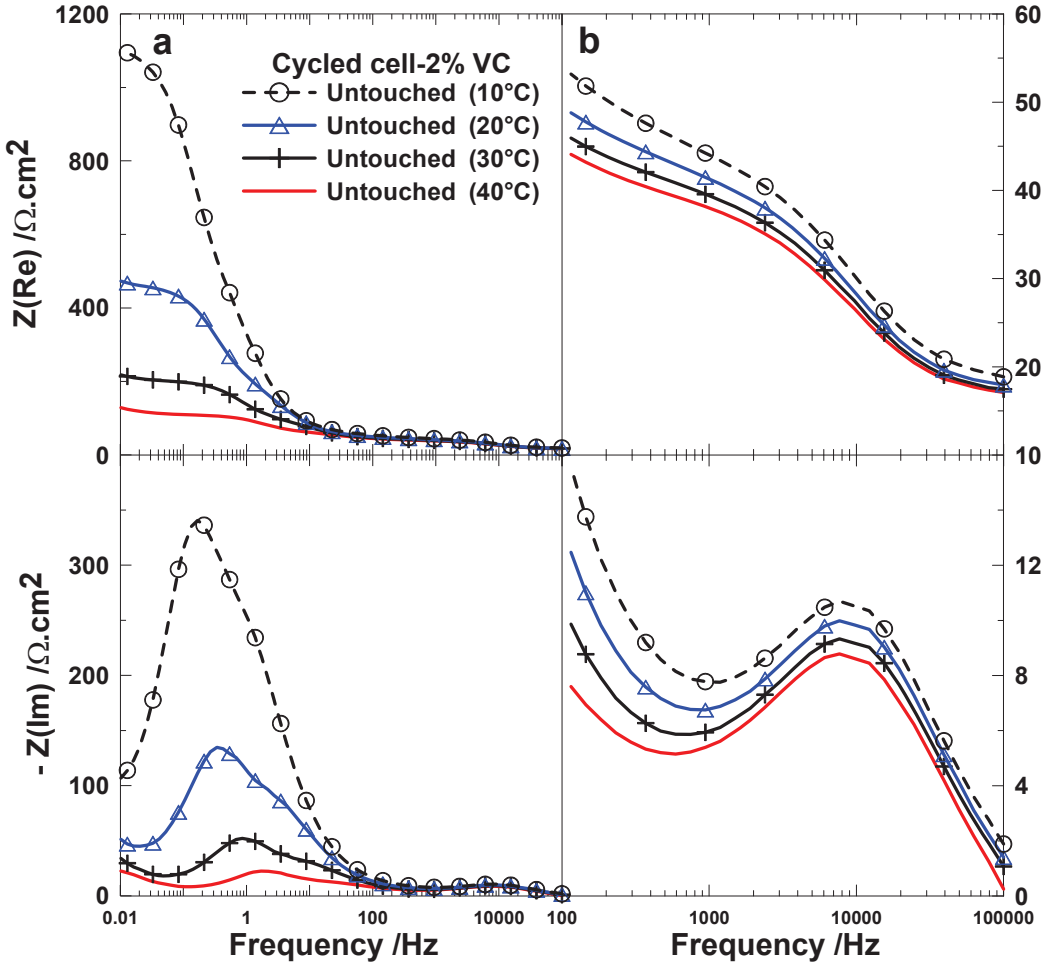

Figure 4.7 Bode representation of the area specific impedance of an untouched HV-LCO/graphite Medtronic cell containing 2% VC after long-term cycling measured at 10°C, 20°C, 30°C, and 40°C (a) and a zoom-in on the high frequency feature (b).

features at medium frequency (100 - 0.1 Hz) that are highly dependent on the temperature, and a low frequency feature (0.1 - 0.01 Hz) that presents a slight dependence on temperature. As introduced in Chapter 3, the full cell impedance is the sum of the contribution from both the positive and negative electrode. The overlapping nature of the features that can be seen in Figure 4.7 does not allow one to assess which electrode the features come from.

Figure 4.8 shows the Bode representation of the area specific impedance measured at 10°C of the full cells, negative symmetric cells divided by two, and calculated positive symmetric cells divided by two (a) reassembled from the untouched HV-LCO/graphite Medtronic cell shown in Figure 4.7, and a zoom-in on the high frequency feature (b). Figure 4.8a shows that the low frequency feature predominantly comes from the negative electrode. The sloping nature of this feature is the signature of the solid state diffusion phenomenon of Li in the particle as introduced in Chapter 3. Figure 4.8a also shows that the two overlapping features in the medium frequency range are a combination of the positive electrode impedance and negative electrode impedance. Figure 4.8b shows that the high frequency feature comes from both the positive and negative electrodes.

Figure 4.9 shows the negative imaginary area specific impedance at 10°C and 40°C of selected full cell, negative symmetric cell divided by two, and calculated positive symmetric cell divided by two, reassembled from the untouched HV-LCO/graphite Medtronic cell shown in Figure 4.7 and Figure 4.8. This figure shows that the high frequency feature of the negative symmetric cell and positive symmetric cell is slightly temperature dependent.

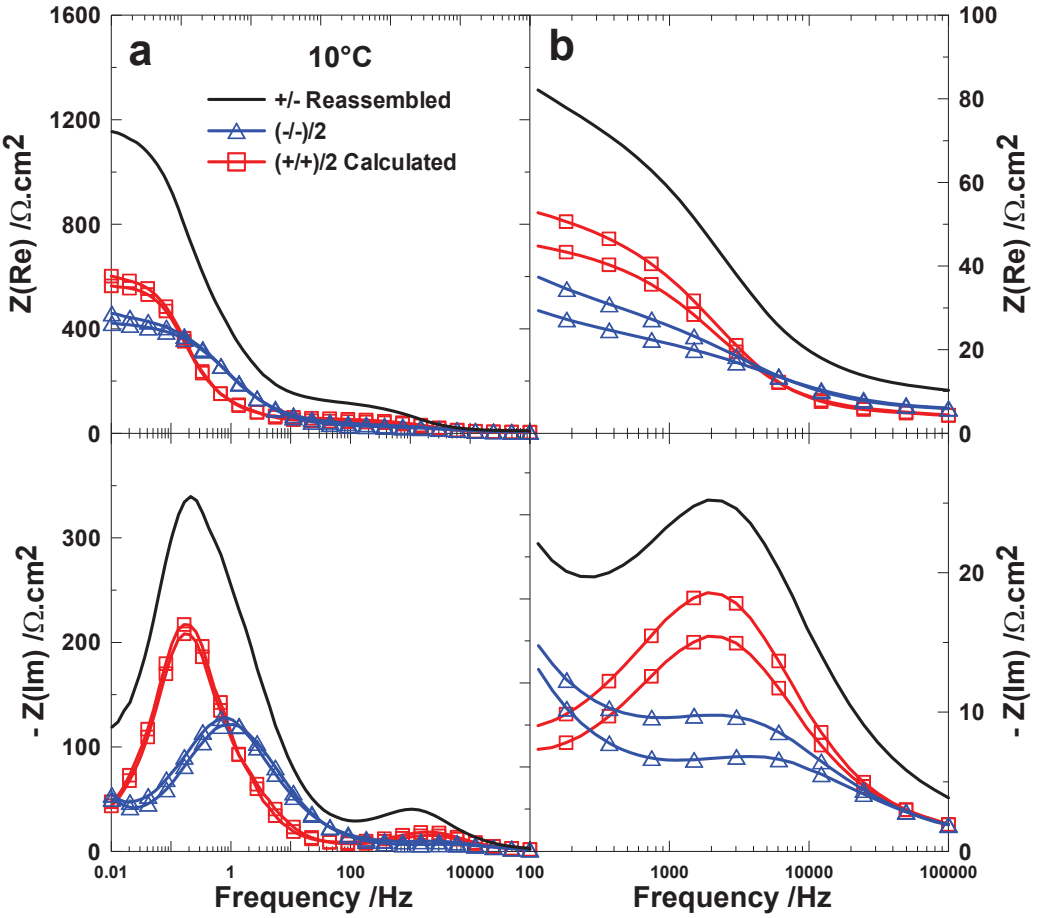

Figure 4.8 Bode representation of the area specific impedance at 10°C of the reassembled full cells, negative symmetric cells divided by two, and calculated positive symmetric cells divided by two (a) from the untouched HV-LCO/graphite Medtronic containing 2% VC cell shown in Figure 4.7 (a) and a zoom-in on the high frequency feature (b).

Simple experiments have been performed on symmetric cells much like the experiments presented by Ogihara et al.,[88] in order to determine the origin of the features of the impedance spectra of both negative and positive electrodes and will be discussed in the next sections.

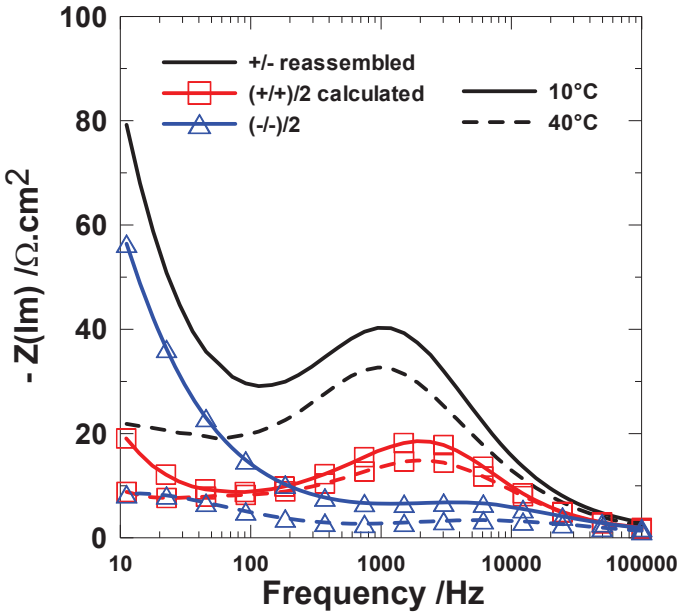

Figure 4.9 Negative imaginary area specific impedance of selected reassembled full cell, negative symmetric cell divided by two, and calculated positive symmetric cell divided by two from the untouched HV-LCO/graphite Medtronic cell shown in Figure 4.7 and Figure 4.8 at 10°C and 40°C.

4.3 ORIGIN OF THE FEATURES IN IMPEDANCE SPECTRA OF LI-ION ELECTRODES

4.3.1 ORIGIN OF THE HIGH FREQUENCY FEATURE

In order to determine whether the high frequency feature comes from a Faradaic process or not, dry machine-made LCO/graphite pouch cells were filled with an electrolyte containing 4 wt.% VC. The electrodes of these cells present almost similar features in the impedance spectrum to the Medtronic LCO/graphite wound cells. The positive electrode of a dry pouch cell presents an extra 45° slope feature in the negative imaginary part of

the impedance as a function of the logarithm of the frequency in the medium frequency range and will be discussed later. The pouch cell containing 4 wt.% VC was cycled for several weeks and taken apart for full cells and symmetric cells to be reconstructed, following the procedure described in Chapter 3. The impedance of the positive symmetric cells and negative symmetric cells was measured at 30°C. The positive symmetric cells and negative symmetric cells were then opened in an argon-filled glove box. From the positive electrodes and negative electrodes of the positive and negative symmetric cells, single electrode cells were reconstructed. The impedance of these single electrode cells was measured at 30°C. Figure 4.10 presents a scheme of the procedure used to determine the origin of the high frequency feature. The single electrode cells were not assembled

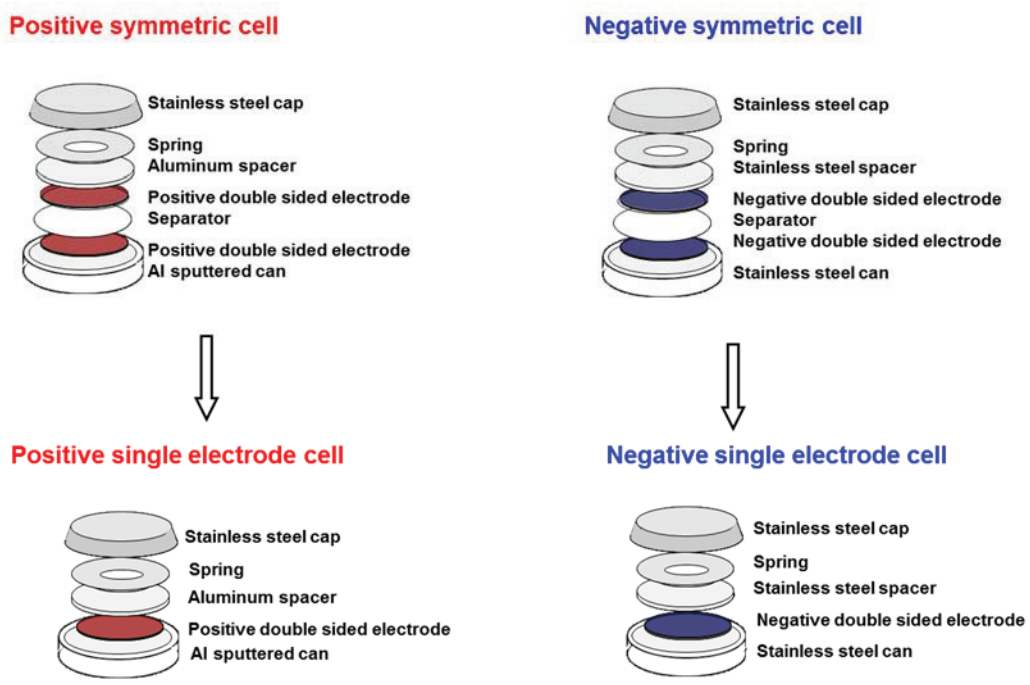

Figure 4.10 Procedure followed to determine the origin of the high frequency feature in the impedance spectrum of the positive electrode and negative electrode.

using any separator. This provides a direct conduction path for the electron from one side of the cell to the other.

Figure 4.11 shows the Bode representation of the area specific impedance of a positive symmetric cell divided by two and a single positive electrode cell (a), of a negative symmetric cell divided by two and of a single negative electrode cell (b). Figure 4.11a shows a good match between the high frequency feature of the positive electrode and the high frequency feature of the impedance of a single positive electrode cell. The small

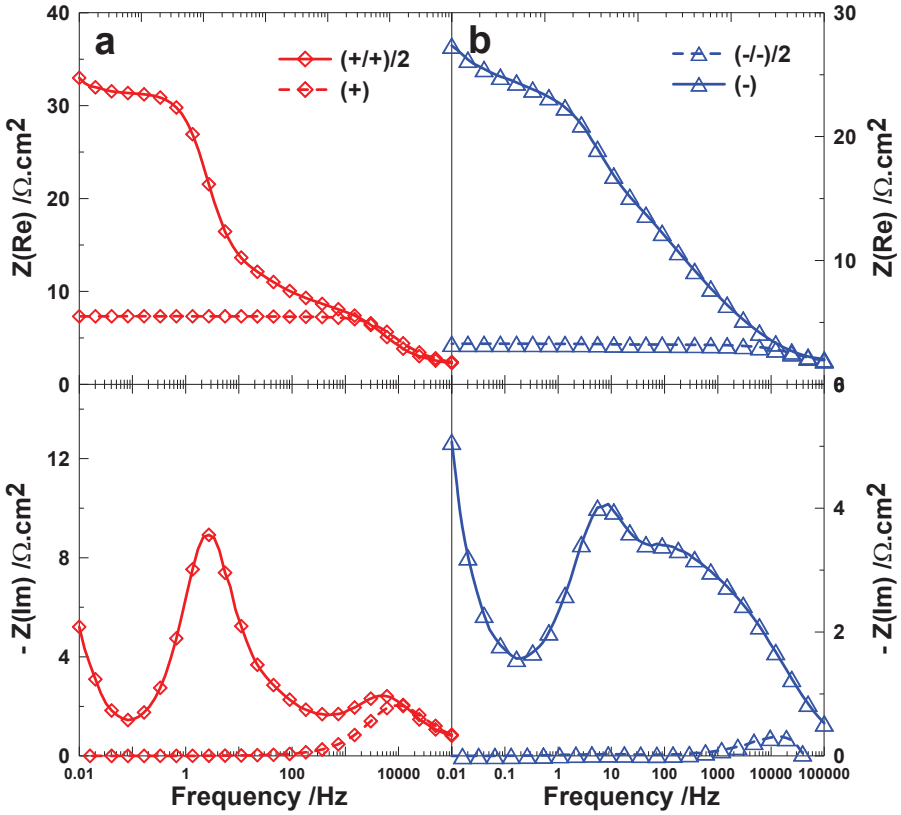

Figure 4.11 Bode representation of the area specific impedance of a positive symmetric cell divided by 2 and a single positive electrode cell (a), and a negative symmetric cell divided by 2 and of a single negative electrode cell.

differences between the two could arise from a slight difference between the high frequency features of the two electrodes in the positive symmetric cells. Also if the electrode is not subjected to the same pressure, the contact resistance could change (more compression would give a better contact between the electrode material and the current collector). On the contrary, Figure 4.11b shows that the high frequency feature of the impedance spectrum of the negative symmetric cells does not match the high frequency feature of the impedance of the single negative electrode cell. This indicates that while the high frequency feature of the impedance spectrum of the positive electrode is due to electronic transport from the current collector to the active particle as proposed by Gaberscek et al.,[85] the high frequency feature of the impedance spectrum of the negative electrode is a combination of the electronic transport and another feature.

In order to make sure that the 45° slope in the positive electrode impedance and that the high frequency feature of the negative electrode does not come from Faradaic processes and from the surface of the particle (*i.e.* Li intercalating in the material through the SEI), symmetric cells were constructed from fresh and uncycled electrodes (*i.e.* in the discharged state and without surface films).

At a state of charge close to 0%, the potential of both the positive electrode and negative electrode varies very sharply for a small amount of Li intercalated (dV/dQ is very large). In this case, with an excitation of +/- 5 mV there is virtually no Li being intercalated or de-intercalated from the active material and the active particle shows a capacitive like feature in the impedance spectrum.[88] The features in the impedance spectrum of symmetric cells constructed with completely discharged electrodes are then due to non-

Faradaic processes. The spectrum then shows a capacitive feature at medium frequency as shown in Chapter 3.

Figure 4.12 shows the Bode representation of the area specific impedance of a positive symmetric cell divided by two, reconstructed from a pouch cell containing 4 wt.% VC and of a positive symmetric cell constructed from fresh electrodes at 0% state of charge (a), and a negative symmetric cell divided by two reconstructed from a pouch cell containing 4 wt.% VC and of a negative symmetric cell constructed from fresh electrodes

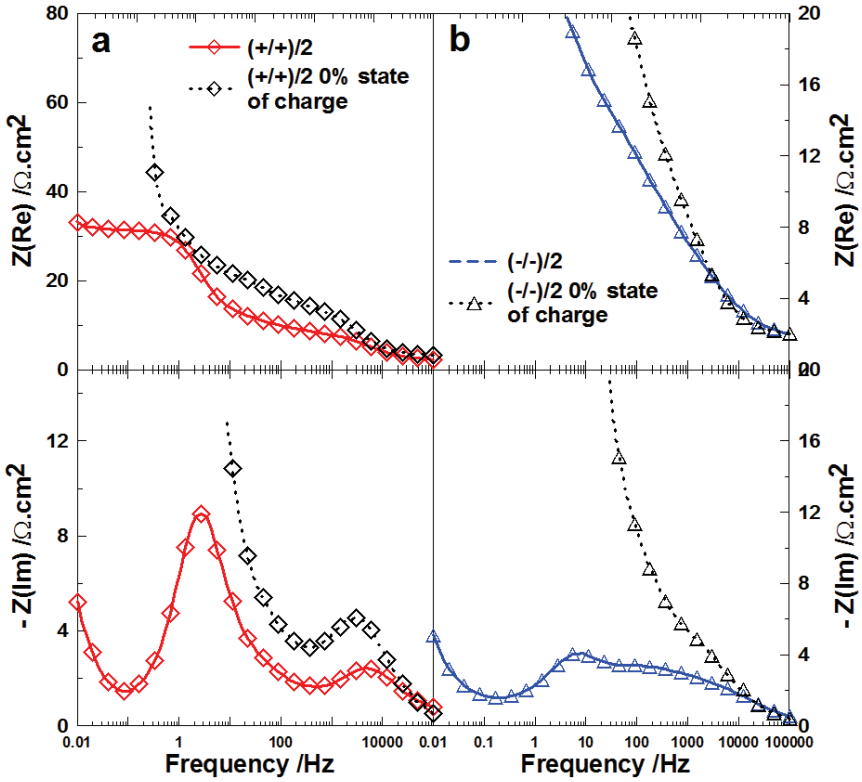

Figure 4.12 Bode representation of the area specific impedance of a positive symmetric cell divided by 2 reconstructed from a pouch cell containing 4 wt.% VC and of a positive symmetric cell constructed from a fresh electrode at 0% state of charge (a), and a negative symmetric cell divided by 2 reconstructed from a pouch cell containing 4 wt.% VC and of a negative symmetric cell constructed from fresh electrode at 0% state of charge (b).

at 0% state of charge (b). Figure 4.12a shows that the impedance spectrum of the positive symmetric cell constructed from fresh electrodes presents the same features as the symmetric cell made from fresh electrodes in the medium-high and high frequency range. This reinforces the hypothesis that the medium frequency feature in the spectrum of the positive electrodes comes from the diffusion of Li^+ in the pores of the electrode as proposed by Ogihara et al.[88]

Figure 4.12b shows that the impedance spectrum of the negative symmetric cell constructed from fresh electrodes presents the same feature as the symmetric cell constructed from fresh electrodes in the high frequency range. This high frequency feature could come from the diffusion of the Li^+ in the pores of the negative electrode, overlapping with the small contribution from the current collector/active particle resistance. The frequency at which the contribution of the diffusion of Li^+ in the pores of the negative electrode appears is not the same as for the positive electrode. This difference in frequency might come from a difference in pore size and shape. As shown by Ogihara et al.[88] the impedance contribution of the diffusion of Li^+ in cylindrical pores strongly depends on the radius and the length of the pores. The negative electrode of the pouch cells used is made of graphite slabs of about 40 x 25 μm. On the contrary, the positive electrode is composed of particle with a radius of about 5 μm. The positive and negative electrodes have different pore sizes.

4.3.2 ORIGIN OF THE MEDIUM FREQUENCY FEATURE

Since the high frequency features and the low frequency features are assigned to electronic conduction processes, Li^+ diffusion in the pores of the electrode and the solid

state diffusion of the Li in the active particle, the medium frequency feature (the step-wise increase in the real part of the impedance and the bell-shaped curve in the negative imaginary part of the impedance) must be due to the transfer of Li^+ from the electrolyte to the active particle, passing through the SEI. If an additive modifies the surface of an electrode, the presence of different additives should affect the medium frequency feature of the impedance spectra.

Figure 4.13 shows the Bode representation of the area specific impedance of untouched (not open) Medtronic LV-LCO/graphite cells containing no additive (control), 1% VC, 2% VC, and 0.3% TMOBX, measured at an open potential of 3.775 V at 10°C. The cells were previously used in automated storage experiments (for a complete history of the cell, see section 3.3). Figure 4.13 shows that while changing the additive content of the electrolyte has a great impact on the medium frequency (100 Hz – 20 Hz) feature of the impedance, it has no pronounced effect on the high frequency feature (100,000 Hz – 100 Hz). Since the impedance of the cells are measured at the same open circuit potential, the change in the impedance spectrum must come from surface alteration induced by the presence of additives in the electrolyte.

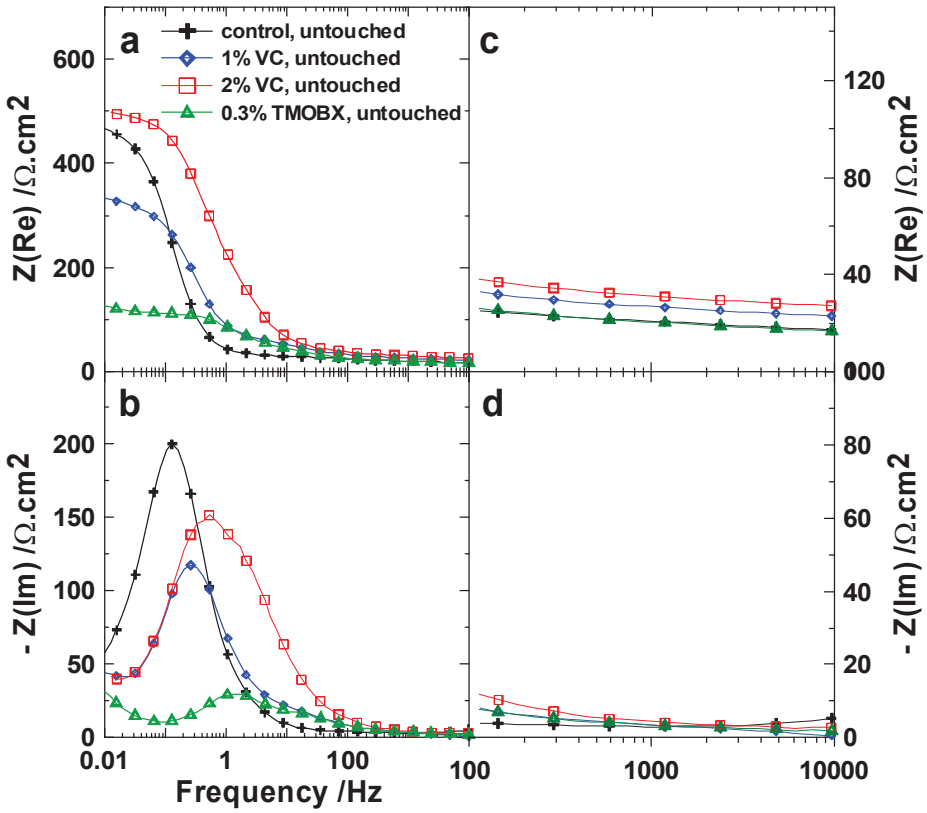

Figure 4.13 Bode representation of the area specific impedance of untouched (not open) Medtronic LV-LCO/graphite cells containing no additive (control), 1% VC, 2% VC, and 0.3% TMOBX, measured at an open potential of 3.775 V at 10°C (a, b), and a zoom-in of the high frequency region (c, d).

4.3.3 SUMMARY OF THE DIFFERENT CONTRIBUTIONS TO THE IMPEDANCE

Figure 4.14 shows the Bode representation of the area specific impedance of a positive symmetric cell (a) and negative symmetric cell (b) reconstructed from a pouch cell containing 0.75 g of electrolyte with 1% VC and cycled at 40°C for 29 days. Figure 4.14 shows the different contributions to the impedance of the negative electrode and positive

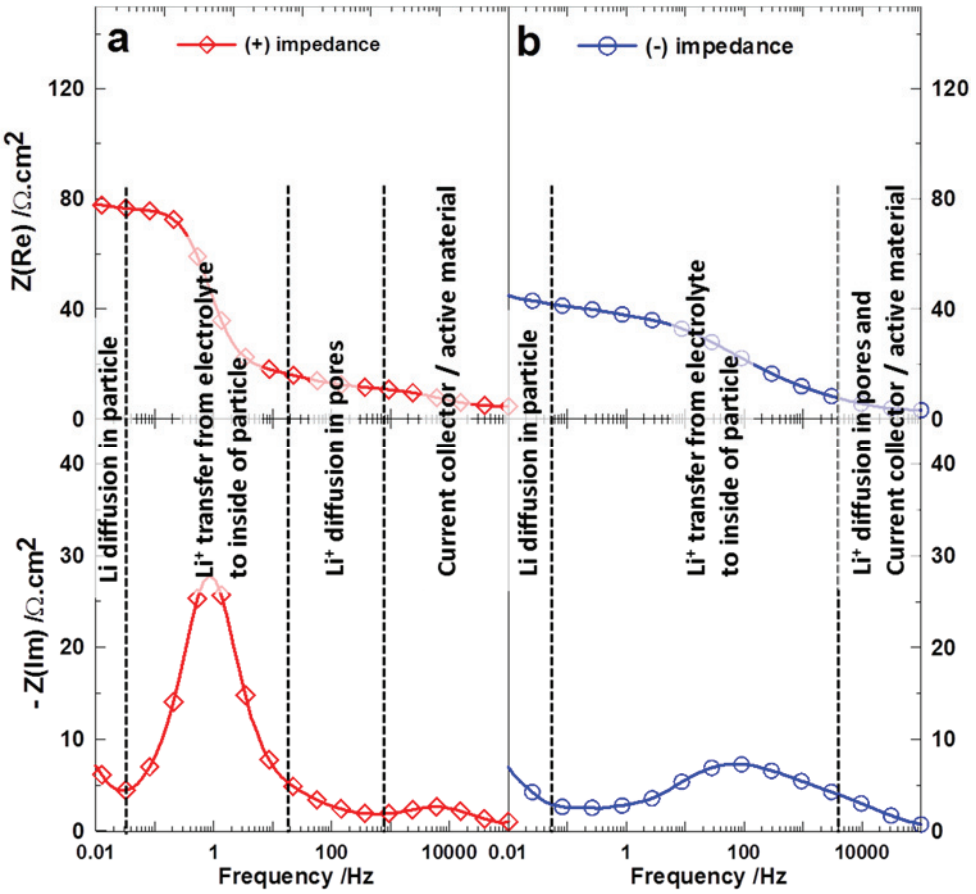

Figure 4.14 Bode representation of the area specific impedance of a positive symmetric cell (a) and negative symmetric cell (b) reconstructed from a pouch cell containing 0.75g of electrolyte with 1% VC. The spectra are separated in different frequency ranges corresponding to different phenomena.

electrode as discussed in sections 4.3.1 and 4.3.2. Figure 4.14.1a shows that at high frequency, the impedance of a positive electrode (the ones used in this thesis) mainly comes from the current collector-active material electronic impedance, that at high-medium frequency, the impedance is mainly due to Li^+ diffusion in the pores (which is not seen in the positive electrode of the Medtronic cells), at medium frequency the impedance comes from the transfer of Li^+ from the electrolyte to the electrode, passing

through the SEI, and at low frequency, the impedance is mainly due to the Li diffusion in the active particle. Figure 4.14b shows that at high frequency the impedance of the negative (graphite) electrode is mainly due to a combination of Li^+ diffusion in the pores and current-collector/active particle electronic impedance, that at medium frequency the impedance is mainly due to the transfer of Li^+ from the electrolyte to the electrode, passing through the SEI, and that at low frequency, the impedance is mainly due to Li diffusion in the active particle as shown by several researchers[82,83]. Figure 4.14 shows that the impedance of Li^+ diffusion in the pores appears at higher frequency for the negative electrode compared to the positive electrode. As mentioned in section 4.3.1, this difference in frequency can come from different pore sizes between the positive electrode and the negative electrode.

CHAPTER 5. STUDY OF ADDITIVES USING EIS ON SYMMETRIC CELLS

This chapter presents the results obtained using the EIS on symmetric cells method discussed in Chapters 3 and 4. Section 5.1 presents the results of the first experiments done on low voltage (LV) $LiCoO_2$/graphite cells manufactured by Medtronic (the electrodes are encased in a hard stainless steel can) containing different combinations of vinylene carbonate (VC) and trimethoxyboroxine (TMOBX). Section 5.2 presents the results of studies made on low-voltage $LiCoO_2$/graphite, high voltage (HV) $LiCoO_2$/graphite, and $Li[Ni_{0.4}Mn_{0.4}Co_{0.2}]O_2$/graphite cells manufactured by Medtronic and containing different combinations of VC, TMOBX, fluoroethylene carbonate (FEC), and lithium bis(trifluoromethanesulfonyl)imide (LiTFSI). Section 5.2 explores the differences (if any) in the effects of additives on the two different positive electrode materials and two different upper potential cut-offs. Section 5.3 presents the results of a comparative study of the effects of VC and vinyl ethylene carbonate (VEC) in $LiCoO_2$/graphite pouch cells using EIS on symmetric cells and high precision coulometry. Finally, section 5.4 presents a study of the effects of VC and TMOBX in $LiCoO_2$/graphite pouch cells using EIS on symmetric cells and high precision coulometry.

5.1 LOW VOLTAGE LCO/GRAPHITE CELLS CONTAINING VINYLENE CARBONATE AND TRIMETHOXYBOROXINE

5.1.1 EXPERIMENTAL

Machine-made low voltage $LiCoO_2$/graphite cells from Medtronic (LV-LCO) used in automated storage experiments were opened to reconstruct symmetric cells following the procedure described in Chapter 3. The history of the cells prior to being opened is described in Section 3.3.

5.1.2 RESULTS AND DISCUSSION

Figure 5.1 shows the Bode representation of the impedance of the reassembled full cells, the calculated positive symmetric cell impedance divided by two, and the measured negative symmetric cell impedance divided by two for electrodes from parent LV-LCO wound cells containing different combinations of VC and TMOBX . In every panel, the results for the control electrolyte have been included as a relative comparison. Figures 5.1a, b and c show that the impedance reduction that 1% VC creates in the full cell is due primarily to its effect on the positive electrode. Figure 5.1b shows that the real part of the impedance at low frequency at the positive electrode changes from 500 $\Omega \cdot cm^2$ to 300 $\Omega \cdot cm^2$ when 1% VC was added. However the impact of 1% VC on the negative electrode is very small and only a slight impedance increase can be seen in Figure 5.1c. Figure 5.1d shows that even though the real part of the impedance at low frequency for the control and the 2% VC-containing cells are very similar, the frequency of the maximum of the negative of the imaginary part is different. This indicates that the contributions to the full cell impedance in the control cell and in the 2% VC cell are

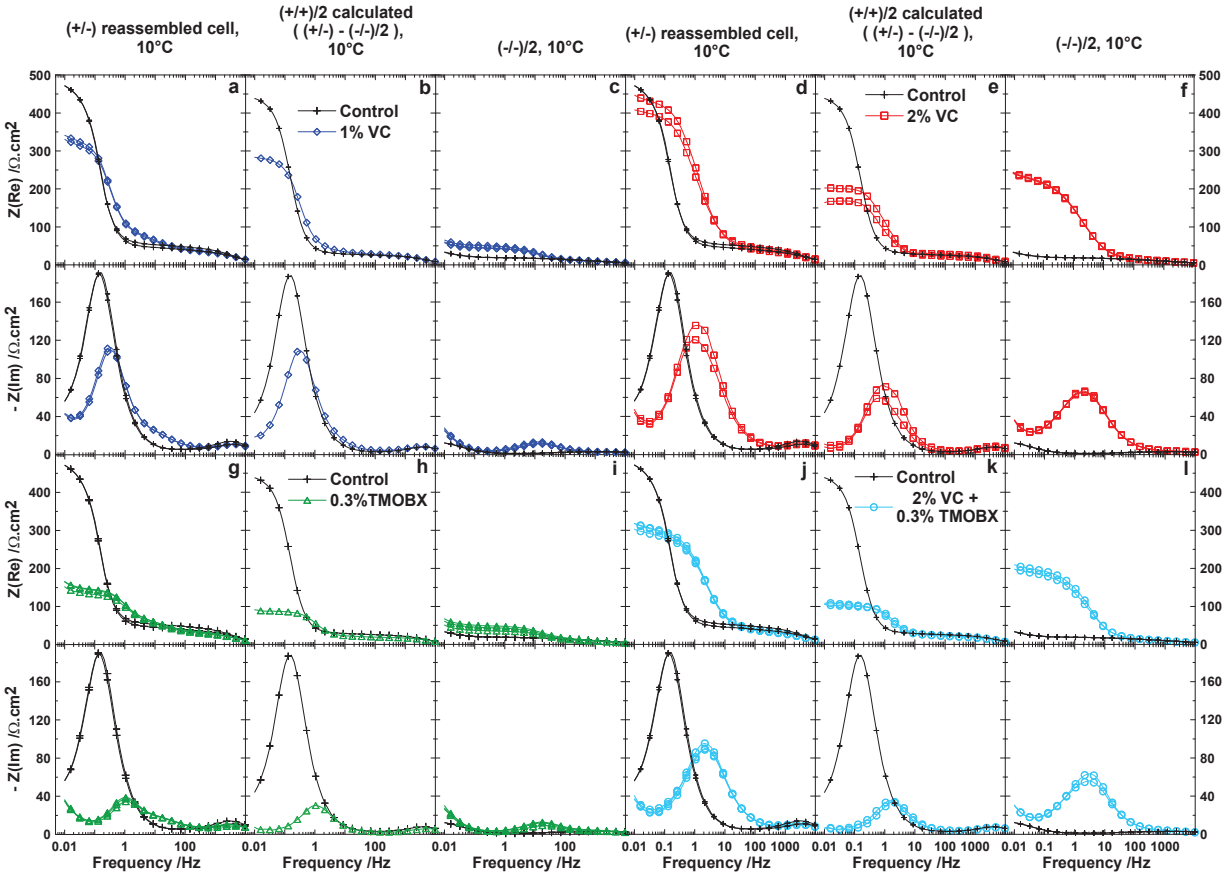

Figure 5.1 Bode representation of the area-specific impedance of the full reassembled coin cells (a, d, g, j), calculated positive symmetric cells impedance divided by two (b, e, h, k) and measured negative symmetric cells impedance divided by two (c, f, i, l) for cells containing 1 wt.% VC (a-c), 2 wt.% VC (d-f), 0.3 wt.% TMOBX (g-i) and 2% VC + 0.3 wt.% TMOBX (j-l). The impedance of the cells containing no additive is shown in each panel. All measurements were made at 10°C. Reproduced with permission from *J. Electrochem. Soc.*, **160**, A117-A124 (2013). Copyright 2003, The Electrochemical Society.

different. Figures 5.1e and 5.1f show clearly how this comes about. Figures 5.1b and 5.1e show that the impedance reduction that 1% VC and 2% VC impart on the positive electrode is similar. However, Figures 5.1c and 5.1f show that their impact on the negative electrode impedance is very different.

Figure 5.1f shows that adding 2% VC greatly increases the negative electrode impedance, presumably because of the well-known thick SEI growth that VC creates[89]. Maybe 2% VC is "too much" as far as the negative electrode side is concerned. Burns et al.[3] showed in precision coulometry studies that the Coulombic efficiency and charge endpoint capacity slippage of LCO/graphite and NMC/graphite cells with 1% or 2% VC additives were basically identical (See Figure 3 in reference 3). Burns et al. also noted that the cells with 2% VC had higher impedance (see Figure 5 in reference 3) but did not determine which electrode caused the increased impedance. Figures 5.1a-f clearly show the negative electrode side is the cause of the increased impedance.

Figures 5.1g, 5.1h and 5.1i show that most of the impedance decrease of the full cell containing 0.3% TMOBX comes from the positive electrode. In this concentration range, TMOBX lowers the positive electrode impedance even more than VC. Figure 5.1i shows that TMOBX raises the negative electrode impedance slightly compared to the control cell. Burns et al.[10] showed that additions of 0.3% TMOBX greatly reduced the impedance of LCO/graphite and NMC/graphite wound cells (See Figure 5 in reference 4**)** but did not identify which electrode was affected. Figures 5.1a-c and 5.1g-i prove that TMOBX has the largest effect on the positive electrode impedance.

Figure 5.1j, 5.1k and 5.1l show the effect of the VC and TMOBX additive mixture. Adding both TMOBX and VC in the same cell retains most of the effect of VC on the negative electrode and the effect of TMOBX on the positive electrode from an impedance perspective. Based on the results in Figure 5.1 and in reference 4**,** excellent low impedance cells with long lifetime could be made using 1% VC and 0.3% TMOBX.

Figures 5.1b, c, e, f, h, i, k, l show that the frequency of the maximum of the negative imaginary part of the feature associated with the charge transfer resistance of the negative electrode is always higher than that for the positive electrode.

Figure 5.2 shows the impedance of the same cells as in Figure 5.2 at 30°C. The conclusions made based on the data collected at 10ºC (Figure 5.2) still apply for the data collected at 30ºC. A careful comparison of Figures 5.1 and 5.2 shows that the negative electrode impedance in the presence of VC decreases more rapidly with temperature than the positive electrode impedance. This suggests that cells destined for dedicated high temperature use could tolerate higher concentrations of VC without developing excessive impedance.

From the data presented in Figures 5.1 and 5.2, the value of the charge transfer resistance at the SEI/electrolyte interface has been assessed using Atebamba's SCR model[90] and an in house fitting software (written by Connor Aiken, summer undergraduate student, Physics and Atmospheric Science, Dalhousie University). Figure 5.3 shows the SCR model. This model comprises a resistor for the electrolyte resistance, R_{el}, a resistor for the active particle/current-collector interface resistance, R_{cr}, a constant phase element (CPE)

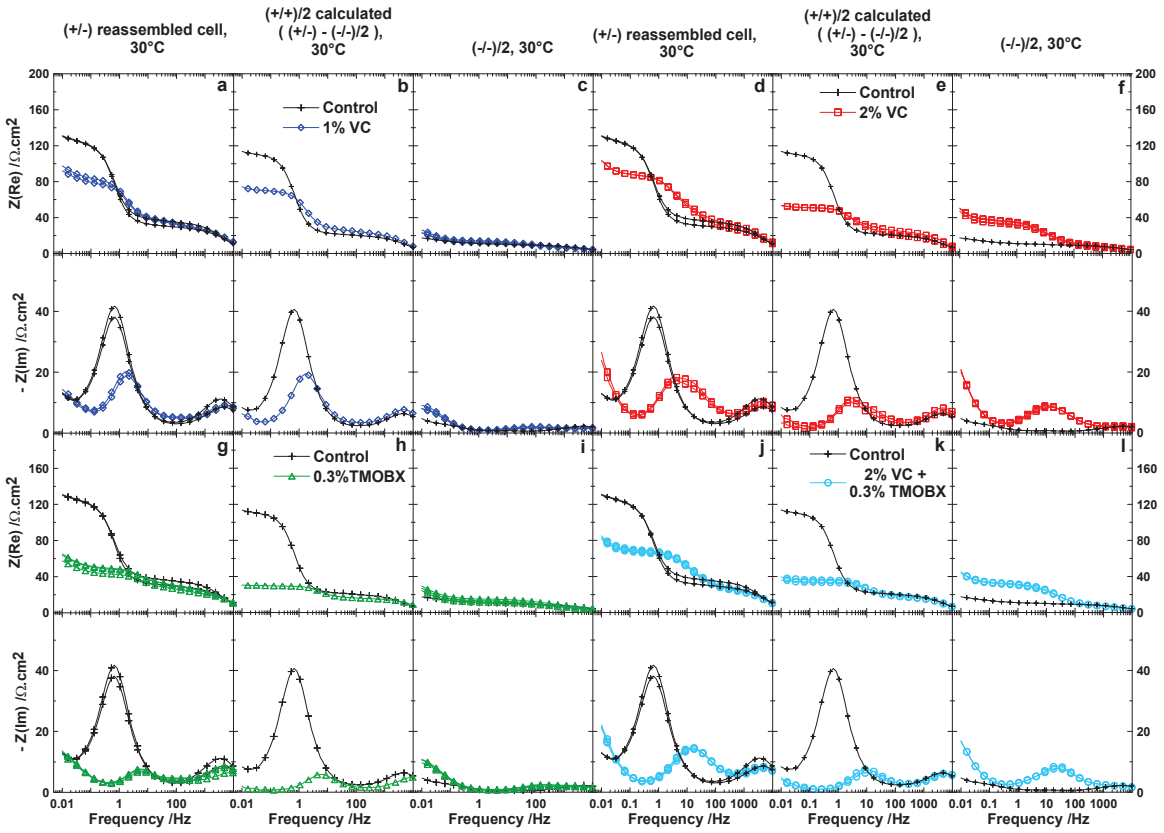

Figure 5.2 Bode representation of the area-specific impedance of the full reassembled coin cells (a, d, g, j), calculated positive symmetric cell impedance divided by two (b, e, h, k) and measured negative symmetric cell impedance divided by two (c, f, i, l) for cells containing 1 wt.% VC (a-c), 2 wt.% VC (d-f), 0.3 wt.% TMOBX (g-i) and 2% VC + 0.3 wt.% TMOBX (j-l). The impedance of the cells containing no additive is shown in each panel. All measurements were made at 10°C. Reproduced with permission from *J. Electrochem. Soc.*, **160**, A117-A124 (2013). Copyright 2003, The Electrochemical Society.

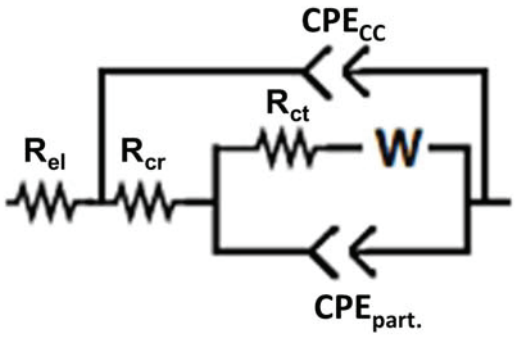

Figure 5.3 SCR model proposed by Atebamba et al.[90]

for the double layer associated with the uncovered part of the current collector, CPE_{cc}, a resistance for the transfer of Li^+ from the electrolyte to the active particle, passing through the SEI, R_{ct}, a CPE for the double layer associated with the active particle, $CPE_{part.}$, and a Warburg-type resistance for the solid state diffusion of Li in the particle, W. The SCR model assumes very good particle to particle electronic conductivity.

The expression for the impedance of the constant phase element, $Z_{CPE}(\omega)$, is given by:

$$Z_{CPE}(\omega) = \frac{1}{(j\omega)^{\alpha}Q} \tag{5.1}$$

where j is the square root of -1, ω is the frequency in rad.s^{-1}, α is a constant ($0 < \alpha < 1$), Q is the capacitance in $Fs^{-\alpha}$. When $\alpha = 1$ the CPE has the same expression as a capacitor. CPEs have been introduced to improve the poor fitting of impedance spectra when normal capacitors were used in the model. It has been proposed that the CPE-like behavior of the electrochemical systems comes from surface inhomogeneity,[91] or a distribution of activation energies for the kinetics of the reactions studied.[92] In the case of

the electrodes of Li-ions cells, surface inhomogeneity is undoubtly present (see Figure 3.6).

The expression for the impedance of the diffusion of Li in the particle is given by:

$$Z_W(\omega) = \frac{\{r_s \coth[r_s c_{sj} j\omega]^p\}}{[r_s c_{sj} j\omega]^p} \tag{5.2}$$

where r_s and c_{sj} are the general resistance and capacitance respectively ($r_s c_{sj}$ is related to the diffusion length and the diffusion coefficient, $r_s c_{sj} = \frac{l^2}{D_{chem}}$ where l is the diffusion length and D_{chem} is the diffusion coefficient of Li in the material), p is an arbitrary constant ($0 < p < 1$) that is used to account for the difference in the slope between the theoretical Warburg resistance and the slope seen in the impedance spectra. Again, p accounts for surface inhomogeneity and the different particle sizes. Clearly α and p are arbitrary factors and reveal the lack of knowledge about their real physical meaning. However, the differences in the shape of the impedance spectra are more important in this thesis than the extraction of specific information such as film thickness, diffusion length, diffusion coefficient, *etc.*

Figure 5.4 shows half of the area specific impedance of a positive symmetric cell (a) and of a negative symmetric cell (b) along with the calculated impedance spectra using the Atebamba et al.[90] model. The model parameters of the calculated spectra were adjusted to give the best fit between experiment and calculation in a least-squares sense. Figure 5.4 shows a very good agreement between the electrochemical impedance spectra and the calculated spectra using the equivalent electrochemical circuit model shown in Figure

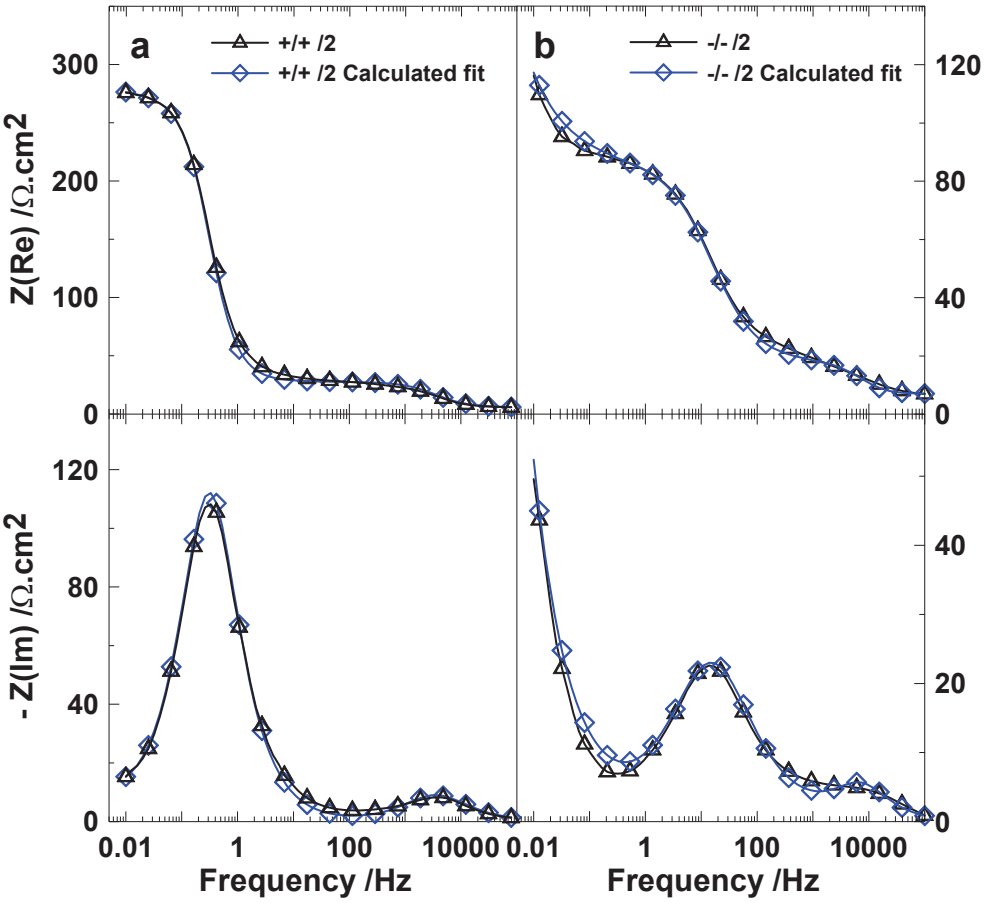

Figure 5.4 Bode representation of the calculated area specific impedance of a positive symmetric cell and its fit (a), and area specific impedance of a negative symmetric cell and its fit (b), using the Atebamba et al. model.[90]

5.3. Since a change in the chemical structure of the SEI changes R_{ct} of an electrode, comparing the value of the charge transfer resistance of the positive electrode and the negative electrode of cells containing different additives to the charge transfer of the electrodes of a cell containing no additive allows assessing at which electrode this additive acts. It is certain that the model is not ideal, especially since it does not take into account the Li^+ diffusion in the pores of neither the positive nor the negative electrode. However, the characteristic frequencies of the Li^+ diffusion in the pores and the transfer

of Li^+ through the SEI are well-separated. As a result, fitting the impedance spectra with the model shown in Figure 5.3 still gives a reliable value for R_{ct}.

Figure 5.5 shows the values of the R_{ct} of the impedance spectra shown in Figure 5.1 and Figure 5.2, calculated using the model shown in Figure 5.3. The error bars are calculated as the standard variation of the R_{ct} of the three replicates fitted using the model presented

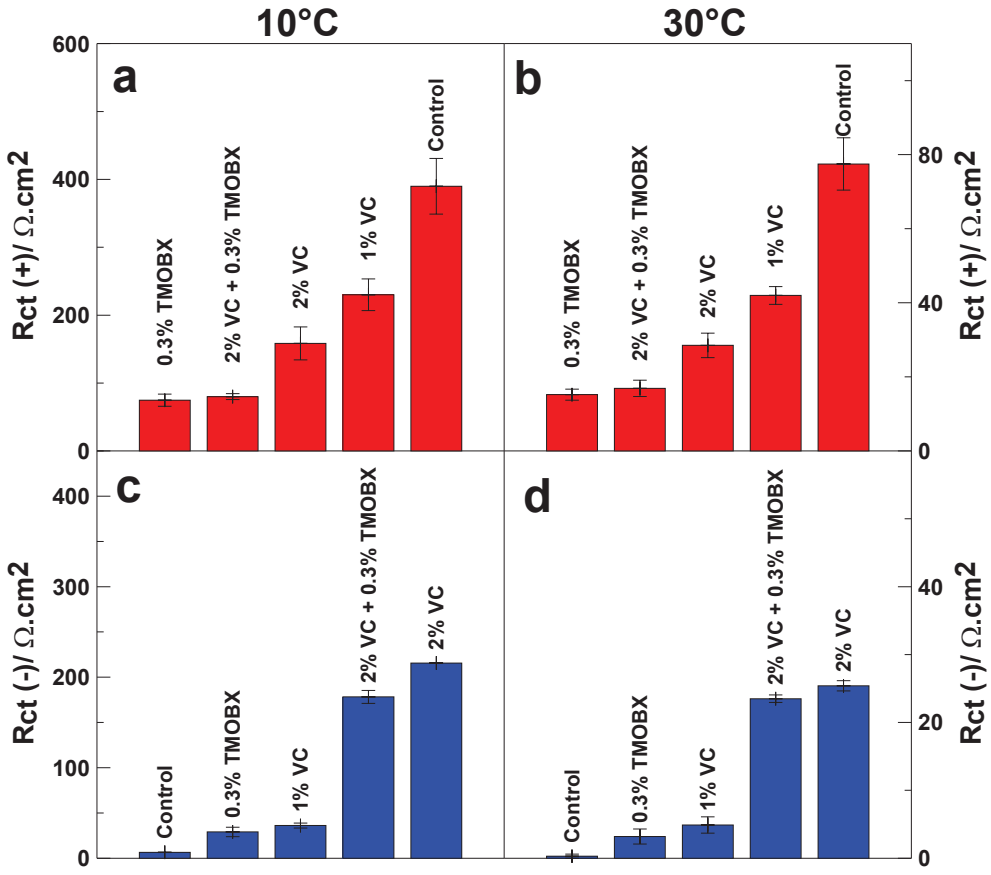

Figure 5.5 Assessed value of the area-specific SEI charge transfer resistance at the particle-electrolyte interface, R_{ct}, at 10°C (a, c) and 30°C (b, d) for the positive electrode (a, b) and negative electrode (c, d) of LV-LCO cells containing VC and TMOBX.

in this chapter. Figure 5.5 shows that the ranking of the charge transfer impedance for both the positive and negative electrode does not change with temperature over this range. That is, cells containing TMOBX have the smallest positive electrode impedance at all temperatures and cells with 2% VC have the highest negative electrode impedance at all temperatures.

5.1.3 CONCLUSION

Using the developed method, the impact of the electrolyte additives, VC and TMOBX, on LCO/graphite cells was studied. VC additions above 1 wt.% dramatically increased the negative electrode charge transfer impedance. VC additions and TMOBX additions both decreased the positive electrode charge transfer impedance. TMOBX is more effective than VC at reducing positive electrode charge transfer impedance. The method also proved to be useful at revealing which additive control the surface composition of the positive electrode and the negative electrode when multiple additives are introduced in the cell at the same time.

5.2 COMPARISON OF THE EFFECT OF VARIOUS ADDITIVES IN LOW-VOLTAGE LCO/GRAPHITE, HIGH VOLTAGE LCO/GRAPHITE, AND NMC/GRAPHITE CELLS FROM MEDTRONIC

5.2.1 EXPERIMENTAL

Machine-made low-voltage $LiCoO_2$/graphite (LV-LCO), high voltage $LiCoO_2$/graphite (HV-LCO), and $Li[Ni_{0.4}Mn_{0.4}Co_{0.2}]O_2$/graphite (NMC) cells from Medtronic previously used in automated storage experiment were opened to reconstruct symmetric cells using the method described in section 3.3. For a more detailed history of the cells prior to being opened, see section 3.3.Table 5.1 lists the additives and in which cell chemistries they were tested. The structures of the additives were presented in Figure 1.5 and Figure 2.2. Some combinations were not tested due to unavailability of cells.

Table 5.1 List of additives studied in this work in Medtronic prismatic wound cells (*yes* means the cell was available for opening; *no* means the cell was not available for opening).

Additive	NMC/graphite 4.225V	LV LCO/graphite 4.075V	HV LCO/graphite 4.175 V
Control	***yes***	***yes***	***yes***
1% VC (Novolyte)	***yes***	***yes***	***yes***
2% VC (Novolyte)	***yes***	***yes***	***no***
0.3% TMOBX (BASF 99.2%)	***yes***	***yes***	***yes***
2% FEC (Novolyte)	***yes***	***yes***	***yes***
2% LiTFSI (3M, 99.9%)	***yes***	***yes***	***yes***
100 ppm additive A	***no***	***yes***	***no***
2% VC + 0.3% TMOBX	***yes***	***yes***	***yes***
2% VC + 2% FEC	***yes***	***yes***	***yes***
2% VC + 2% LiTFSI	***yes***	***yes***	***yes***
2% VC + 100ppm additive A	***yes***	***no***	***no***
2% VC + 1000 ppm additive A	***no***	***yes***	***no***
2% VC + 2 % LiTFSI + 100 ppm additive A	***no***	***yes***	***no***
2% VC + 2% LiTFSI + 1000 ppm additive A	***yes***	***yes***	***no***
2% VC + 0.3% TMOBX + 100 ppm additive A	***no***	***yes***	***no***

5.2.2 RESULTS AND DISCUSSION

Figure 5.6 presents the charge transfer resistance of the positive electrode of NMC cells (a, b), LV-LCO cells (c, d) and HV-LCO cells (e, f) at 10°C (a, c, e) and 30°C (b, d, f) obtained by fitting the inferred electrochemical impedance spectra of the reassembled positive symmetric cells ((+/+) = 2(+/-) - (-/-)) using the equivalent circuit model shown in Figure 5.3. Figure 5.6 shows that all additives and additive combinations used affected the positive electrode surface in all cell chemistries studied (NMC/graphite, LV-LCO/graphite, and HV-LCO/graphite). Almost every additive used reduced the charge transfer impedance of the positive electrode with the exemption of additive A and LiTFSI when used alone in the LV-LCO cells. Figure 5.6 shows that TMOBX is an effective additive for reducing the charge transfer resistance at the positive electrode in all cell chemistries studied.

Figure 5.6 also helps to determine which additive controls the surface chemistry at the positive electrode when more than one additive is included in the electrolyte. For instance, when VC and TMOBX are added in LV-LCO and HV-LCO cells, the value of the R_{ct} at the positive electrode is the same as for TMOBX alone. This suggests that TMOBX controls the surface chemistry of LCO electrodes when combined with VC. The error bars for R_{ct} for the mix of TMOBX and VC in NMC cells does not allow one to suggest which additive is controlling the surface chemistry. Figures 5.6a and 5.6c show that LiTFSI has a different effect on the positive electrode surface of NMC cells, LV-LCO cells, and HV-LCO cells. Adding LiTFSI to NMC cells significantly reduces R_{ct}

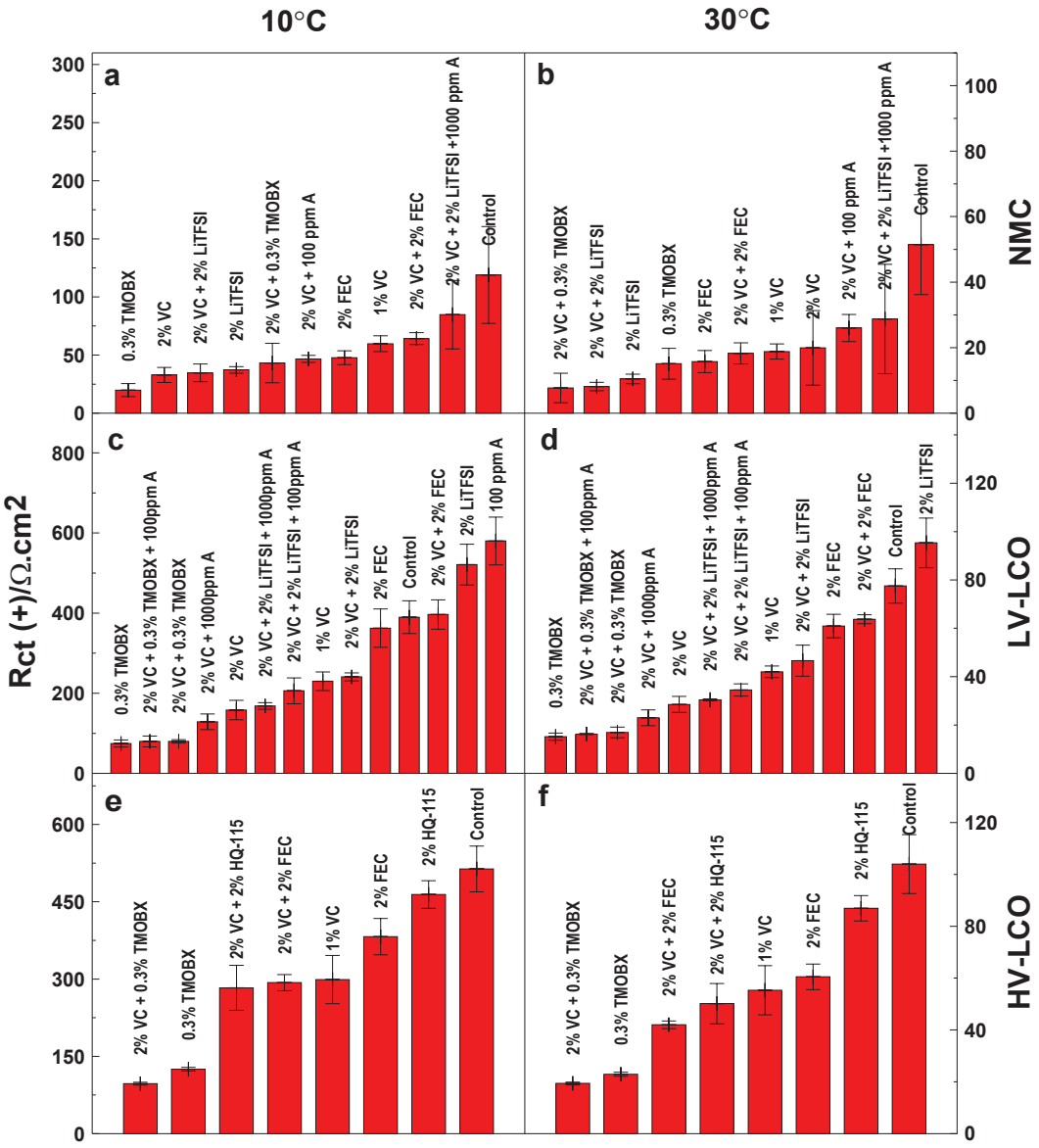

Figure 5.6 Charge transfer resistance, of the positive electrode, $R_{ct}(+)$, of NMC cells (a, b), LV-LCO cells (c, d), and HV-LCO cells (e, f) at 10°C (a, c, e) and 30°C (b, d, f) obtained by fitting the calculated area specific electrochemical impedance spectra of the positive symmetric cells using the equivalent circuit proposed by Atebamba et al.[90]

compared to control, adding LiTFSI to HV-LCO cells slightly reduces R_{ct} of the positive electrode and adding LiTFSI to LV-LCO cells increases R_{ct} of the positive electrode.

This might indicate a dependence of the effect of LiTFSI on the type of positive material used or on the potential to which the cells were exposed. R_{ct} values of the positive electrode of the HV-LCO and LV-LCO cells containing 2% LiTFSI are the same. It seems that LiTFSI keeps the SEI of the positive electrode unchanged when the higher voltage cut-off is increased.

Based on Figures 5.6c and 5.6d, both LiTFSI and VC affect the positive electrode chemistry when introduced together in LCO cells. The similarity of the impact of LiTFSI and VC on R_{ct} of the positive electrode of the NMC cells does not allow one to distinguish which additive controls the surface chemistry of the positive electrode when both additives are present. Figures 5.6a, 5.6c, and 5.6d show that FEC and VC have different impacts on R_{ct} of the positive electrode of NMC cells and LV-LCO cells (2% VC in HV-LCO cells were not available). This indicates that the effects of FEC and VC at the positive electrode are different.

Figure 5.6 shows that adding 100 ppm of additive A to NMC and LV-LCO cells containing VC, TMOBX, VC + TMOBX, VC + LiTFSI affects R_{ct} slightly indicating that VC, TMOBX, LiTFSI, and their combination control most of the surface chemistry of NMC and LCO electrodes when only 100 ppm of additive A is introduced. Adding 1000 ppm of additive A to NMC and LV-LCO cells containing VC, and VC + LiTFSI affects R_{ct} significantly indicating that additive A participates in the formation of the SEI at the positive electrode when a larger concentration is introduced. Every wound cell containing additive A used in this study showed a brownish color on the separator once they were opened and had an unusually bad adhesion of the negative electrode to the

copper foil. The adhesion of the positive electrode to the current collector was not altered by the addition of additive A (compared to cells containing other additives), except for the cell containing 2% VC and 100 ppm additive A.

Figure 5.7 shows the charge transfer resistance of the negative electrode of NMC cells (a, b), LV-LCO cells (c, d) and HV-LCO cells (e, f) at 10°C (a, c, e) and 30°C (b, d, f) obtained by fitting the electrochemical impedance spectra of the reassembled negative symmetric cells using the equivalent circuit model presented in Figure 5.3. The error bars were calculated as the standard deviation of the fitted R_{ct} value of the three replicates.

Figure 5.7 shows that all additives used increased R_{ct} of the negative electrode, except for LiTFSI, which did not show any significant effect at the negative electrode of LV-LCO cells and HV-LCO cells. LiTFSI appears to have reduced the impedance of the negative electrode of NMC cells. Except for LiTFSI-containing cells, the value of R_{ct} of the negative electrode of NMC cells, LV-LCO cells and HV-LCO cells containing the same electrolyte formulation are very similar. This indicates that the positive electrode material and upper voltage cut-off (**in the voltage range studied**) do not have any significant effect on the surface of the negative electrode.

As indicated in an earlier publication,[3] varying the concentration of VC from 1 wt.% to 2 wt.% has a great impact on R_{ct} of the negative electrode without improving the Coulombic efficiency or the voltage drop during an automated storage experiment. As a

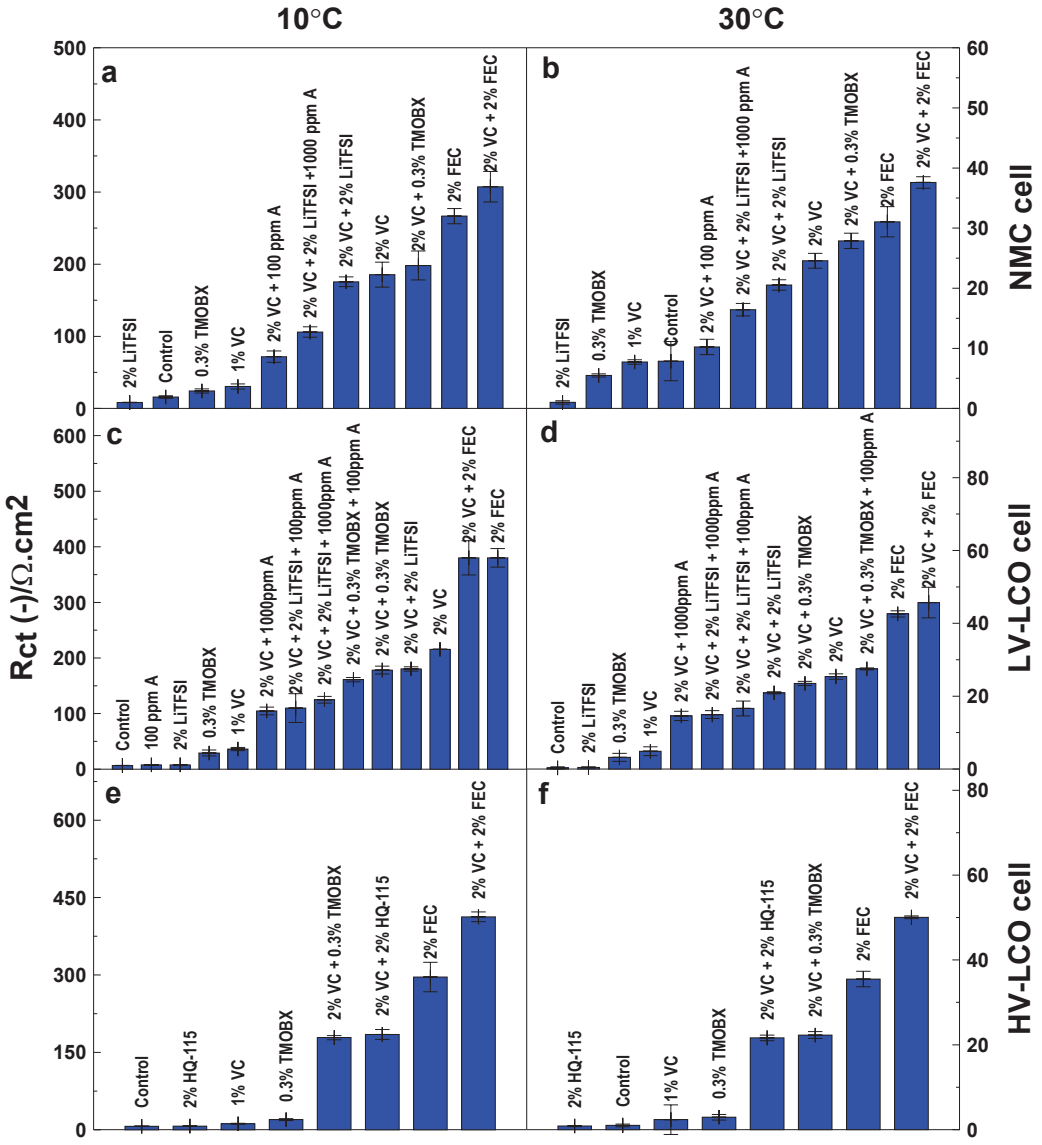

Figure 5.7 Charge transfer resistance of the negative electrode of NMC cells (a, b), LV-LCO cells (c, d), and HV-LCO cells (e, f) at 10°C (a, c, e) and 30°C (b, d, f) obtained by fitting the area specific electrochemical impedance spectra of the negative symmetric cells using the equivalent circuit proposed by Atebamba et al.[90]

consequence, introducing a large amount of VC will have a negative impact on the rate capability of a cell. Figure 5.7 shows that TMOBX affects the surface of the negative

electrode slightly. When VC and TMOBX are introduced in the same cell, R_{ct} of the negative electrode is the same as for cells containing VC only, indicating that VC controls the surface chemistry of the negative electrode over TMOBX.

Figure 5.7 also shows that FEC and VC have different effects on R_{ct} of the negative electrodes. FEC caused a greater R_{ct} at the negative electrode than VC did. This indicates that the SEI at the negative electrode that FEC creates is different from the one that VC does. Figure 5.7c shows that additive A does not have any significant impact on the R_{ct} of the negative electrode when introduced alone. Figures 5.7a-f show that the effect of FEC on the negative electrode surface prevails when introduced with VC.

Figures 5.7a-d show that introducing additive A to cells containing VC, VC and LiTFSI, VC and TMOBX reduces R_{ct} of the negative electrode. This indicates that additive A modifies the nature of the SEI of the negative electrode of cells containing VC, LiTFSI, and TMOBX. It also indicates that the electrode which additive A affects depends on the additive added to the cell and points towards an interaction between additive A and the by-products of the degradation of other additives.

Figure 5.8 shows side by side the R_{ct} of the positive electrode (a, b) and negative electrode (c, d) of LV-LCO cells and HV-LCO cells. This figure helps to determine the effect, if any, of a higher cut-off potential on the effects of additives. For instance,

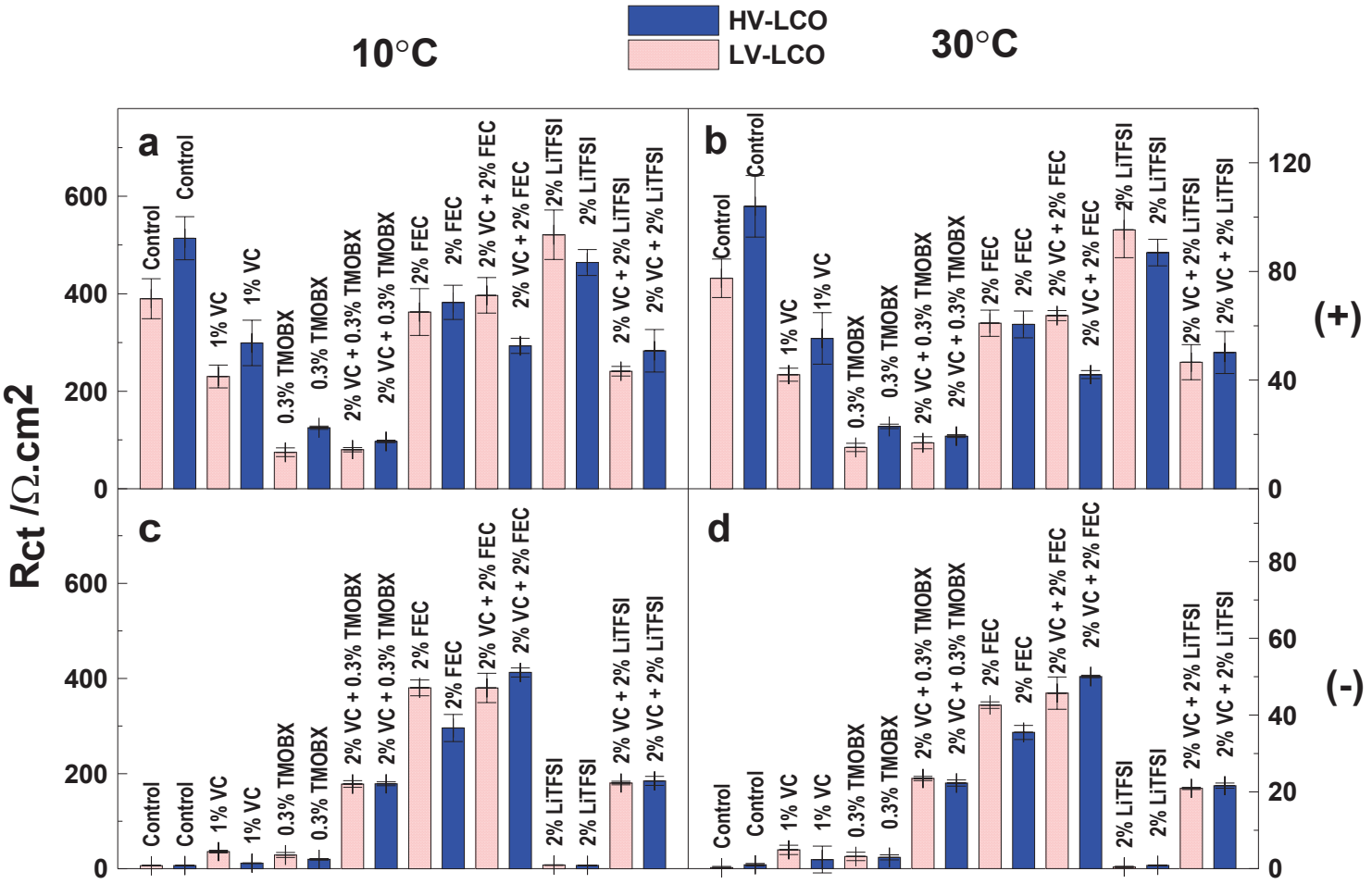

Figure 5.8 Comparison of the charge transfer resistance of the positive electrode of LV-LCO and HV-LCO cells (blue) at 10°C (a) and 30°C (b) and the charge transfer resistance of the negative electrode of LV-LCO (red) and HV-LCO cells at 10°C (c) and 30°C (d).

Figures 5.8a and 5.8b show that the positive electrode of cells containing no additive, 1% VC, 2% VC and 0.3% TMOBX have a higher R_{ct} when charged to a higher cut-off voltage. This is not surprising and is expected since a higher voltage promotes electrolyte oxidation at the positive electrode from which reaction by-products can form at the surface of the electrode. However, cells containing 2% VC + 0.3% TMOBX, 2% FEC, 2% LiTFSI, 2% VC + 2% LiTFSI do not have a higher R_{ct} when charged to higher voltage. This suggests that for these cells the SEI of the positive electrode does not change when the voltage cut-off is increased by 100 mV near 4.1 V. However this does not necessarily indicate a reduction in the rate of electrolyte oxidation as the by-products can be soluble and not participate in the thickening of the SEI. Cells containing 2% VC +2% FEC have a lower R_{ct} at the positive electrode when the cell is charged at a higher voltage cut-off. This may indicate the creation of a slightly different SEI when the cell is charged at a different cut-off.

Figures 5.8c and 5.8d show that that R_{ct} of the negative electrode of HV-LCO is very similar to the R_{ct} of the negative electrode of LV-LCO cells containing the same electrolyte formulation, with the exception of cells containing 2% FEC and 1% VC. It seems that for most of the cells studied, the difference in the higher cut-off voltage (in the range used) does not influence the SEI of the negative electrode. Figure 5.9 shows the Coulombic inefficiency (CIE) during cycling on a high precision charger[8] (a, c, e) and the voltage drop during automated storage experiments (b, d, f) for wound prismatic LV-LCO cells, HV-LCO cells and NMC cells containing different electrolyte additives and additive combinations. The CIE data were collected during C/20 cycling at 40^{o}C and are

reported for the average of the 14th to 16th cycles of all cells. Each data set is the average of duplicate cells. The error bars are calculated as the standard deviation of the value of the duplicate. The cells used in the automated storage experiments are the same cells used for the EIS on symmetric cells study. The data for the cells containing no additive, TMOBX, VC, and LiTFSI, shown in Figure 5.9, were already presented in earlier publications[3,4,77]. The voltage drop during the automated storage experiment measures the rate of parasitic reactions at the positive electrode[6,9]. The greater the voltage drop, the greater the rate of the parasitic reactions at the positive electrode. Normally, cells with the longest cycle life have the smallest CIE.

Figure 5.9 allows some general comments to be made on the effect of an additive on the cycling behavior of a cell. Compared to the control, the addition of either VC (1 wt.% and 2 wt.%), or 2 wt.% FEC reduces the CIE (good) and the voltage drop (good) for both cell chemistries (NMC and LCO) which indicates a reduction in the parasitic reactions between the electrodes and the electrolyte. Compared to the control, the addition of LiTFSI reduces the CIE slightly (good) but does not have any significant impact on the voltage drop (neutral) for both NMC and LCO cells. Compared to the control, the addition of TMOBX reduces the CIE (good) and does not have any impact on the voltage drop (neutral) of LV-LCO cells, reduces the CIE (good) and increases the voltage drop (bad) of HV-LCO cells, and increases the CIE (bad) and voltage drop (bad) of the NMC cells. This suggests that the effect of the addition of TMOBX worsens (in terms of parasitic reactions at the positive electrode) as the voltage cut-off of the cell is increased from 4.075 to 4.175 to 4.225 V.

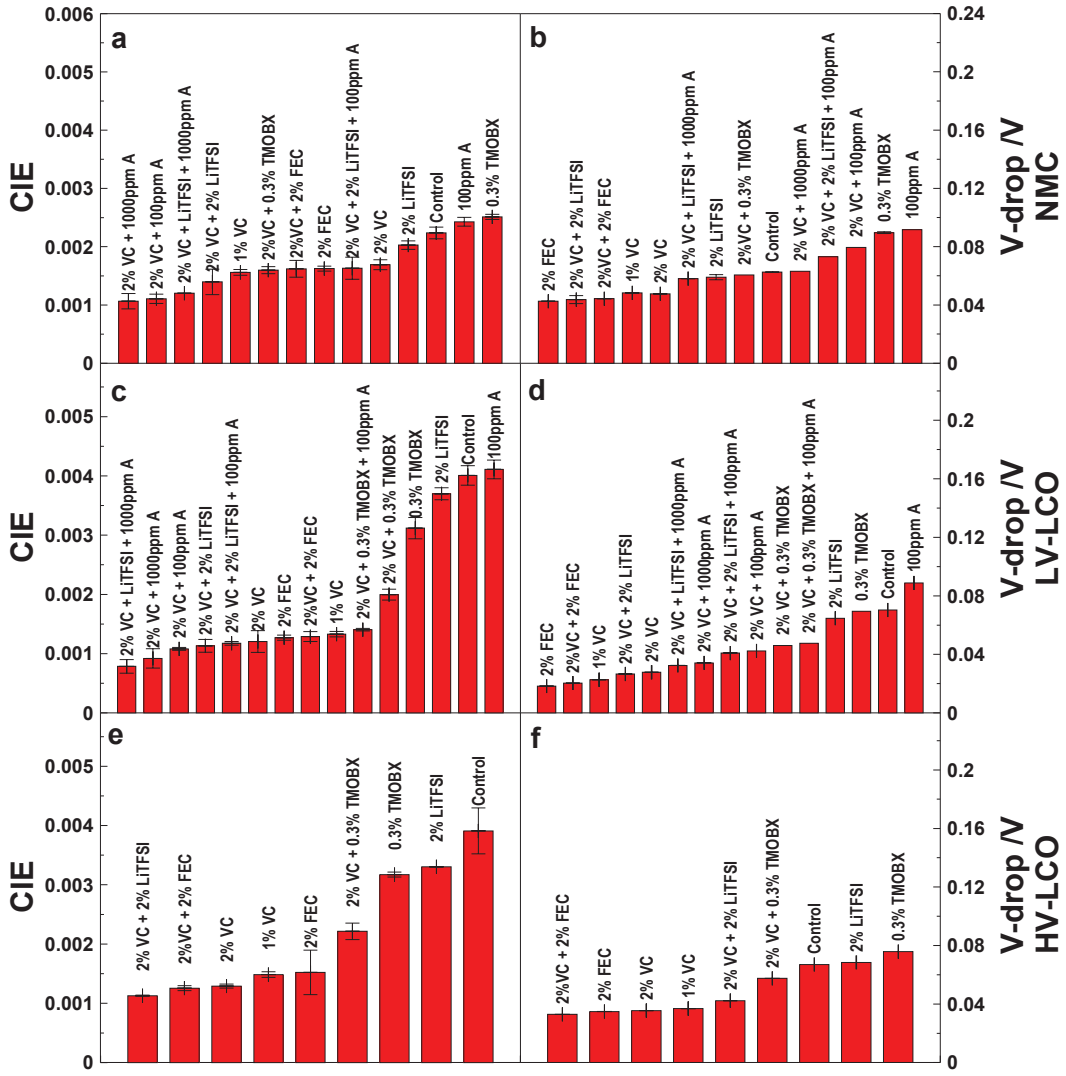

Figure 5.9 Coulombic inefficiency (a, c , e) during cycling on a high precision charger and Voltage drop (b, d, f) during automated storage experiments for NMC/Graphite cells charged to 4.225 V (a, b), LCO/Graphite cells charged to 4.075 V (c, d), and LCO/Graphite cells charged to 4.175 V (e, f). All measurements were made by Chris Burns, PhD candidate and Nupur Sinha, PDF, Department of Physics and Atmospheric Science, Dalhousie, Halifax, NS (2011).

Figure 5.9 shows that compared to the control, 100 ppm of additive A increases somewhat the CIE and voltage drop of NMC and LV-LCO cells. Adding 2% LiTFSI to 2% VC does not seem to have any noticeable impact on the cycling performances of all

cell chemistries compared to VC by itself. Adding 0.3% TMOBX to 2% VC increases the CIE of LV-LCO and HV-LCO, doesn't have any noticeable effect on the CIE of the NMC cells, and increases the voltage drop of all cell chemistries. However, the CIE and voltage drop of VC + TMOBX cells are still significantly lower than the control cells. Adding 100 ppm additive A to 2% VC improves the CIE of the NMC cells but does not have any noticeable effect on the CIE of LV-LCO cells, and increases the voltage drop of both NMC and LV-LCO cells. Compared to 2% VC + 100 ppm Additive A, 2% VC + 1000 ppm A improves the CIE slightly and reduces the voltage drop (the voltage drop is still greater than 2 wt.% VC by itself). Adding 100 ppm additive A to 2% VC + 2% LiTFSI increases the CIE and voltage drop of NMC and LCO cells. Compared to 2% VC + 2% LiTFSI + 100 ppm additive A, increasing the concentration of additive A to 1000 ppm reduces the CIE (CIE is even lower than 2% VC + 2% LiTFSI) and the voltage drop of both NMC cells and LV-LCO cells (V-drop is still higher than 2% VC + 2% LiTFSI). Adding 100 ppm of additive A to 2% VC + 0.3% TMOBX reduces the CIE and leaves the voltage drop unchanged of LV-LCO cells.

Combining the information contained in Figures 5.6 to 5.9 allows one to make some conclusions about the properties of the additives studied. For example, TMOBX does not have any beneficial effect in terms of CIE and voltage drop for cells operating at high voltage, if anything; it makes it worse. The only advantage of using TMOBX alone would be for the reduction of the impedance. From the EIS on symmetric cells study, this impedance reduction comes from the SEI at the positive electrode that TMOBX creates. VC and FEC have the same effect on the CIE and voltage drop of all tested cells (they reduce them both) imparting a good cycle life to the cell. From the EIS study on

symmetric cells, VC and FEC act both at the positive and negative electrode but create different SEIs. VC might be more advantageous than FEC due to smaller charge transfer resistances at both the negative and positive electrodes compared to FEC.

LiTFSI brings some improvements to the CIE and voltage drop (does not slow down the parasitic reactions significantly). From the EIS on symmetric cell study, LiTFSI has no effect at the negative electrode and some effect at the positive electrode. From these results, LiTFSI is a good additive for lowering the charge transfer resistance of the positive electrode of cells used at high voltage. Adding LiTFSI to 2% VC does not have any strong impact on the CIE and voltage drop of all tested cells. From the EIS study, VC controls the formation of the SEI at the negative electrode and both LiTFSI and VC control the SEI at the positive electrode. However compared to VC, the modification of the SEI at the positive electrode produced by the addition of LiTFSI does not affect the reduction of the rate of the parasitic reactions that VC creates. As a consequence, adding LiTFSI to 2% VC does not bring any improvement and increases R_{ct} at the positive electrode.

Adding 2% FEC to 2% VC does not have any impact on the CIE and the voltage drop of the cells. This is not surprising since FEC and VC have exactly the same effect when introduced separately in these cells. When VC and FEC are added together, FEC seems to control the formation of the SEI at the negative electrode and both FEC and VC seem to control the SEI at the positive electrode. As a consequence, adding FEC to VC does not bring any improvement in these cells, and worsens R_{ct} at both electrodes, reducing the power capability of the cell.

Adding 0.3% TMOBX to 2% VC increases the CIE and voltage drop slightly. However it decreases the R_{ct} of the positive electrode and leaves the R_{ct} of the negative electrode unchanged. This indicates that the SEI at the positive electrode that TMOBX creates is responsible for the increase of the rate of the parasitic reactions. From the EIS study, TMOBX controls the formation of the SEI at the positive electrode and VC controls the formation of the SEI at the negative electrode.

Adding 100 ppm of additive A to control cells worsens the cycling behavior of LV-LCO cells and NMC cells. Based on the EIS study, it seems like most of the effects of additive A (when introduced alone) are at the positive electrode. Adding 100 ppm of additive A to 2% VC + 0.3% TMOBX improves the CIE and does not have any significant effect on the voltage drop. From the EIS study, it seems like additive A modifies the SEI at the negative electrode and leaves the SEI at the positive electrode unchanged. This is somewhat expected since the voltage drop is unchanged with the addition of additive A. Adding 100 ppm of additive A in 2% VC cells, and 2% VC + 2% LiTFSI improves the CIE somewhat and increases the voltage drop. However, adding 1000 ppm of additive A to the 2% VC, and 2% VC + 2% LiTFSI cells improves the CIE even more and reduces the voltage drop. From the EIS study on LV-LCO cells, adding 100 ppm of additive A to 2% VC, and 2% VC + 2% LiTFSI has a slight impact on the positive electrode and a great impact (reduces the R_{ct}) on the negative electrode. Adding more additive A to the 2% VC + 2% LiTFSI seems to have a greater effect on the positive electrode than on the negative electrode. This indicates a complex reactivity of additive A. The electrode that additive A affects depends on both the additives added with it, along with its own concentration.

5.2.3 CONCLUSION

The study of electrolyte additives using the EIS on symmetric cells method described in Chapter 3 allowed studies of the effect of several additives and additive combinations on the positive and negative electrodes separately to be made. Combining this study with high precision coulometry and automated storage experiments allowed an assessment of the effect of additives on the cycling performance of NMC/graphite and LCO/graphite cells along with determining on which electrode they act. Being able to correlate cycling behavior to the effect of an additive on each electrode helps to shed light on the complicated mechanisms involved in the way additives work.

This study showed that the behavior of an additive depends on the presence or absence of other additives and that in some cases some additives control the formation of the SEI at the positive electrode, or the negative electrode, or both. For example, VC controls the formation of the SEI at the negative electrode when introduced with LiTFSI and TMOBX but not with FEC. TMOBX controls the formation of the SEI at the positive electrode when introduced with VC.

This study also showed that the effect of varying the concentration of an additive does not always result in additive behavior. For instance, increasing the concentration of VC from 1 wt.% to 2 wt.% resulted in an unexpected increase of the negative electrode impedance. Also, adding 100 ppm of additive A in cells containing VC affected the negative electrode more than the positive electrode, but introducing 1000 ppm of additive A had a greater impact on the positive electrode than on the negative electrode.

This study shows that to achieve good cycling performance (low CIE, voltage drop and impedance) additives must be used. The ideal additive or additive combination should help create SEI layers at both the positive and negative electrodes that have low charge transfer resistance and that slow down the parasitic reactions.

5.3 COMPARATIVE STUDY OF VINYL ETHYLENE CARBONATE (VEC) AND VINYLENE CARBONATE (VC) IN LCO/GRAPHITE POUCH CELLS USING HIGH PRECISION COULOMETRY AND ELECTROCHEMICAL IMPEDANCE SPECTROSCOPY ON SYMMETRIC CELLS

5.3.1 EXPERIMENTAL

The LCO/graphite pouch cells were filled with 0.75 g of 1 M $LiPF_6$ EC:EMC (Novolyte Technologies, now BASF) in a ratio of 3:7 by weight with 0 wt.% VC (Novolyte Technologies, now BASF) and 0 wt.% VEC (Novolyte Technologies, now BASF) called control, 0.5 wt.% VC, 1 wt.% VC, 2 wt.% VC, 4 wt.% VC, 6 wt.% VC, 0.5 wt.% VEC, 1 wt.% VEC, 2 wt.% VEC, 4 wt.% VEC and 6 wt.% VEC. After electrolyte filling, cells were vacuum-sealed. However the VEC-containing cells were not centrifuged. After electrolyte filling, the VEC-containing cells were connected to a Maccor series 4000 and held at 2 V for 24 h in a 40°C (+/- 0.1°C) temperature controlled box. After the 24 h period, the cells were charged to 4.2 V at 15 mA (~C/15) and discharged to 3.7 V at 22.5 mA (~C/10). The cells were then transferred in an argon-filled glove box to be opened and re-vacuum-sealed. Pairs of cells with 0%, 0.5%, 1%, 2%, 4%, and 6% VEC were then connected to the High Precision Charger (HPC) built at Dalhousie University[8] where cells were cycled at 40°C for ~350 hours to measure Coulombic efficiency and charge endpoint capacity slippage. Pairs of cells containing 0% and 2% VEC were connected to the HPC and cycled at 30°C and 60°C. The other pairs of cells containing 0.5%, 1%, 4%, and 6% VEC were connected to a Maccor cycler and cycled at 30°C and 60°C for the same amount of time using the same currents and between the same voltage limits as the

cells connected to the HPC. After ~350 h of cycling, cells were put at ~3.7 V and stored in a freezer (~-15°C) until further use. Prior to performing the EIS on symmetric cells study, the VEC-containing cells were held at 3.79 V and their EIS spectra were taken at 10°C (+/- 0.1°C) and 30°C (+/- 0.1°C) with a 10 mV excitation from 100 kHz to 10 mHz.

Two batches of LCO/graphite pouch cells containing VC were made (due to a power failure during testing, the first batch was inadvertently brought to high voltage after power resumption and subsequently disposed of). After filling the first batch, the cells were connected to a Maccor 4000 series charger and held at 2 V for 24 h to promote wetting. After 24 h, the cells were connected to a Moli cycler in a 40°C (+/- 0.1°C) temperature-controlled box where they were charged to 4.2 V at 15 mA (~C/15) and discharged to 3.7 V at 22.5 mA (C/20). They were then de-gassed and cycled on a Maccor series 4000 at 40°C between 2.8 V and 4.2 V at 15 mA (~C/15) for 18 days. The cells were then moved to the HPC where they were cycled at 40°C between 4.2 V and 2.8 V at 15 mA for ~350 hours to measure Coulombic efficiency and charge endpoint capacity slippage. After filling the second batch, the cells were put in a centrifuge at an acceleration of 50 g-force for 20 min. The cells were then connected to a Maccor series 4000 charger in 40°C boxes and held at 1.5 V for 24 h to promote wetting. The cells were then charged at 2 mA for the first 10 h to collect well-defined differential capacity of the reduction of the additives and electrolyte components. The cells were then charged to 4.2 V and discharged to 3.775 V at 15 mA. The cells were de-gassed and cycled on a Maccor series 4000 for 29 days under the same conditions as the first VC-containing cells. After the 29 days of cycling and before performing the EIS on symmetric cells study, the cells

were put at 3.80 V and their EIS spectra were taken at 10°C (+/- 0.1°C) and 30°C (+/- 0.1°C) with an excitation of 10 mV and a frequency range of 100 kHz-10 mHz.

The EIS on symmetric cells study procedure followed the one described in section 3.3, except for the VEC-containing pouch cells. These cells were opened at an open circuit potential of 3.79 V instead of a potential of 3.80 V.

5.3.2 RESULTS AND DISCUSSION

Figure 5.10 shows the cell terminal voltage as a function of capacity for the first 60 mAh of the first charge (during formation) (a, c) along with the differential capacity as a function of cell potential (b, d) for the VEC-containing cells (a, b) and the VC-containing cells (c, d). Figure 5.10 shows the good reproducibility the machine-made pouch cells provided. Figures 1a and 1c show that VC and VEC have very different reaction mechanisms at the negative electrode. Figure 1a shows that the VEC containing cells have a plateau at 2.7 V (graphite electrode near 1.1 V vs. Li /Li^+) that grows with increasing amounts of VEC. This growing plateau with VEC amounts indicates that this first reaction of VEC with the graphite surface does not produce a passivating film. Figure 1a shows a second growing plateau around 3.2 V (graphite electrode near 0.6 V vs. Li /Li^+) appears at concentrations of VEC of 4% and greater. This may indicate a change in the reaction pathway when the concentration of VEC is high enough.

Figure 5.10b shows the differential capacity versus voltage (dQ/dV vs. V) data of Figure 5.10a. The plateaus in Figure 5.10a appear as peaks in differential capacity plots. Figure 5.10b shows three sets of peaks. The first set of peak appears at 2.7 V. This corresponds

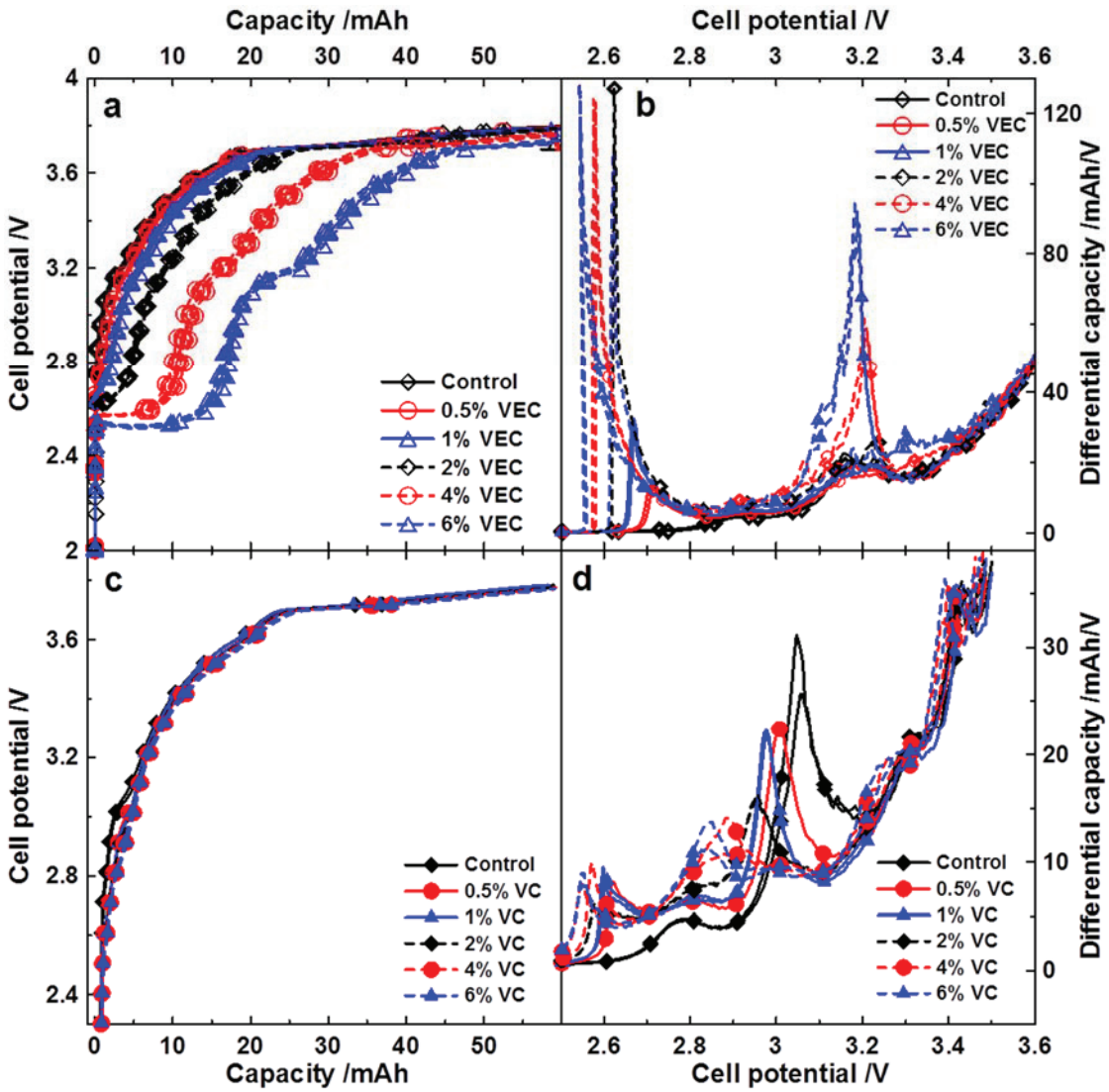

Figure 5.10 Cell terminal voltage as a function of capacity of the first 60 mAh of the first charge (during formation) (a, c) and the differential capacity as a function of cell voltage (b, d) of pouch cells containing VEC (a, b) and pouch cells containing VC (c, d). The formation was performed at 40°C. The pouch cells containing VEC have 6 replicates for each concentration; the pouch cells containing VC have 2 replicates for each concentration. The data for the VEC-containing cells were collected by Courtney Henry, Honor's student, Department of Physics and Atmospheric Science, Dalhousie University, Halifax, NS (2013).

to the reduction of VEC at the graphite surface, since it is not present for cells without

VEC. The peak at 2.7 V shifts to lower potential as the VEC concentration is increased. The second set of peaks (small; dQ/dV maximum) appears around 2.9 V in all cells, including the cells without VEC. This peak might correspond to the reduction of EC. The third set of peaks appears around 3.2 V. This peak is also present for all cells and might correspond to the reduction of EC on the graphite surface. The peak at 3.2 V is not affected by the addition of VEC from 0.5% to 2%. This indicates once again the absence of any passivation from VEC. At concentrations of 4% and 6% the peak at 3.2 V grows considerably. It is unlikely that the amount of EC reduced at the graphite surface increases with the addition of VEC. The by-products of VEC reduction might be reduced at the graphite surface at the same potential as EC and give overlapping peaks in the dQ/dV plot.

Figure 5.10c shows that the VC-containing cells do not present any extensive plateau due to VC reduction. Figure 5.10d shows three sets of peaks. The first set of peak appears around 2.6 V and is present for every VC concentration except for control. This indicates that this peak corresponds to the reduction of VC. The peak area does not seem to increase with increasing VC concentration which might indicate some sort of passivation of the graphite surface. The peak also shifts toward lower potentials as the concentration of VC increases. The second set of peaks appears around 2.8 V. This peak is present for the control cell and might correspond to the first reduction of EC. The area of the peak does not seem to grow significantly from 0% to 2% VC (apart from peak overlap). The third set of peaks appears around 3.05 V (for control) and changes slightly with the addition of VC in concentrations higher than 2%. The change is even more dramatic at

concentrations of VC of 1% and higher which might indicate a change in the reaction pathways when the concentration of VC is increased from 1% to 2%.

Figure 5.11 shows the capacity between 2.0 V - 2.9 V (a), and 2.9 V - 3.4 V (b) during

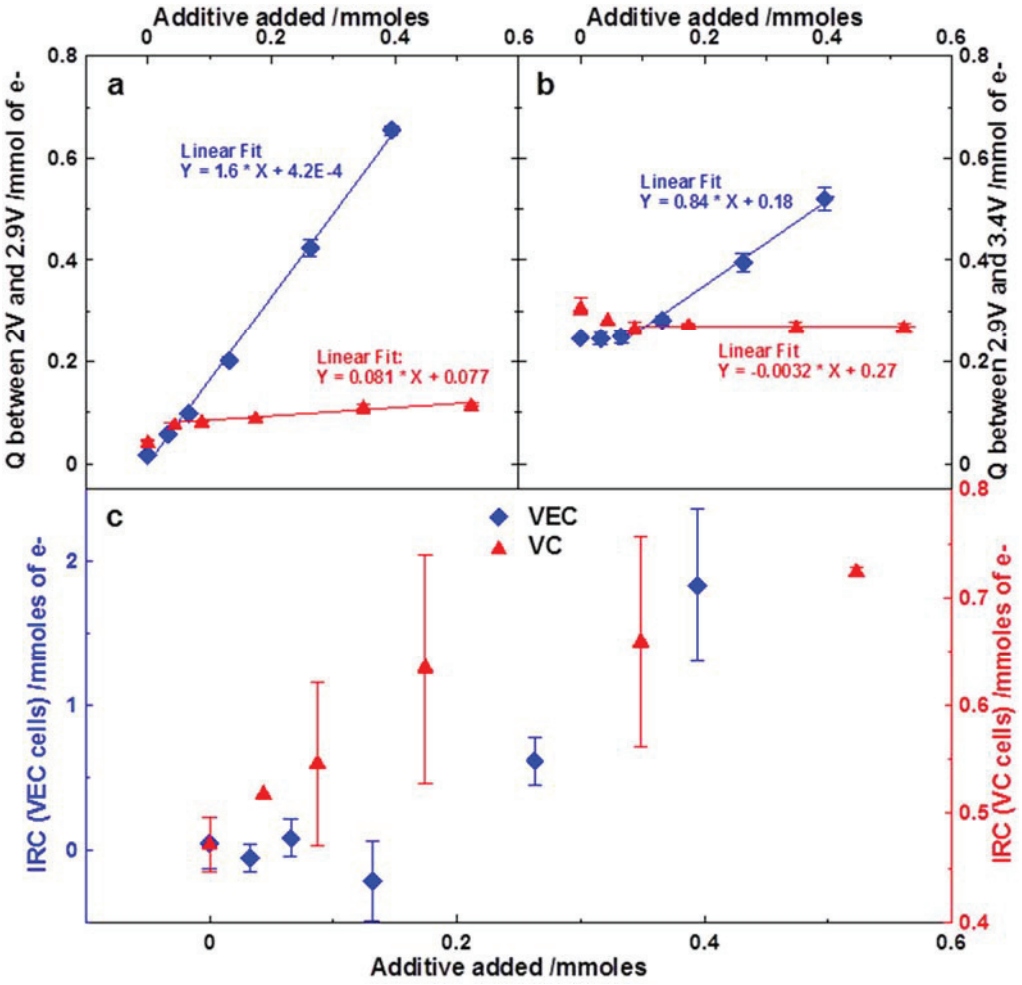

Figure 5.11 Capacity between 2 V and 2.9 V (a), and between 2.9 V and 3.4 V (b) during the first charge (formation) and irreversible capacity calculated as the capacity of the first charge minus the capacity of the second discharge (c) for VC-containing cells and VEC-containing cells. The data for the VEC-containing cells were collected by Courtney Henry, Honor's student, Department of Physics and Atmospheric Science, Dalhousie University, Halifax, NS (2012).

the first charge and the irreversible capacity (IRC) calculated as the difference between the capacity of the first charge and second discharge (due to the formation protocol). The error bars are calculated as the standard deviation of the two duplicate for the VC containing cells, and of six cells for the VEC-containing cells. The voltage range in Figure 5.11a comprises the peaks corresponding to the reduction of VEC and VC and the first peak assigned to the reduction of EC. Figure 5.11a shows that the capacity in this voltage range grows linearly with the amount of VEC added. The slope is 1.6 electrons per molecule of VEC assuming **all** VEC added to the cell is reacted. This suggests that all the VEC accessible to the negative electrode (even that initially in the separator and in the positive electrode) is reduced at the negative electrode in a two electron step (some VEC might be outside the jelly roll where the diffusion time to the negative electrode is too long leading to the measured slope of 1.6 instead of 2). VC also shows a linear behavior, however the slope is significantly smaller than for VEC (0.08 electrons per VC molecule versus 1.6 electrons per VEC molecule). The small slope (significantly less than 1 electron per VC molecule) indicates that VC does not react completely at the graphite surface.

Figure 5.11b shows the capacity between 2.9 V and 3.4 V during the first charge for cells containing different amounts of VEC and VC. The VEC-containing cells show a stable capacity from 0% to 1% and then a linear increase in capacity between 1% and 6%. This indicates a change in reaction pathways (the appearance of a new reaction) at the graphite surface. The slope fitted for the data points of the cells containing between 1% and 6% of VEC is 0.84 electrons per VEC molecule and suggests a 1 electron reaction. The VC-containing cells show two different regions. The first region shows a steep decrease in

capacity with increasing VC between 0% and 1%. The second region shows a stable capacity for cells containing between 1% and 6% VC. The initial decrease in capacity is presumably due to partial passivation of the graphite surface resulting in a decrease in the amount of EC reduced. The second region is due to the peak shifting to lower potential (lower than the 2.9 V - 3.4 V region).

Figure 5.11c shows the irreversible capacity (IRC) for the VC and VEC-containing cells. Even though the scatter is substantial, Figure 5.11c unveils a clear trend. Adding increasing amounts of VEC and VC to the cell imparts higher IRCs. The IRC for the VEC-containing cells is greater than for the VC-containing cells. The VEC-containing cells and VC-containing cells showed very different gas generation during formation. While increasing amounts of VEC produced increasing amounts of gas (the cells swelled extensively for 4% and 6% VEC), the VC-containing cells did not produce any visible amount of gas, at any concentration.

Figure 5.12 shows the charge endpoint capacity (a, d, g), discharge capacity (b, e, h) and Coulombic efficiency (CE) (c, f, i) as a function of cycle number for cells containing VEC and cells containing VC. Figure 5.12a shows the charge endpoint capacity as a function of cycle number for cells cycled at 40°C and containing different amounts of VEC. The data in Figure 5.12a has been normalized to zero capacity at the end of the first charge after the formation cycle (the second charge of the cell). The charge endpoint capacity slippage gives information about the rate of parasitic reactions at the positive electrode[9]. A steeper slope of the charge endpoint capacity as a function of cycle number is the result of a higher rate of parasitic reactions, presumably electrolyte oxidation, at the

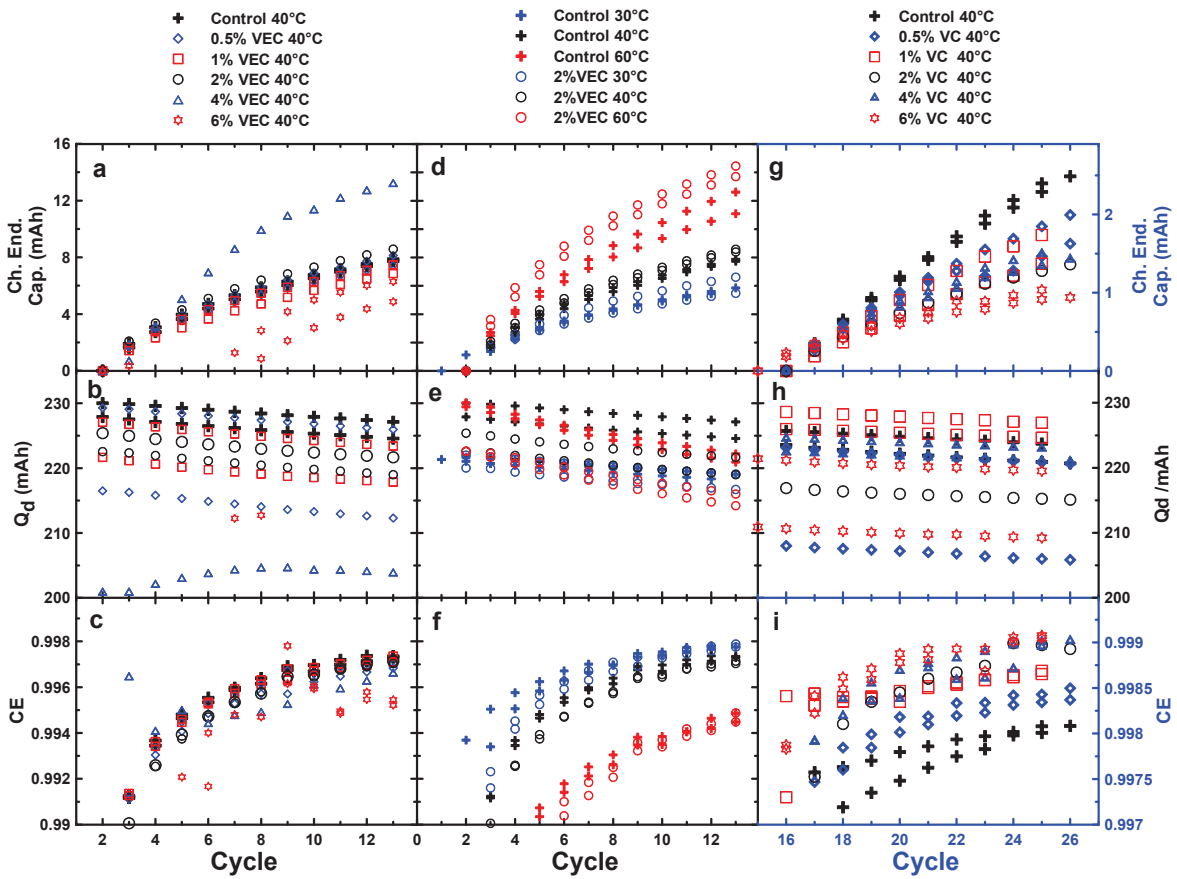

Figure 5.12 Charge endpoint capacity (a, d, g), discharge capacity (b, e, h) and Coulombic efficiency (c, f, i) as a function of cycle number for VEC-containing cells cycled at 40°C (a, b, c), control, 2% VEC cells cycled at 30°C, 40°C, 60°C (d, e, f) and VC-containing cells cycled at 40°C (g, h, i). The data for the VEC-containing cells were collected by Courtney Henry, Honor's student, Department of Physics and Atmospheric Science, Dalhousie University, Halifax, NS (2012).

positive electrode.[9] Figure 5.12a shows that VEC does not bring any apparent improvement to the rate of parasitic reactions at the positive electrode.

The charge endpoint capacity versus cycle number of the 4% VEC and 6% VEC cells are somewhat erratic which could be due to the large volume of gas produced during formation. The pouch cells have a compartment which can accommodate a certain amount of gas. In the case of the cells with the two highest VEC concentrations, the gas generated was so great that the pouches swelled extensively. This could have affected the adhesion of the active material to the current collectors which in turn could be responsible for the erratic data points in Figures 5.12a, b, and c.

Figures 5.12b and 5.12c show the discharge capacity and Coulombic efficiency, respectively, as a function of cycle number for the VEC-containing cells cycled at 40°C. The CE depends on the rate of parasitic reactions at both the positive electrode and the negative electrode.[9] Usually, a higher CE imparts a higher cycle life and calendar life. Again there is no apparent beneficial effect from the addition of VEC. Figures 5.12d, 5.12e, and 5.12f show the charge endpoint capacity, the discharge capacity and Coulombic efficiency as a function of cycle number respectively for cells containing no VEC and cells containing 2% VEC, cycled at 30°C, 40°C, and 60°C. These figures show that when formed at 40°C, VEC does not bring any improvement to the cycling of $LiCoO_2$/graphite cells pouch, at any temperature (in the range tested).

Figures 5.12g, 5.12h, and 5.12i show the charge endpoint capacity, the discharge capacity and Coulombic efficiency respectively as a function of cycle number for cells cycled at

40°C and containing various amounts of VC (after cycling first for 18 days on a "regular charger"). Figure 5.12g shows that increasing the concentration of VC increasingly reduces the charge endpoint capacity slippage. This indicates that VC has a great impact on the parasitic reactions at the positive electrode as showed by Burns et al.[3]. Based on Figure 5.12h, it is difficult to draw any conclusion about the effect of VC on the discharge capacity fade, mainly because of the scale of the axis and the fade rates of the cells. Figure 5.12i shows that introducing VC in cells improves the Coulombic efficiency at concentrations as low as 0.5%. However, the improvement in CE with increasing amounts of VC is very small at concentrations above 2%. This is in agreement with the recent work presented by Burns et al., on the impact of VC in wound Li-ion cells of various chemistries.[93]

Figure 5.13 shows a summary of the Coulombic inefficiency (CIE = 1 - CE) (a), charge endpoint slippage (slope of the charge endpoint capacity versus cycle number calculated from the last 5 measured data points) (b), short-term fade rate (slope of the discharge capacity as a function of cycle number) and polarization change per cycle (calculated as the slope of the difference of the mean voltage during charge and discharge as a function of cycle number) (d) of VC-containing cells and VEC-containing cells cycled at 40°C on the HPC. The CIE, charge slippage, fade rate, and polarization change between the control of the VEC containing cells and the VC containing cells are different. This difference is caused by the history of the cells prior to being put on the high precision charger. The VEC containing cells were put on the HPC after formation; meanwhile, the VC containing cells were put on the HPC after having been cycled for several weeks. Figures 5.13a, b and c show that VEC, alone, does not bring any improvement to the cell,

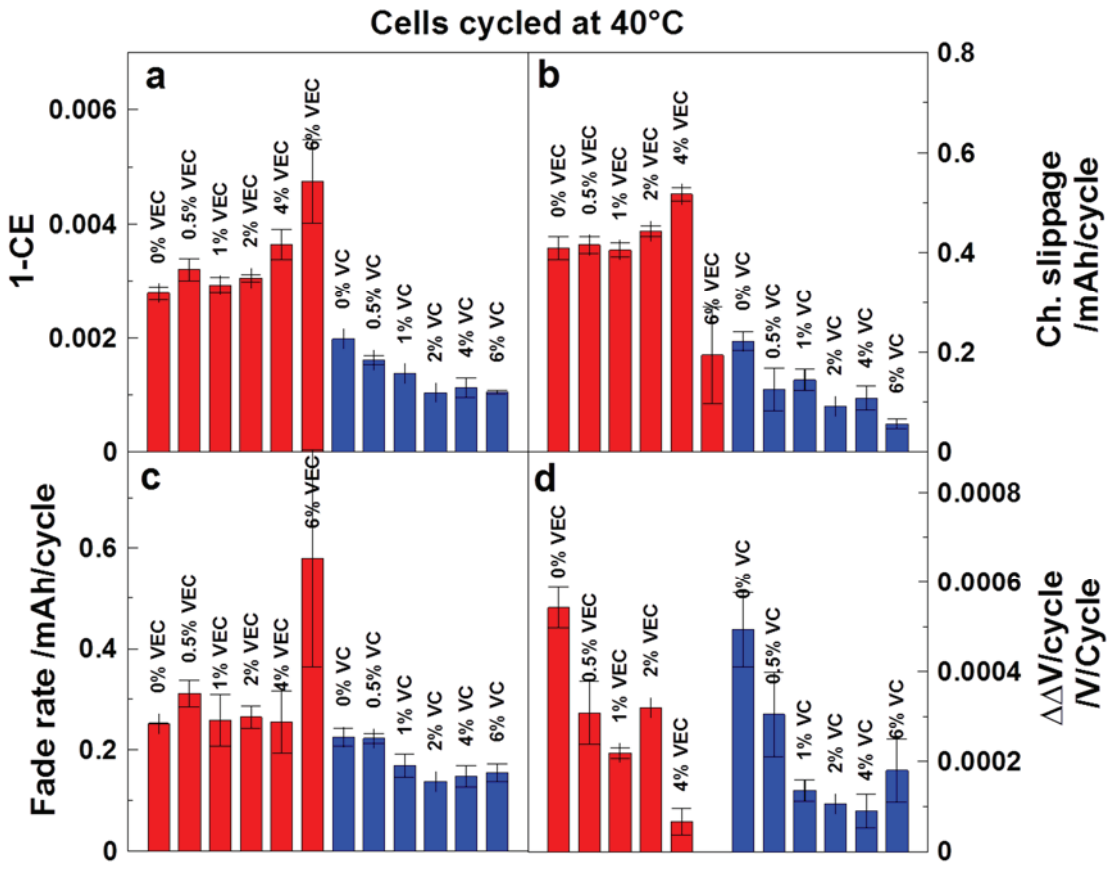

Figure 5.13 Summary of the coulombic inefficiency (CIE = 1 - CE) (a), charge endpoint slippage (b), fade rate, and polarization change per cycle (d) of cells containing VEC (red) and VC (blue) cycled at 40°C. The data for the VEC-containing cells were collected by Courtney Henry, Honor's student, Department of Physics and Atmospheric Science, Dalhousie University, Halifax, NS (2013).

whether it is in terms of CIE, parasitic reactions at the positive electrode, and fade rate. Figure 5.13d shows that adding VEC lowers the change in polarization as a function of cycle. However this advantage probably does not outweigh the disadvantages the introduction of VEC brings (gas generation, potential cost, *etc.*). Figure 5.13 shows that adding VC improves the CIE, charge endpoint slippage, fade rate and polarization change with cycle number. This shows that VC, alone, is superior to VEC, alone, at any

concentration. Figure 5.13 also shows that 2% VC offers a good compromise between CIE, charge slippage fade rate and polarization change as a function of cycle number. 6% VC brings better charge slippage and comparable CIE, however it seems to bring slightly higher fade rate (during the early life of the cell at least) and greater polarization increase during cycling.

Figure 5.14 shows the Bode plot of the area specific impedance of VEC-containing cells cycled at 30°C (a, b) and VC-containing cells cycled at 40°C (c, d). Figures 5.14a and b show that VEC does not have any significant impact on the impedance of the pouch cells in concentrations ranging from 0.5% to 2%. At concentrations of 4% VEC and 6% VEC, the impedance dramatically increases. However it is not possible to say if this feature comes from the direct reaction of VEC with one electrode or both electrodes or from the gas generated and possible damage of the electrode during the formation cycle. Figures 5.14c and d show that VC has a significant impact on the impedance, even at low concentration. The appearance of a second time constant between 10 Hz and 100 Hz indicates that the contribution to the impedance changes going from 1% to 2% VC. However it is not possible to assess which time constant belongs to which electrode.

Figure 5.15 shows the Bode plot of half of the average area specific impedance of the negative symmetric cells, reconstructed from the electrodes of pouch cells containing various amount of VEC (a, b) and various amounts of VC (c, d). The error bars are calculated as the standard deviation of the data points of each replicate. Figures 5.15a and 5.15b show that the impedance of the negative electrode of cells containing VEC is not significantly different from the impedance of the cells containing no VEC. This indicates

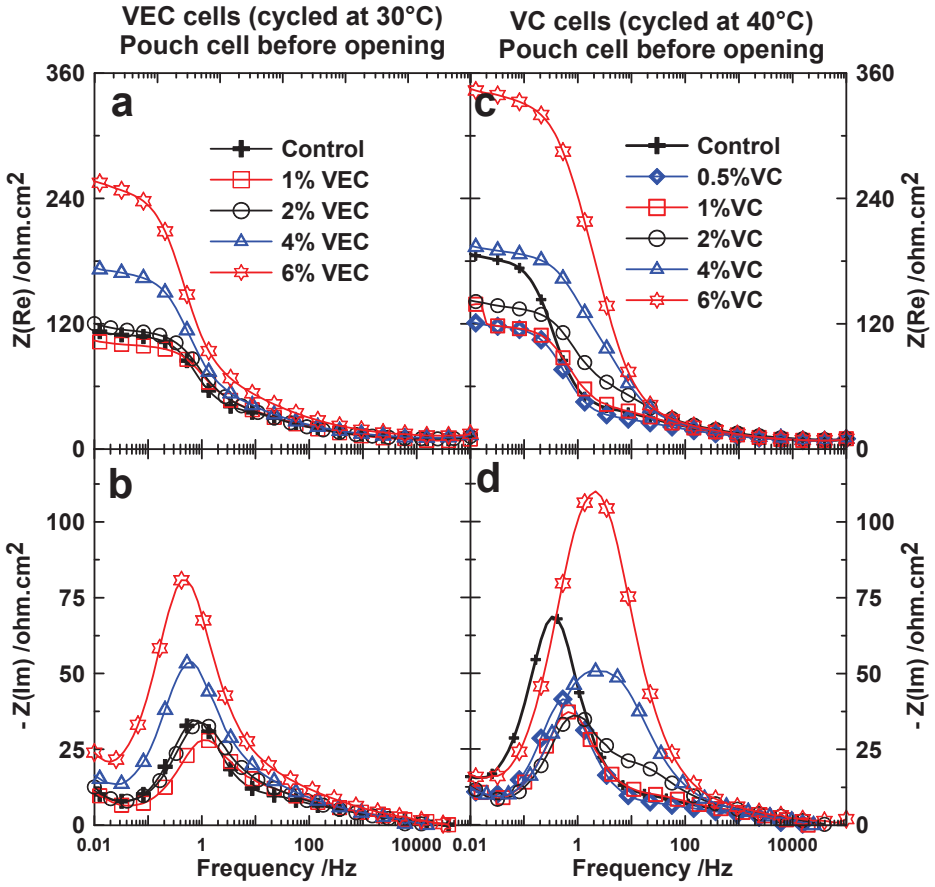

Figure 5.14 Area-specific real impedance (a, c) and area-specific negative imaginary impedance as a function of the logarithm of the frequency (b, d) for pouch cells containing VEC (a, b), and VC (c, d) before opening. All EIS measurements were done at 10°C. The data for the VEC-containing cells were collected by Courtney Henry, Honor's student, Department of Physics and Atmospheric Science, Dalhousie University, Halifax, NS (2013).

that VEC does not affect the surface of the negative electrode in these experimental conditions (formation at 40°C and cycling between 2.8 V and 4.2 V at 30°C). This indicates that none of the by-products of the reaction of VEC during the first cycle precipitated on the graphite surface which is consistent with the results in Figures 5.10 and 5.11. One should keep in mind that the gas evolving during the formation cycle is

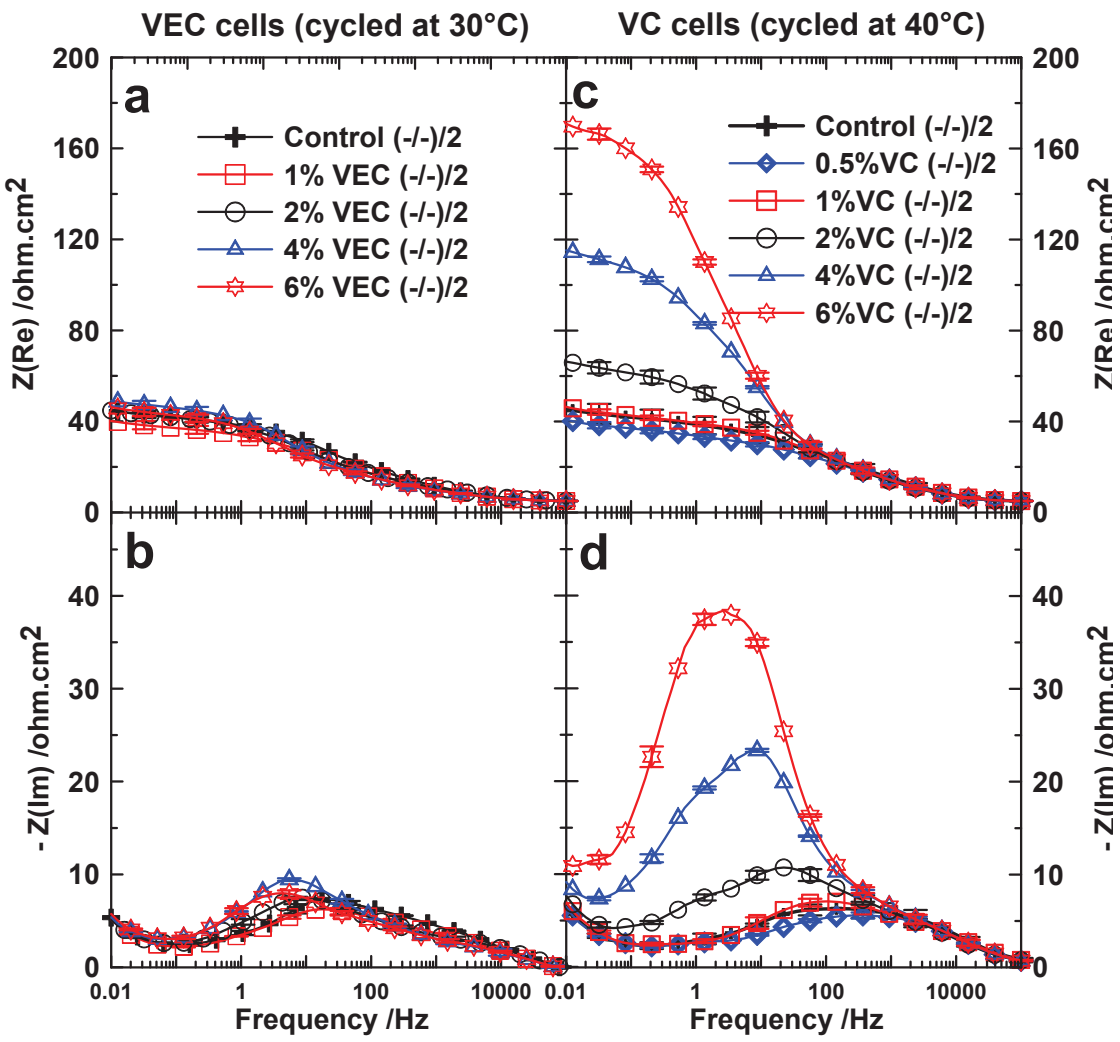

Figure 5.15 Average area-specific real impedance (a, c) and average area-specific negative imaginary impedance (b, d) as a function of the logarithm of the frequency of negative symmetric cells reassembled from pouch cells containing VEC and cycled at 30°C (a, b), and containing VC cycled at 40°C (c, d). All EIS measurements were made at 10°C. The data for the VEC-containing cells were collected by Courtney Henry, Honor's student, Department of Physics and Atmospheric Science, Dalhousie University, Halifax, NS (2012)

removed during the de-gassing step. Hard can cells, such as for the experiments described in sections 5.1 and 5.2 can withstand great pressure. At high pressure, the solubility of gases is higher than at low pressure. On the contrary, pouch cells are made of a soft

plastic envelope that expands when gas is generated. This does not allow great pressure to develop in the cell and prevent the gaseous compounds from solubilizing in the electrolyte. It is possible that the gaseous compounds generated during the reduction of VEC at the graphite surface are key for the development of a good SEI. Further studies should be carried to determine whether these gaseous compounds play a role in the development of the SEI.

Figures 5.15c and 5.15d show that the impedance of the negative electrode is not affected by addition of VC up to 1% VC. At concentrations of 2% and higher, the impedance of the negative electrode increases with increasing amount of VC. This indicates that VC does not affect the negative electrode significantly at concentrations lower than 2%. One can also notice that the concentration of VC at which the change of the negative electrode impedance occurs corresponds to the concentration where the dQ/dV peaks in the early times of the first charge (see Figure 5.10) start to change significantly.

Figure 5.16 shows the Bode plot of half of the average area specific impedance of the positive symmetric cells, calculated from the impedance of the full cells and negative symmetric cells reconstructed from the electrodes of the pouch cells containing various amounts of VEC cycled at 30°C (a, b), and of the area specific impedance of positive symmetric cells reconstructed from pouch cells containing various amounts of VC and cycled at 40°C (c, d). The error bars are calculated as the standard deviation of the data points of each replicate. The positive electrode containing the control electrolyte for the cells cycled at 30°C was damaged during the process of the pouch cell opening and cell reconstruction. For that reason no data is presented in Figures 5.16a and b for the control

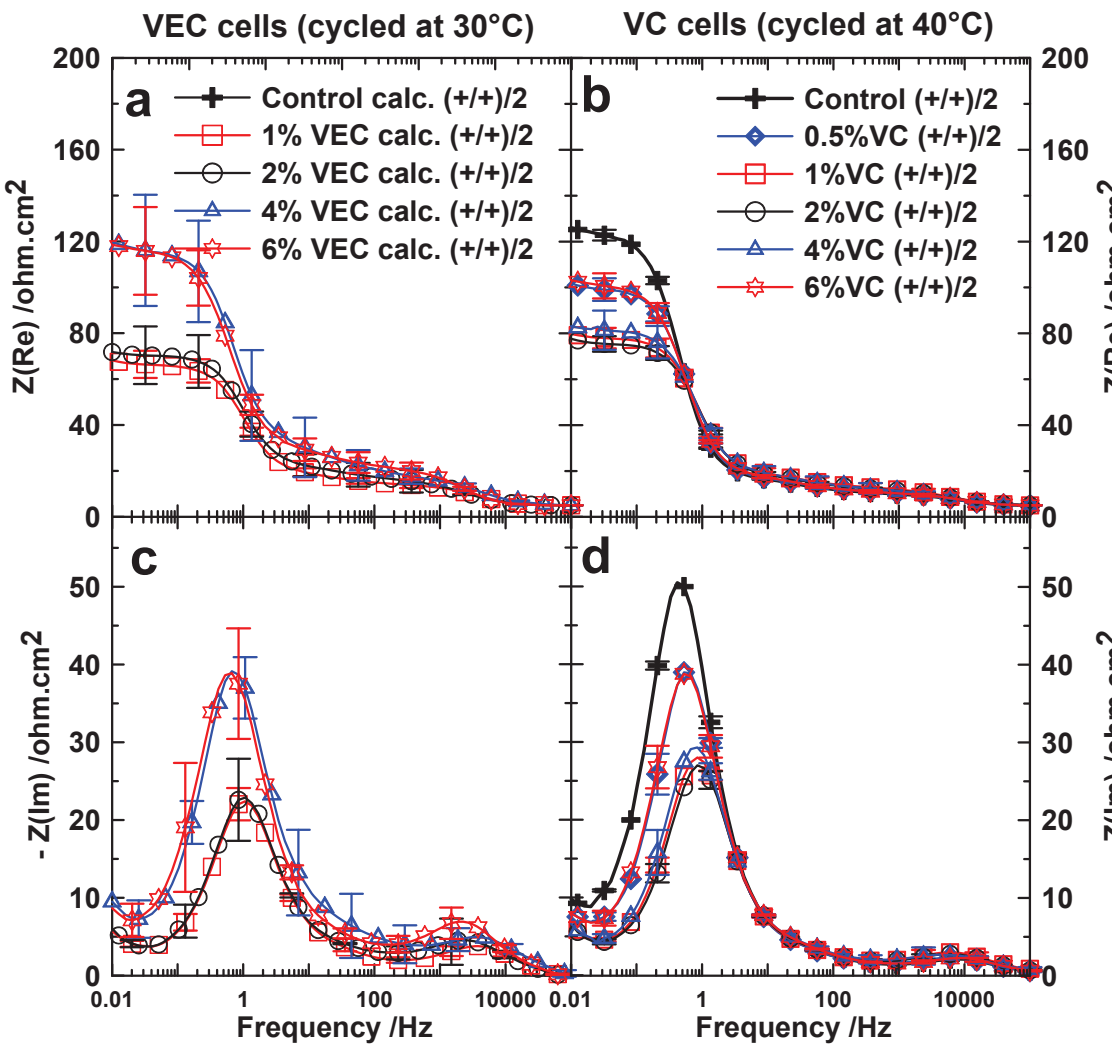

Figure 5.16 Average area-specific real impedance (a) and average area-specific negative imaginary impedance (b) as a function of the logarithm of the frequency of the positive symmetric cells containing VEC, calculated from full cells and negative symmetric cells reassembled from pouch cells containing VEC and cycled at 30°C. Area-specific real impedance (c) and area-specific negative imaginary impedance (d) as a function of the logarithm of the frequency of positive symmetric cells reassembled from pouch cells containing VC cycled at 40°C. All EIS measurements were made at 10°C. The data for the VEC-containing cells were collected by Courtney Henry, Honor's student, Department of Physics and Atmospheric Science, Dalhousie University, Halifax, NS (2013).

cell. However, since the impedance spectra of the pouch cells containing no VEC, 1% VEC, and 2% VEC were almost identical and the impedance spectra of the negative symmetric cells reconstructed from the same pouch cells were also almost identical, the impedance of the positive electrode of the control cell should then be very similar to the impedance of the cells containing 1% VEC and 2% VEC. Figures 5.16a and 5.16c show that VEC does not have any impact on the impedance of the positive electrode in concentrations between 0% to 2%. At concentrations higher than 4%, the impedance of the positive electrode increases a lot. This might be due to either to VEC reacting at the positive electrode or electrode damage due to gassing during formation. One has to notice that this increase in the positive electrode impedance happens at the same concentration where the sharp rise of the dQ/dV peak at 3.2 V appeared. This rise in the positive electrode impedance might come from a reaction and precipitation at the positive electrode of the products of the reduction seen in Figure 5.10b around 3.2 V. Even though VEC might have an impact on the surface of the positive electrode, this change does not bring any improvement to the cycling performances of the cell.

Figures 5.16b and d show that VC affects the positive electrode in all concentrations tested. Adding VC to the cell initially decreases the impedance of the positive electrode. However, at concentration higher than 2% VC, the impedance of the positive electrode starts to rise again. This might indicate a change in the reaction pathway VC undertakes when present in higher concentration. It is also at this particular concentration that the peak around 3 V in the dQ/dV vs. V plot during the first cycle starts to change drastically.

Figure 5.17 shows the charge transfer resistance of cells containing different amounts of VC at 10°C normalized to the R_{ct} of the control cell as a function of VC content (in wt.%) for prismatic wound LCO/graphite charged to different voltage cut-offs, NMC/graphite cells made by Medtronic (presented in sections 5.1 and 5.2), LCO/graphite pouch cells (presented in section 5.3) and NMC/graphite 18650 cells (hard stainless steel can). The pouch cells, prismatic wound cells and 18650 cells had different electrolyte mass to active material mass ratios and different solvent compositions. Figure 5.17 shows that the total R_{ct} of cells containing VC presents the same trend with increasing amount of VC, no matter what the cell chemistry is. That is a decrease of the R_{ct} with low VC concentration, and an increase of the R_{ct} at higher VC concentration. However, the concentration at which the minimum in the total R_{ct} appears is not the same for all cell types. Figure 5.18 shows the charge transfer resistance (R_{ct}) of cells containing different amount of VC at

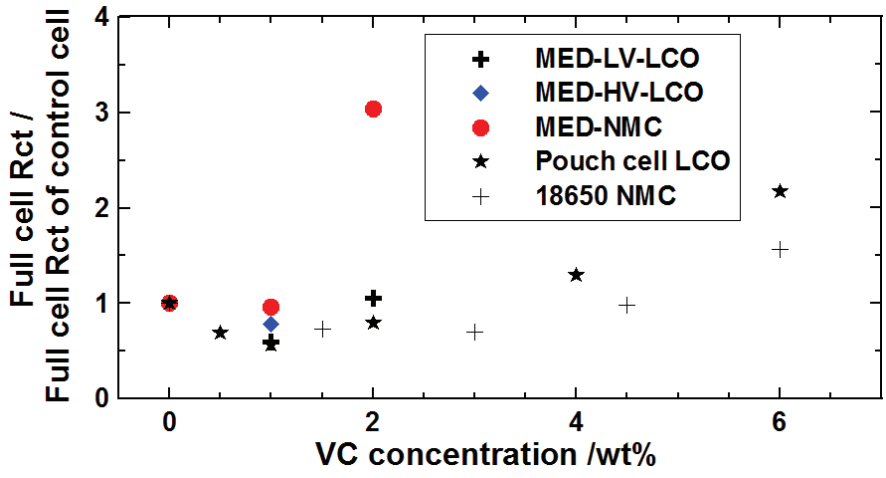

Figure 5.17 Charge transfer resistance (R_{ct}) of cells containing different amount of VC at 10°C normalized to the R_{ct} of the control cell as a function of VC content (in wt.%) . The EIS measurements for the 18650 NMC cells were made by Chris Burns, PhD candidate and Nupur Sinha, PDF, Department of Physics and Atmospheric science, Dalhousie, Halifax, NS (2013).

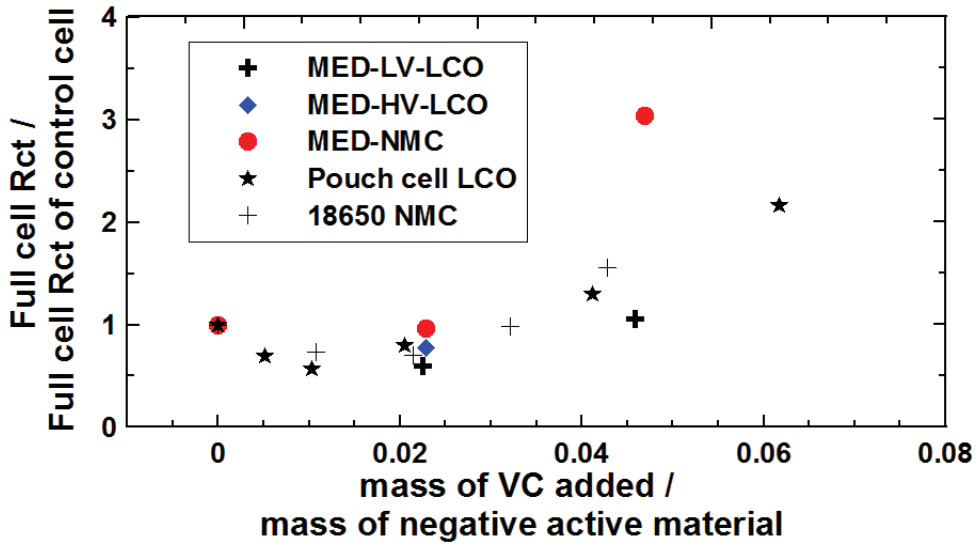

Figure 5.18 Charge transfer resistance (R_{ct}) of cells containing different amount of VC at 10°C normalized to the R_{ct} of the control cell as a function of the ratio of the mass of VC added in the cell to the mass of negative active material. The EIS measurements for the 18650 NMC cells were made by Chris Burns, PhD candidate and Nupur Sinha, PDF, Department of Physics and Atmospheric Science, Dalhousie, Halifax, NS (2013).

10°C normalized to the R_{ct} of the control cell as a function of the ratio of the mass of VC added in the cell to the mass of negative active material. Figure 5.18 shows that the minimum in the total R_{ct} of cells containing VC appears at the same ratio of the mass of VC added to the cell to the mass of negative material. This indicates that the ratio of the mass of additive added (in the case of VC at least) to the mass of active material matters, and not the concentration. One has to note that the mass of negative active material has been arbitrarily chosen instead of the mass of positive active material. That is because the ratio of the mass of negative active material to the mass of active positive material is very similar from one cell configuration to the other.

Figure 5.19 shows the value of the charge transfer resistance (R_{ct}) of the positive electrode and negative electrode of cells containing various amounts of VEC (a, b) and VC (c, d). R_{ct} represents the resistance to the transfer of Li^+ from the electrolyte to the electrode (passing through the SEI). The value of the R_{ct} was calculated by fitting the impedance spectra shown in Figure 5.15 and Figure 5.16 with the equivalent circuit model proposed by Atebamba et al.[90] shown in Figure 5.3. Figures 5.19a and 5.19b show

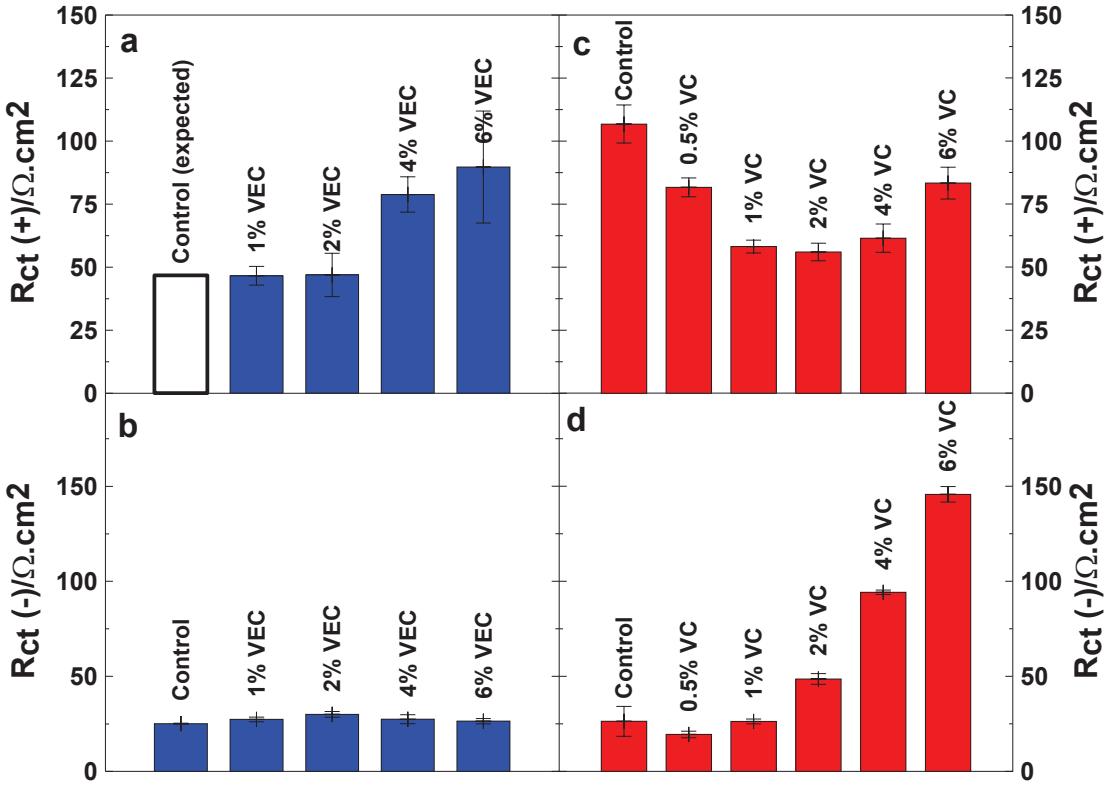

Figure 5.19 Charge transfer resistance of the positive electrode of pouch cells containing VEC cycled at 30°C (a), of cells containing VC cycled at 40°C (b), and charge transfer resistance of the negative electrode of pouch cells containing VEC and cycled at 30°C (c), of cells containing VC and cycled at 40°C (d) obtained by fitting the area specific electrochemical impedance spectra shown in Figures 5.14 and 5.16 using the equivalent circuit proposed by Atebamba et al.[90]

that VEC does not affect the negative electrode at all concentrations tested and that it affects the positive electrode when present at high concentration. Figure 5.19c shows that VC affects the positive electrode when present at all concentrations, even at concentrations as low as 0.5%. Figure 5.19d shows that VC affects the negative electrode mainly at concentration higher than 1%. Figures 5.19c and 5.19d indicate that introducing VC at concentration higher than 2% gives high impedance and might affect the power capability of the cell. Figure 5.19c and d support the findings on VC-containing Medtronic cells. At low concentration, VC has a great impact on the positive electrode and almost no effect at the negative electrode. At higher concentration, VC has a great impact on the negative electrode.

5.3.3 CONCLUSION

The effects of VC and VEC on the cycling performance and on the surface of the electrodes of machine-made $LiCoO_2$/graphite pouch cells have been probed using high precision coulometry and EIS on symmetric cells reconstructed from the electrodes of pouch cells. High precision coulometry measurements showed that VEC, alone, does not have any beneficial impact on the cycling performance at any temperature (30°C - 60°C) for the cell design tested and produced great amounts of gas during the formation cycle. VC yields better Coulombic efficiency, lower parasitic reaction rate at the positive electrode and good capacity retention. EIS on symmetric cells showed that VEC had no impact on the negative electrode at any concentration tested and modified the positive electrode surface at concentrations higher than 4%. VC impacts the positive electrode at every concentration tested and had an impact at the negative electrode at concentrations

higher than 1%. The study revealed that adding 2% VC to the electrolyte offers a good compromise between Coulombic efficiency, rate of parasitic reactions at the positive electrode, capacity retention, and impedance. It also revealed that VEC brings only drawbacks when added alone to $LiCoO_2$/graphite pouch cells.

5.4 STUDY OF THE EFFECT OF VC AND TMOBX IN LCO/GRAPHITE POUCH CELLS BY EIS ON SYMMETRIC CELLS AND HIGH PRECISION COULOMETRY

In order to test if the effect of TMOBX and VC is the same on different cell configurations, machine-made pouch cells were filled with different amounts of VC and TMOBX. The ratios of VC and TMOBX introduced in the pouch cells were not studied in the prismatic wound cells made by Medtronic. The concentration range of VC and TMOBX used were selected to be equivalent to 1% VC and 0.3% TMOBX in the Medtronic cells in terms of ratio of the mass of additive added to the mass of negative active material. This concentration range was chosen to attempt to achieve a low impedance cell with good cycling performance as per the findings made in the Medtronic cells presented in sections 5.1 and 5.2. The following section presents the results of the high precision coulometry measurements and EIS on symmetric cells study.

5.4.1 EXPERIMENTAL

Machine-made 225 mAh $LiCoO_2$/graphite wound pouch cells were filled with 0.75 g of 1 M $LiPF_6$ in EC:EMC (BASF) in a ratio of 3:7 by weight as control electrolyte and electrolytes containing different additive amounts of VC and TMOBX. Once filled, the pouch cells were centrifuged, formed and de-gassed following the method described in section 3.3. The pouch cells were then connected to the High Precision Charger (HPC) built at Dalhousie University[8] where cells were cycled at 40°C for ~450 hours at a current of 15 mA (~C/15) to measure Coulombic efficiency and charge endpoint capacity slippage. The cells were then stored in a fridge (~ 1°C) at an open circuit potential of 3.80

V until used for the EIS on symmetric cells study. The EIS on symmetric cells study was performed following the method described in Chapter 3.

5.4.2 RESULTS AND DISCUSSION

Figure 5.20 shows the values of the Coulombic inefficiency (CIE = 1 – CE) (a), charge endpoint capacity slippage (b), fade rate (c), and polarization change per cycle (d) for pouch cells containing various combinations of VC and TMOBX. The Coulombic inefficiency was calculated as the average of the CIE of cycles 13 to 15. The charge endpoint capacity slippage was calculated as the slope of the charge endpoint capacity versus cycle number, from cycles 11 to 15, the fade rate was calculated as the slope of the discharge capacity as a function of cycle number from cycles 11 to 15, and the polarization change per cycle was calculated as the slope of the difference of the average voltage of the charge and discharge as a function of cycle number, from cycles 11 to 15. The error bars were calculated as the standard deviation of the values of the pair cells. Figure 5.20a shows that adding incremental amounts of TMOBX to the cells increases the CIE (bad) up to 0.3% and then decreases the CIE. However from 0.3% TMOBX to 0.53% TMOBX, the CIE does not decrease below the value of the CIE of the control cell. Adding 2% VC to a control electrolyte greatly improves the CIE, and adding TMOBX to the cell containing VC does not impact the CIE very much, up to 0.3% TMOBX. Adding 0.6% TMOBX to a cell containing 2% VC makes the CIE worse (almost on par with control). Cells containing 1% VC and 0.3% TMOBX have a higher CIE than cells containing 2% VC and 0.3% TMOBX which is not surprising based on the results of section 5.3 (2% VC shows better CIE, charge slippage and fade rate than 1% VC). Cells

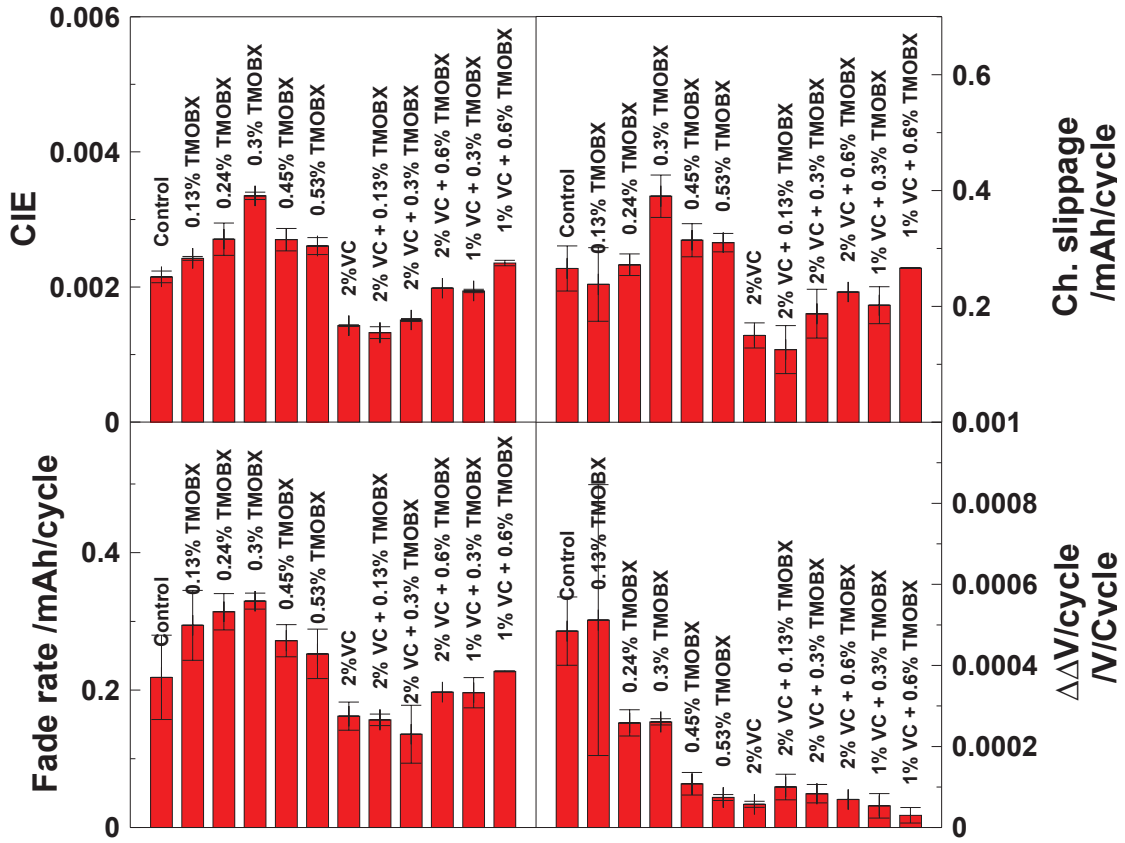

Figure 5.20 Coulombic inefficiency (CIE) (a), charge endpoint capacity slippage (b), fade rate (c), and polarization change per cycle (d) for pouch 220 mAh cells containing various combinations of VC and TMOBX

containing 1% VC and 0.6% TMOBX have a higher CIE than the cell containing 1% VC and 0.3% TMOBX as was the case for cells containing 2% VC with 0.3% and 0.6% TMOBX.

Figure 5.20 b shows that adding incremental amounts of TMOBX increases the charge slippage (increases the rate of electrolyte oxidation at the positive electrode) up to 0.3% TMOBX. At concentrations higher than 0.3% TMOBX, the charge slippage seems to get smaller. The change in the way TMOBX affects the charge slippage with concentration

follows the same trend as the way it affects the CIE. This could indicate a change in the SEI composition that TMOBX produces at either electrode. Adding 2% VC to a control electrolyte greatly improves the charge slippage as shown in section 5.3. Adding 0.13% TMOBX to a cell containing 2% VC does not seem to affect the charge slippage, and adding 0.3% or 0.6% TMOBX seem to make it worse.

Figure 5.20c shows the same trend in the effect of TMOBX and VC on the fade rate than on the CIE and charge slippage. That is, incremental amounts of TMOBX added to the cell, up to 0.3% makes the cell capacity fade more quickly. However, the fade rate seems to get better with addition of more TMOBX, without getting better than the control. Adding 2% VC again makes the fade rate a lot better and the addition of up to 0.3% TMOBX does not seem to affect the fade rate. Adding 0.6% TMOBX to 2% VC makes the fade rate worse than 2% VC (but better than control). Cells with 1% VC and TMOBX (0.3% and 0.6%) have a greater fade rate than cells with 2% VC and TMOBX (0.13%, 0.3%, and 0.6%).

Figure 5.20d shows the polarization change per cycle. A high polarization means that the there is a significant difference between the mean voltage during charge and the mean voltage during discharge and is essentially the equivalent of the impedance measured using a direct current. A positive polarization change as a function of cycle number means that the polarization increases during cycling and that the cell power capability drops. A low polarization change with cycle number is then preferred. Figure 5.20 shows that adding TMOBX reduces the polarization change with cycle number. However it does

not reduce it as much as adding 2% VC does. Adding TMOBX to a cell containing 2% VC seems to increase slightly the polarization change.

Figure 5.21 shows the Bode representation of the area-specific impedance of cells containing various amounts of TMOBX (a), and various amounts of TMOBX and VC (b), after cycling for ~450 h at 40°C. Figure 5.21a shows that adding incremental amounts of TMOBX has different effects on the cell impedance. Generally adding TMOBX to the cell reduces the impedance, except for 0.24%. It is not clear if the inconsistency in the effect of TMOBX with concentration at 0.24% is real or due to some other factors. Starting at a concentration of 0.45% TMOBX, a new feature around 50 Hz appears. The feature in the impedance spectra associated to the transfer of Li^+ through the SEI generally appears at higher frequency for the negative electrode compared to the positive electrode. This new feature appearing around 50 Hz might then be a growth of the negative electrode R_{ct}. It is also at this particular concentration that the effect of TMOBX on cycling performance starts to be significant (CIE, charge slippage, and fade rate all begin to decrease).

The difference in impedance between the control cell and the cell containing TMOBX is not as dramatic as the difference seen in the Medtronic cell presented in sections 5.1 and 5.2. However the pouch cells have been cycling for only 450 h and stored at ~1°C, whereas the Medtronic cells have been stored around 3.9 V at room temperature for about a year. As shown in figure 5.20d, the change in polarization is faster in the control cell than in the cells containing TMOBX. Based on this trend, storing the pouch cells for a

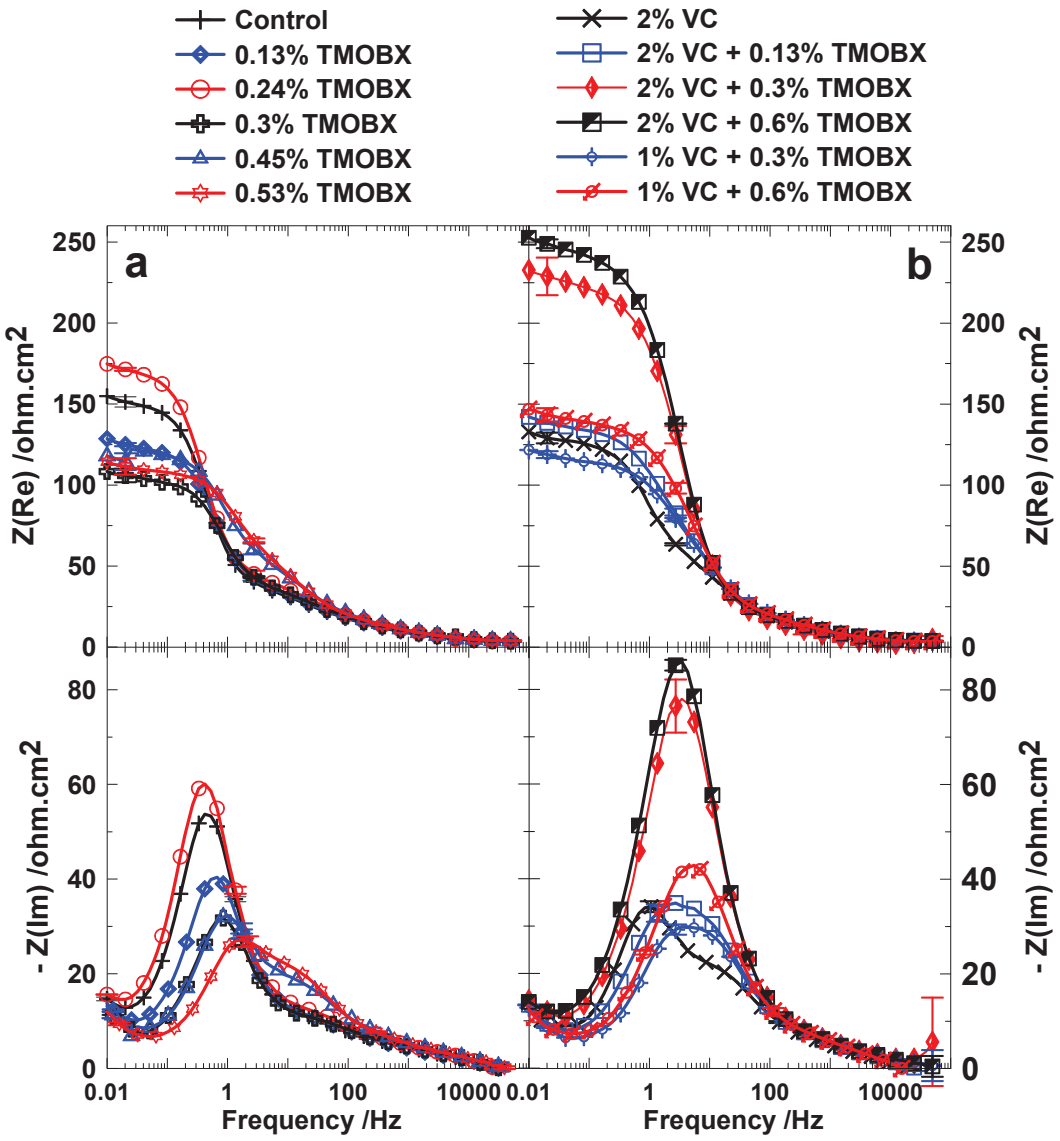

Figure 5.21 Bode representation of the area-specific impedance of $LiCoO_2$/graphite pouch cells containing various amounts of TMOBX (a), and various amounts of TMOBX and VC (b), after cycling for ~450 h at 40°C. All measurements were made at 10°C

longer period of time at room temperature might have made the difference in impedance between the control cell and the cells containing TMOBX greater.

In order to determine at which electrode TMOBX alone and combinations of TMOBX and VC act, selected cells have been opened and symmetric cells have been reconstructed following the procedure described in Chapter 3.

Figure 5.22 shows the Bode representation of the average impedance of the negative symmetric cells reconstructed from pouch cells containing VC alone or TMOBX alone (a, b) and combinations of VC and TMOBX (c, d). The error bars are calculated as the standard deviation of the data points of each replicate. Figures 5.22a and b show that TMOBX has different effect on the negative electrode impedance depending on its concentration. The impedance of the negative electrode of cells containing 0.45% TMOBX is greater than the impedance of the negative electrode of cells containing lower TMOBX concentration. This is consistent with the study of Burns et al.[10] made on the effect of TMOBX on the impedance of graphite in graphite/Li half cells. However, the impedance of the negative electrode of cells containing 0.24% TMOBX is greater than the impedance of cells containing 0.3% TMOBX.

The impedance of the negative electrode of cells containing 0.24% TMOBX being higher than the impedance of the negative electrode of cells containing 0.3% TMOBX could come from several factors. The first factor could be a difference in water content present in the cells. Cells containing 0.3% TMOBX and 0.24% TMOBX were filled on two different occasions. It is possible that the water content of the cells used for the two different TMOBX concentrations was different. Differences in water content for such a low additive concentration might have a big impact as TMOBX reacts with water. For instance, water measurements done on a dry pouch cell indicated the presence of about 1

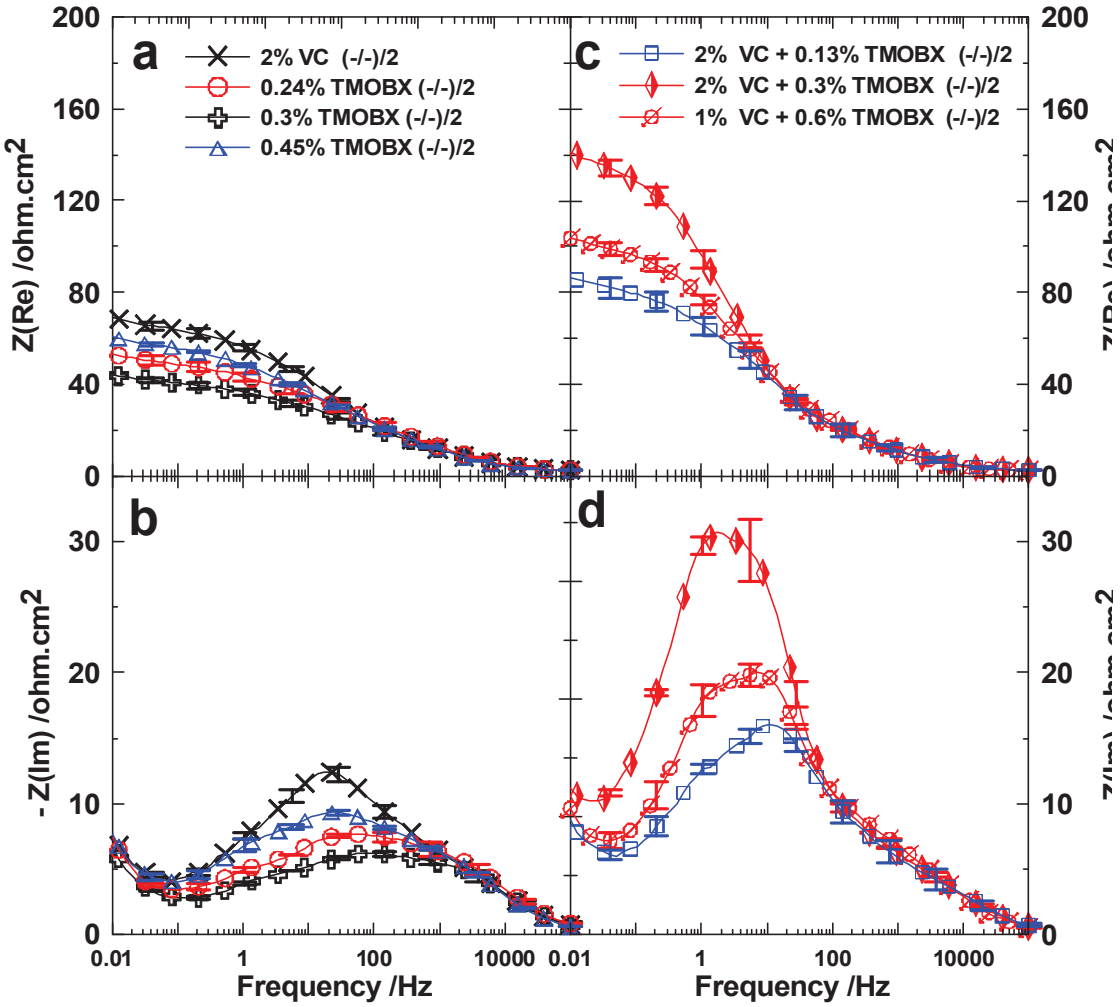

Figure 5.22 Average area-specific real impedance (a, c) and average area-specific negative imaginary impedance (b, d) as a function of the logarithm of the frequency of negative symmetric cells reassembled from pouch cells containing VC **or** TMOBX and cycled at 30°C (a, b), and containing VC **and** TMOBX cycled at 40°C (c, d). All EIS measurements were made at 10°C.

mg of water adsorbed on the electrodes. A concentration of 0.24% TMOBX corresponds to a total mass of 1.8 mg of TMOBX introduced in the cell (assuming that the cells were filled with 0.75 g of electrolyte). This corresponds to a ratio of about 0.5 by mass water-

TMOBX. A difference in the water content of cells from one batch to the other could then have an effect on the way TMOBX affects the surface of the electrodes.

Figures 5.22a-d show that the effect of the addition of TMOBX and VC on the negative electrode impedance when introduced together is very different from the effect of VC alone or TMOBX alone. This is not consistent with the findings presented in sections 5.1 and 5.2. The difference in the effect again could arise for different reasons. The first reason could be the difference in the ratio of the mass of additive added to the mass of active negative material. It was shown in section 5.3 that the effect of VC on the impedance of the cells depends on the ratio of the mass of additive to the mass of active material (see Figures 5.17 and 5.18). Based on the difference in the ratio of mass of electrolyte to active material added in the pouch cells compared the ratio in the Medtronic cells presented in sections 5.1 and 5.2, a concentration of 2% VC and 0.3% TMOBX in the pouch cells would correspond to 1% VC and 0.15% TMOBX in the Medtronic cells. It is possible that in this concentration range, VC does not control the negative electrode SEI formation anymore and that both additives play a role in it. Moreover, the water contents of the two cell configurations (pouch cells and Medtronic cells) might be different. The two cell configurations are also treated differently. While the gas produced during the first cycle is removed from the pouch cells, the gas produced in the cells made by Medtronic is not. The gas produced during the first cycle such as carbon dioxide, or ethylene might play an important role in the formation of the SEI. The removal of the gas generated during the first cycle in the pouch cells might then alter the way additives affect each electrode. The cell configurations also had different negative material particle

morphologies (spherical versus slab-shaped), and slightly different upper cut-off potentials.

Figures 5.22c and d also show that increasing the concentration of TMOBX in a cell containing 2% VC and 0.13% TMOBX imparts greater impedance to the negative electrode. This again indicates that TMOBX has an impact on the negative electrode surface in these cells. Finally, Figures 5.22c and d show that cells containing 1% VC and 0.6% TMOBX have lower negative electrode impedance than 2%VC and 0.13% or 0.3% TMOBX. This indicates again that VC plays also a role in the composition of the SEI at the negative electrode.

Figure 5.23 shows the Bode representation of the average impedance of the positive symmetric cells reconstructed from pouch cells containing VC alone or TMOBX alone (a, b) and mixes of VC and TMOBX (c, d). The error bars are calculated as the standard deviation of the data points of each replicate. Figures 5.23a and b show that the impedance of the positive electrode of cells containing 0.3% TMOBX and 0.45% TMOBX is identical and significantly lower than the impedance of the positive electrode of cells containing 0.24% TMOBX. Figures 5.23c and d show that the impedance of the positive electrode of cells containing mixtures of VC and TMOBX is smaller than the impedance of cells containing VC only or TMOBX only. This indicates again that both additives play a role in the formation of the SEI at the positive electrode. This is somewhat different from the findings presented in sections 5.1 and 5.2. The difference in the way TMOBX and VC control the impedance at the positive electrode in the pouch

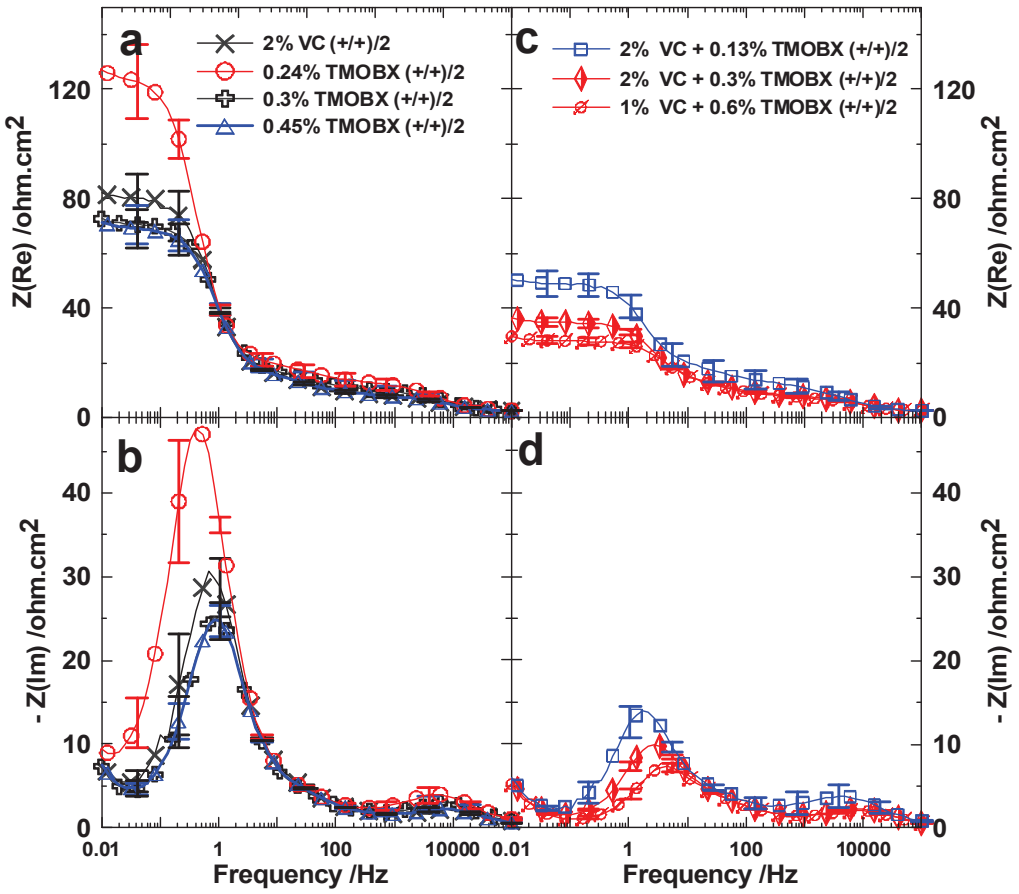

Figure 5.23 Average area-specific real impedance (a, c) and average area-specific negative imaginary impedance (b, d) as a function of the logarithm of the frequency of positive symmetric cells reassembled from pouch cells containing VC **or** TMOBX and cycled at 30°C (a, b), and containing VC **and** TMOBX cycled at 40°C (c, d). All EIS measurements were made at 10°C.

cells and in the wound prismatic cells made by Medtronic could arise for the same reasons enumerated previously for the negative electrode impedance.

5.4.3 CONCLUSION

The effects of TMOBX and combinations of VC and TMOBX on the cycling performance and on the electrode impedance in LCO/graphite pouch cells have been

investigated used high precision coulometry and EIS on symmetric cells. Cells containing TMOBX showed worse cycling performance (CE, charge slippage) and similar impedance at 10°C compared to cells containing 2% VC. It has been shown that adding TMOBX to cells containing VC does not improve the cell cycling performance in any way as opposed to the great impedance decrease imparted by the addition of TMOBX to VC-containing cells in the wound prismatic cells in sections 5.1 and 5.2.

EIS on symmetric cells showed that TMOBX (when introduced alone in the cell) seems to increase the impedance of the negative electrode at high concentrations. At lower concentrations, the effect of TMOBX does not seem to follow specific rules. It was proposed that this might come from different water contents in the cells used for this study. EIS on symmetric cells also showed that both VC and TMOBX seem to control the formation of the SEI at the positive and negative electrode as opposed to the findings presented in sections 5.1 and 5.2. It was proposed that this difference in behavior might come from differences in water content, differences in particle morphology (surface areas), and differences in additive concentration range. Further studies should be carried to reveal the origin of the different behavior of the combination of TMOBX and VC in pouch cells and in prismatic wound cells. Cells with similar ratios of additive mass to active material mass between the prismatic wound cells presented in sections 5.1 and 5.2 and the pouch cells should be tested.

CHAPTER 6. CONCLUSION

A method using electrochemical impedance spectroscopy (EIS) on symmetric cells has been developed to study the effects of additives at the negative and positive electrodes separately.

A brief review on EIS in Li-ion cells and the relation between the impedance of a cell and the impedance of each electrode was presented in Chapter 3. In the same chapter, the experimental details of the method that allows the impedance of the positive and negative electrode from a commercial cell to be measured independently have been presented. This technique uses machine-made cells containing long electrodes. The long electrodes of the cell were salvaged to reconstruct positive symmetric cells and negative symmetric cells. The impedance of the symmetric cells was measured to determine the effects of additives at the negative and positive electrodes separately.

Chapter 4 presented the experimental details of the method proposed in the previous chapter. The proposed method allows the electrodes to be salvaged without any damage and offers good cell to cell reproducibility thanks to the machine-made cells. Chapter 4 also explored the origins of the different features of the impedance spectra of the positive and negative electrodes using different cell configurations and electrodes at different states of charge. It has been shown that the impedance spectra of both electrodes can be separated into three different frequency ranges. At high to medium frequency, the impedance mainly comes from the contact resistance between the current collector and the active material as proposed by Gaberscek et al.[85], and from the diffusion of Li^+ in the

electrolyte in the pores of the material as proposed by Ogihara et al.[88] At medium to low frequency, the impedance mainly comes from the transfer of Li^+ from the electrolyte to the active particle, passing through the SEI. This contribution to the impedance is the key feature that allows the impact of an additive at the surface of an electrode to be detected. Lastly, in the low frequency range, the impedance comes primarily from the diffusion of Li in the active particle. The analysis of the origin of the different features showed that many researchers misinterpret impedance data and report resistances associated with the SEI that are actually resistance due to the contact resistance between the current collector and the active particles.

Chapter 5 presented the results of the study of the effects of electrolyte additives in Li-ion cells. Section 5.1 presented the first results obtained on the effect of vinylene carbonate (VC) and trimethoxyboroxine (TMOBX) in $LiCoO_2$/graphite wound prismatic cells made by Medtronic. In this cell configuration, VC acted primarily at the positive electrode at low concentration, and greatly affected the negative electrode at higher concentration. The introduction of small quantities of TMOBX greatly lowered the positive electrode impedance without affecting the negative electrode too much. When VC and TMOBX were mixed together, VC controlled the surface chemistry at the negative electrode and TMOBX controlled the surface chemistry of the positive electrode. Section 5.1 presented the model proposed by Atebamba et al.[90] used to extract the value of the charge transfer resistance of Li^+ from the electrolyte to the electrode. Even though imperfect, this model was still useful to extract the charge transfer resistance in order to easily compare the effects of multiple additives at the same time.

Section 5.2 presented the result of the study of the effects of multiple additives in LCO/graphite cells charged to 4.075 V and to 4.175 V and in $Li[Ni_{0.4}Mn_{0.4}Co_{0.2}])O_2$/graphite (NMC/graphite) cells. Section 5.2 showed that all additives tested impact the surface of both the positive and negative electrodes. While almost every additive tested reduced the impedance of the positive electrode, almost every additive tested increased the impedance of the negative electrode.

Section 5.2 showed that when multiple additives were introduced in the same cell, in some cases one additive controlled the formation of the surface of one electrode and the other additive controlled the formation of the surface of the other electrode. In other instances, additives introduced in the same cell shared the formation of the surfaces of both electrodes. Section 5.2 also showed that the effect of an additive at either electrode depends on the amount introduced in the cell. For example some additives affected one electrode at low concentration, and affected the other electrode at higher concentration. It also showed that the effect of an additive at the surface of the LCO positive electrode was very similar to its effect on the NMC positive electrode. Most additives were shown to impart higher impedance at the positive electrode when the cell was charged to a higher voltage except for LiTFSI. Changing the upper-voltage cut-off of the cell from 4.075 to 4.175 V was shown not to affect the impedance of the negative electrode.

Section 5.3 presented a comparative study of the effects of different concentrations of VC and vinyl ethylene carbonate (VEC) in LCO/graphite pouch cells using EIS on symmetric cells and high precision coulometry. VC improved the cycling performance in all concentrations (0.5% to 6%). From low concentration to 2%, VC reduced the impedance

of the cell, and at higher concentration, increased the impedance a lot. The introduction of 2% VC offered a good compromise between cycling performance and overall impedance of the cell. EIS on symmetric cells showed that at low concentrations, VC affected the positive electrode surface even though evidence of the reduction of VC at the negative electrode appeared in the early first cycle. This might indicate that the products of the reduction of VC are soluble and do not affect the negative electrode surface, migrate to the positive electrode where it reacts, modifying its surface. At concentrations of 2% and above, VC greatly affected the negative electrode and its effects on the positive electrode changed (the impedance of the positive electrode started to rise again).

VEC did not improve the cycling performance of the cells, at any concentration tested (0% - 6%) and at any temperature tested (30, 40, and 60°C). EIS on symmetric cells showed that the surface of the negative electrode was not affected by the presence of VEC even though this additive was proposed as a film forming additive at the negative electrode[74]. This absence of any effect at the negative electrode could come from the removal of the gaseous by-products of the reduction of VEC during the de-gassing step. It is possible that these gaseous by-products are key in the formation of a good SEI at the negative electrode. The surface of the positive electrode was shown to be affected by VEC only when present at high concentration. However these changes at the positive electrode did not bring any benefit to the cell.

Finally, section 5.4 presented a study of the effect of VC and TMOBX in LCO/graphite pouch cells. Both VC and TMOBX seemed to play a role in the formation of the SEI of both electrodes in LCO/graphite pouch cells. This is different from the findings on the

LCO/graphite cells made by Medtronic where TMOBX seemed to control the formation of the SEI at the positive electrode and VC seemed to control the formation of the SEI at the negative. This difference in the behavior of additives has been proposed to be the result of several factors such as cell configuration (soft plastic cans as opposed to hard metal cans), difference in the concentration range of VC and TMOBX from one study to the other, removal of the gas formed during the formation cycle, differences in potential cut-offs (4.20 V as opposed to 4.175 V), etc.

Throughout Chapters 4 and 5, the method presented has been shown to be very useful for studying the effects of electrolyte additives. However, this technique has several limitations. Even though the method allows changes at the surface of an electrode to be detected, it does not provide any chemical information about the composition of the SEI. Furthermore, if two different SEIs have similar resistance values, then the method will give the false impression that the two surface films are identical. The method described constitutes an additional tool for the analysis of the effects of electrolyte additives in Li-ion cells and should be used along with different measurement techniques, such as infrared spectroscopy, x-ray photoelectron spectroscopy, scanning electron microscopy, high precision coulometry, *etc.*

6.1 FUTURE WORK

Chapter 4 presented the equivalent circuit model proposed by Atebamba et al.[90] used for the extraction of the value of R_{ct}. However this model does not take the diffusion of Li^+ in the pores into account. Even though the contribution of the diffusion of Li^+ in the pores and the charge transfer were shown not to overlap in the frequency domain, it is

important to improve the equivalent circuit model. Ogihara et al.[88] proposed an equivalent circuit model that takes the Li^+ diffusion in the pores into account. However this model does not include the contact resistance. It would then be useful to combine both models and compare the results to real impedance spectra of symmetric cells.

EIS on symmetric cells allows changes in the surface of the electrodes to be detected. Nevertheless, understanding the way additives work is a huge task. The fate of additives after cycling and the nature of the by-products of their reaction are unknown. The use of gas chromatography coupled with mass spectrometry (GC-MS) could reveal the fate of additives and the nature of their by-products. Gas chromatography separates neutral compounds that can exist in the gas phase, and mass spectrometry provides information on the chemical structure of the compounds. GC-MS is very useful to determine the fate of neutral compounds and to determine the structure of the by-products of the reaction of additives.

A method for the extraction of the electrolyte of a cycled Li-ion cell has already been developed (Tony Gozdz, A123 Systems, Boston, USA). This extraction technique allows the neutral organic compounds to be separated from the salt, thus protecting the GC-MS setup from the corrosive $LiPF_6$. Figure 6.1 shows a chromatogram (total ion counts) of a mixture of additives (some names have been replaced by letters for proprietary reasons) as well as common carbonate solvents and co-solvents used in Li-ion cells. Figure 6.1 shows that additives along with solvents can be well-separated in a rapid manner. GC-MS can be used to quantify the relative amounts of the organic constituents of the electrolyte

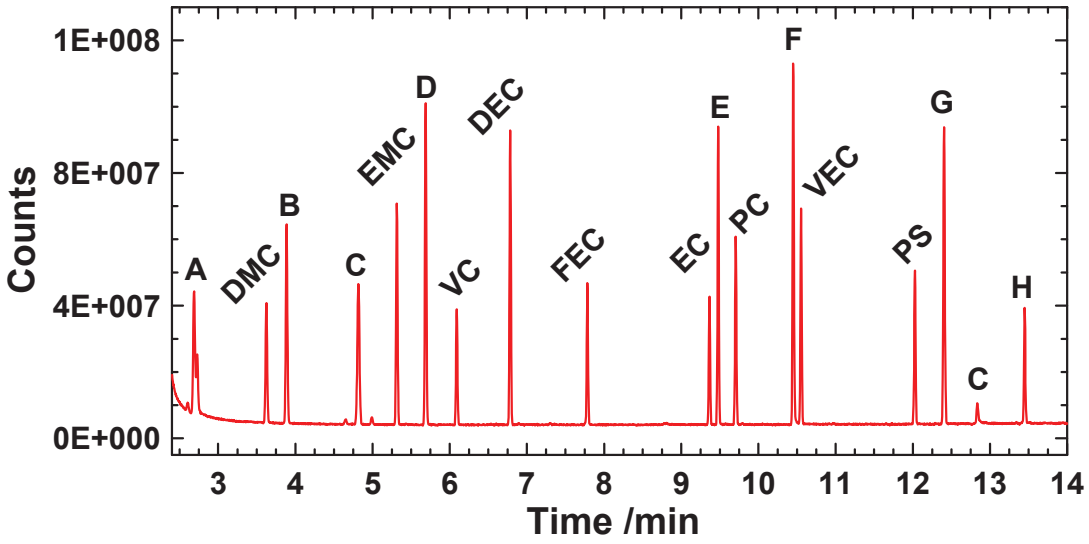

Figure 6.1 Chromatogram (total ion counts) of a mixture of electrolyte additives and carbonate solvents used in Li-ion cells (mass spectrometry was used as detection technique), additives A to H are proprietary compounds.

which makes this technique very useful to determine the fate of the additives after cycling.

Figure 6.2 shows the chromatogram (total ion counts) of the extraction of the electrolyte of a commercial 18650 Li-ion cell. Figure 6.2 shows that the electrolyte components can be effectively extracted from a Li-ion cell and can be analyzed by GC-MS.

The structure that makes a stable SEI and that slows parasitic reactions needs to be determined. Knowing the desired SEI structure would allow new and better additives to be identified. However, the scale of the size of the SEI makes it difficult to analyze and requires sensitive surface techniques to be used. Fourier transform infrared spectroscopy (FT-IR) using attenuated total reflectance sampling techniques allows only the surface (top micron) of particles to be probed. FT-IR provides information on the nature of the

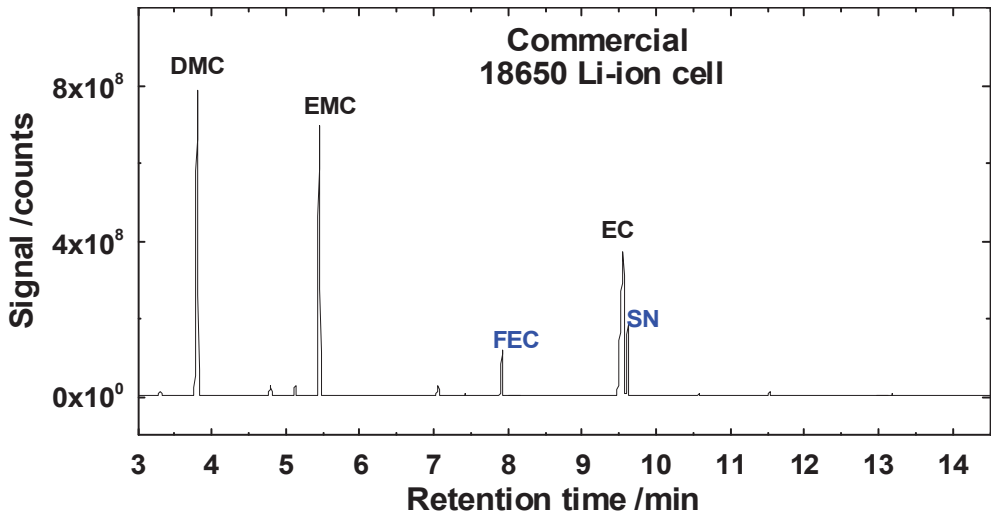

Figure 6.2 Chromatogram (total ion counts) of the extraction of the electrolyte of a commercial 18650 Li-ion cell.

chemical groups (carbonyl, unsaturated or saturated carbons, alcohols, *etc*.) of chemicals present in the SEI. FT-IR spectra of known compounds can also be compared to the spectra of the surface of the electrodes and could allow the compounds in the SEI to be determined.

X-ray photoelectron spectroscopy (XPS) is also a useful technique for the determination of the chemical nature of the SEI. XPS probes only the first few tens of nanometers of the surface of the sample. This surface sensitive technique gives information on the atoms and bonding present in the constituents of the SEI. Combining these different surface sensitive techniques would enable the composition of efficient SEIs to be determined.

Section 5.3 presented a comparative study of the effects of VEC and VC in LCO/graphite pouch cells. This study showed that VEC has no effect on the surface of the graphite at any concentration and no effect on the surface of the LCO at concentrations below 4%. It

has been proposed that this absence of any effect might be due to the removal of the gas formed after the formation process. The role of the gas in the formation of the SEI should be investigated. The determination of the nature of the gas could provide information on the reaction pathway which the additive undertook. The structure of the gas can be revealed once again by GC-MS.

The role of the gas in the formation cycle can be investigated using a compression device. This device could be made of two slabs of PVC with the shape of the pouch cell milled into it. The cell would fit between the two slabs that would be tightly screwed together. This would provide very little space for the gas to expand. The gas would then be partially dissolved in the electrolyte and could react at either electrode. Comparing the cycling performance of a pouch cell that would sit in the compression device and cycled without de-gassing to the cycling performance of a cell that would be de-gassed (treated as in section 5.3) would reveal if the gas is playing a key role in the formation of the SEI.

The anodic and cathodic stability of each additive should be tested with inert electrodes such as glassy carbon electrodes. This would provide insights in the stability of the additives and reveal if the different active materials have some catalytic properties in the degradation of additives. Putting these additives in presence or absence of Li metal during the anodic stability tests could reveal some of the reaction pathways of the interactions between the positive and negative electrodes.

The role of the composition and morphology of the active material on the effect of additive should also be studied. It is still not clear to this date if the composition and

morphology of the active material affect the rate of the parasitic reactions. When additives are studied in cells using different materials, the cells are often cycled to different cut-off potentials and active materials with different surface areas are often used. This casts doubts on whether the difference in the effects of an additive is due to the active material of the electrodes or to the difference in the potential cut-offs and surface areas.

There is a high probability that the next generation of Li-ion cells will be charged to higher voltage than the current generation. This indicates that the effect of higher cut-off potentials must be investigated in order to validate that the current "best" additives can still be used and investigate the difference in their behavior at higher potential. NMC/graphite (can be operated up to 4.7 V) pouch cells can be used for this purpose along with high precision coulometry, EIS on symmetric cells, GC-MS, micro-calorimetry, FT-IR and cyclic voltammetry.

The effect of the nature of the carbonate solvents on cycle life has not yet been investigated. Using the measurement techniques mentioned above would allow the determination of which solvent is the best for cycle life and their function in the formation of the SEI. Carbonate solvents are generally used for the improved stability of the graphite they provide. However, the existence of additives that passivate the graphite surface allows for different solvents such as lactones, esters, ketones, *etc.* to be tested, provided that the thermal stability is not compromised. Using different solvents might enable better electrolyte-additive systems.

It is important to study the role of additive structures in a systematic manner, much like the screening of the efficiency of catalysts. For instance, different molecules of the same class (ketones, lactones, esters, carbonates, ethers, organosilicates, sulfones, sulfoxides, phosphates, phosphites, borates, *etc.*) whose structure varies by one or several carbons or by one or more oxygens could be screened, along with their isomers, by high precision coulometry and automated storage experiments. Figure 6.3 shows the structure of cyclic organosulfates differing by one carbon and one isomer (a) along with the volume of gas produced during the formation cycle (b). Figures 6.3a and b show that even though the

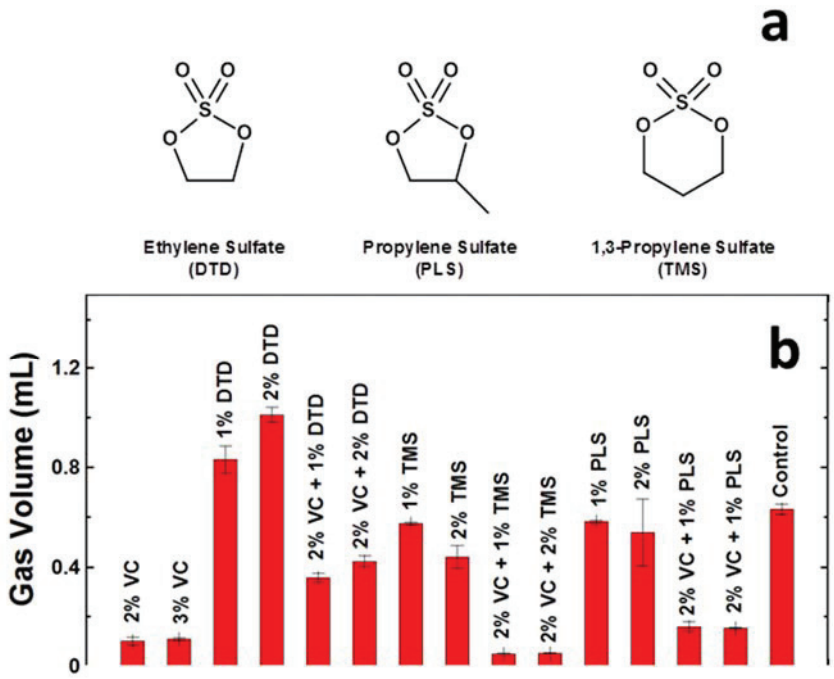

Figure 6.3 Structure of molecules of the same family (a), and volume of gas produced in the pouch during the formation cycle of a 220mAh NMC/graphite pouch cell. Measurements were done by Jian Xia, visiting student, Department of Physics and Atmospheric Science, Dalhousie University, Halifax, NS (2013).

structure of these compounds is very similar from one molecule to the next, the volume of gas produced during the formation cycle is very different. This indicates that these compounds either give very different by-products or form different SEIs. Simple experiments like these could help understand which factors, such as electronic environment or size of the side chain, are the most important in the formation of a good SEI.

Another area to explore is the boundary between solvent and additives. Chapter 5 showed that the effects of additives with concentration do not follow a linear behavior. However the concentration range tested was quite narrow (0% - 6%). Higher concentrations should be tested to investigate the difference in behavior between low concentrations and very high concentrations. It would also determine if high concentrations of additives always lead to higher impedance as was the case with VC and TMOBX in this thesis.

Recently an *in operando* gas volume measurement system has been developed (Connor Aiken, summer student, Department of Physics and Atmospheric Science, Dalhousie University, Halifax, NS) based on Archimedes principle. Since gas is the product of parasitic reactions, this technique constitutes one more tool for the analysis of the effects of additives. It also allows the nature of the by-products to be determined (gaseous versus not gaseous).

REFERENCES

(1) Prud'homme, R.; Koning, M. *Transp. Policy* **2012**, *23*, 60–69.

(2) Broussely, M.; Biensan, P.; Bonhomme, F.; Blanchard, P.; Herreyre, S.; Nechev, K.; Staniewicz, R. J. *J. Power Sources* **2005**, *146*, 90–96.

(3) Burns, J. C.; Sinha, N. N.; Coyle, D. J.; Jain, G.; VanElzen, C. M.; Lamanna, W. M.; Xiao, A.; Scott, E.; Gardner, J. P.; Dahn, J. R. *J. Electrochem. Soc.* **2011**, *159*, A85–A90.

(4) Burns, J. C.; Sinha, N. N.; Jain, G.; Ye, H.; VanElzen, C. M.; Lamanna, W. M.; Xiao, A.; Scott, E.; Choi, J.; Dahn, J. R. *J. Electrochem. Soc.* **2012**, *159*, A1105–A1113.

(5) Burns, J. C.; Jain, G.; Smith, A. J.; Eberman, K. W.; Scott, E.; Gardner, J. P.; Dahn, J. R. *J. Electrochem. Soc.* **2011**, *158*, A255–A261.

(6) Sinha, N. N.; Smith, A. J.; Burns, J. C.; Jain, G.; Eberman, K. W.; Scott, E.; Gardner, J. P.; Dahn, J. R. *J. Electrochem. Soc.* **2011**, *158*, A1194–A1201.

(7) Zhang, S. S. *J. Power Sources* **2006**, *162*, 1379–1394.

(8) Smith, A. J.; Burns, J. C.; Trussler, S.; Dahn, J. R. *J. Electrochem. Soc.* **2010**, *157*, A196–A202.

(9) Smith, A. J.; Burns, J. C.; Xiong, D.; Dahn, J. R. *J. Electrochem. Soc.* **2011**, *158*, A1136–A1142.

(10) Burns, J. C.; Xia, X.; Dahn, J. R. *J. Electrochem. Soc.* **2013**, *160*, A383–A386.

(11) Chen, C. .; Liu, J.; Amine, K. *J. Power Sources* **2001**, *96*, 321–328.

(12) Reddy, T. *Linden's Handbook of Batteries, 4th Edition*; McGraw Hill Professional, 2010.

(13) Aurbach, D.; Ein-Eli, Y. *J. Electrochem. Soc.* **1995**, *142*, 1746–1752.

(14) Dudley, J. T.; Wilkinson, D. P.; Thomas, G.; LeVae, R.; Woo, S.; Blom, H.; Horvath, C.; Juzkow, M. W.; Denis, B.; Juric, P.; Aghakian, P.; Dahn, J. R. *J. Power Sources* **1991**, *35*, 59–82.

(15) Xu, W.; Angell, C. A. *Electrochem. Solid-State Lett.* **2001**, *4*, E1–E4.

(16) Paillard, E.; Iojoiu, C.; Alloin, F.; Guindet, J.; Sanchez, J.-Y. *Electrochimica Acta* **2007**, *52*, 3758–3765.

(17) Zhang, X.; Kostecki, R.; Richardson, T. J.; Pugh, J. K.; Ross, P. N. *J. Electrochem. Soc.* **2001**, *148*, A1341–A1345.

(18) Egashira, M.; Takahashi, H.; Okada, S.; Yamaki, J. *J. Power Sources* **2001**, *92*, 267–271.

(19) Aurbach, D. *J. Power Sources* **2005**, *146*, 71–78.

(20) Peled, E. *J. Electrochem. Soc.* **1979**, *126*, 2047–2051.

(21) Aurbach, D.; Levi, M. D.; Levi, E.; Schechter, A. *J. Phys. Chem. B* **1997**, *101*, 2195–2206.

(22) Gnanaraj, J. S.; Levi, M. D.; Levi, E.; Salitra, G.; Aurbach, D.; Fischer, J. E.; Claye, A. *J. Electrochem. Soc.* **2001**, *148*, A525–A536.

(23) Aurbach, D.; Koltypin, M.; Teller, H. *Langmuir* **2002**, *18*, 9000–9009.

(24) Yazami, R. *Electrochimica Acta* **1999**, *45*, 87–97.

(25) Jeong, S.-K.; Inaba, M.; Abe, T.; Ogumi, Z. *J. Electrochem. Soc.* **2001**, *148*, A989–A993.

(26) Inaba, M.; Tomiyasu, H.; Tasaka, A.; Jeong, S.-K.; Ogumi, Z. *Langmuir* **2004**, *20*, 1348–1355.

(27) Aurbach, D.; Markovsky, B.; Weissman, I.; Levi, E.; Ein-Eli, Y. *Electrochimica Acta* **1999**, *45*, 67–86.

(28) Momose, H.; Honbo, H.; Takeuchi, S.; Nishimura, K.; Horiba, T.; Muranaka, Y.; Kozono, Y.; Miyadera, H. *J. Power Sources* **1997**, *68*, 208–211.

(29) Verma, P.; Maire, P.; Novák, P. *Electrochimica Acta* **2010**, *55*, 6332–6341.

(30) Andersson, A. .; Henningson, A.; Siegbahn, H.; Jansson, U.; Edström, K. *J. Power Sources* **2003**, *119–121*, 522–527.

(31) Andersson, A. M.; Edström, K. *J. Electrochem. Soc.* **2001**, *148*, A1100–A1109.

(32) Peled, E.; Golodnitsky, D.; Ardel, G. *J. Electrochem. Soc.* **1997**, *144*, L208–L210.

(33) Zaban, A.; Aurbach, D. *J. Power Sources* **1995**, *54*, 289–295.

(34) Aurbach, D.; Markovsky, B.; Shechter, A.; Ein-Eli, Y.; Cohen, H. *J. Electrochem. Soc.* **1996**, *143*, 3809–3820.

(35) Aurbach, D.; Ein-Eli, Y.; Markovsky, B.; Zaban, A.; Luski, S.; Carmeli, Y.; Yamin, H. *J. Electrochem. Soc.* **1995**, *142*, 2882–2890.

(36) Aurbach, D.; Gofer, Y.; Ben-Zion, M.; Aped, P. *J. Electroanal. Chem.* **1992**, *339*, 451–471.

(37) Kominato, A.; Yasukawa, E.; Sato, N.; Ijuuin, T.; Asahina, H.; Mori, S. *J. Power Sources* **1997**, *68*, 471–475.

(38) Kang, S.-H.; Abraham, D. P.; Xiao, A.; Lucht, B. L. *J. Power Sources* **2008**, *175*, 526–532.

(39) Zhuang, G. V.; Ross, P. N. *Electrochem. Solid-State Lett.* **2003**, *6*, A136–A139.

(40) Mori, S.; Asahina, H.; Suzuki, H.; Yonei, A.; Yokoto, K. *J. Power Sources* **1997**, *68*, 59–64.

(41) Zhang, H.-L.; Li, F.; Liu, C.; Tan, J.; Cheng, H.-M. *J. Phys. Chem. B* **2005**, *109*, 22205–22211.

(42) Aurbach, D.; Moshkovich, M. *J. Electrochem. Soc.* **1998**, *145*, 2629–2639.

(43) Augustsson, A.; Herstedt, M.; Guo, J.-H.; Edström, K.; Zhuang, G. V.; P. N. Ross, J.; Rubensson, J.-E.; Nordgren, J. *Phys. Chem. Chem. Phys.* **2004**, *6*, 4185–4189.

(44) Aurbach, D. *J. Power Sources* **2003**, *119–121*, 497–503.

(45) Peled, E.; Bar Tow, D.; Merson, A.; Gladkich, A.; Burstein, L.; Golodnitsky, D. *J. Power Sources* **2001**, *97–98*, 52–57.

(46) Kanamura, K.; Tamura, H.; Takehara, *Z. J. Electroanal. Chem.* **1992**, *333*, 127–142.

(47) Odziemkowski, M.; Irish, D. E. *J. Electrochem. Soc.* **1993**, *140*, 1546–1555.

(48) Ng, S. H.; Vix-Guterl, C.; Bernardo, P.; Tran, N.; Ufheil, J.; Buqa, H.; Dentzer, J.; Gadiou, R.; Spahr, M. E.; Goers, D.; Novák, P. *Carbon* **2009**, *47*, 705–712.

(49) Novák, P.; Ufheil, J.; Buqa, H.; Krumeich, F.; Spahr, M. E.; Goers, D.; Wilhelm, H.; Dentzer, J.; Gadiou, R.; Vix-Guterl, C. *J. Power Sources* **2007**, *174*, 1082–1085.

(50) Aurbach, D.; Markovsky, B.; Rodkin, A.; Cojocaru, M.; Levi, E.; Kim, H.-J. *Electrochimica Acta* **2002**, *47*, 1899–1911.

(51) Moshkovich, M.; Cojocaru, M.; Gottlieb, H. .; Aurbach, D. *J. Electroanal. Chem.* **2001**, *497*, 84–96.

(52) Aurbach, D.; Gamolsky, K.; Markovsky, B.; Salitra, G.; Gofer, Y.; Heider, U.; Oesten, R.; Schmidt, M. *J. Electrochem. Soc.* **2000**, *147*, 1322–1331.

(53) Goodenough, J. B.; Kim, Y. *Chem. Mater.* **2010**, *22*, 587–603.

(54) Dillon, S. J.; Sun, K. *Curr. Opin. Solid State Mater. Sci.* **2012**, *16*, 153–162.

(55) Dubarry, M.; Truchot, C.; Liaw, B. Y.; Gering, K.; Sazhin, S.; Jamison, D.; Michelbacher, C. *J. Power Sources* **2011**, *196*, 10336–10343.

(56) Wang, E.; Ofer, D.; Bowden, W.; Iltchev, N.; Moses, R.; Brandt, K. *J. Electrochem. Soc.* **2000**, *147*, 4023–4028.

(57) Boeuve, J.-P.; Simon, B. Rechargeable lithium electrochemical cell. US5626981 A, May 6, 1997.

(58) Lee, J.-T.; Lin, Y.-W.; Jan, Y.-S. *J. Power Sources* **2004**, *132*, 244–248.

(59) Wrodnigg, G. H.; Besenhard, J. O.; Winter, M. *J. Electrochem. Soc.* **1999**, *146*, 470–472.

(60) Naji, A.; Ghanbaja, J.; Willmann, P.; Billaud, D. *Electrochimica Acta* **2000**, *45*, 1893–1899.

(61) Xiong, D.; Burns, J. C.; Smith, A. J.; Sinha, N.; Dahn, J. R. *J. Electrochem. Soc.* **2011**, *158*, A1431–A1435.

(62) Shin, J.-S.; Han, C.-H.; Jung, U.-H.; Lee, S.-I.; Kim, H.-J.; Kim, K. *J. Power Sources* **2002**, *109*, 47–52.

(63) Ein-Eli, Y.; Thomas, S. R.; Koch, V. R. *J. Electrochem. Soc.* **1997**, *144*, 1159–1165.

(64) Wang, C.; Nakamura, H.; Komatsu, H.; Yoshio, M.; Yoshitake, H. *J. Power Sources* **1998**, *74*, 142–145.

(65) Mao, H.; Reimers, J. N.; Sacken, U. V. Additives for improving cycle life of non-aqueous rechargeable lithium batteries. US5891592 A, April 6, 1999.

(66) Heider, U.; Schmidt, M.; Amann, A.; Niemann, M.; Kühner, A. Use of additives in electrolyte for electrochemical cells. US6548212 B1, April 15, 2003.

(67) Xu, K.; Zhang, S.; Jow, T. R.; Xu, W.; Angell, C. A. *Electrochem. Solid-State Lett.* **2002**, *5*, A26–A29.

(68) Komaba, S.; Watanabe, M.; Groult, H.; Kumagai, N.; Okahara, K. *Electrochem. Solid-State Lett.* **2006**, *9*, A130–A133.

(69) Koiwai, A.; Shiga, T.; Takechi, K. Nonaqueous electrolytic solution for battery and nonaqueous electrolytic solution battery. US6077628 A, June 20, 2000.

(70) Takechi, K.; Shiga, T. Nonaqueous electrolytic solution for battery and nonaqueous electrolytic solution battery using the same. US6235431 B1, May 22, 2001.

(71) Zhang, S. S.; Xu, K.; Jow, T. R. *Electrochem. Solid-State Lett.* **2002**, *5*, A206–A208.

(72) Aurbach, D.; Gamolsky, K.; Markovsky, B.; Gofer, Y.; Schmidt, M.; Heider, U. *Electrochimica Acta* **2002**, *47*, 1423–1439.

(73) Chalasani, D.; Li, J.; Jackson, N. M.; Payne, M.; Lucht, B. L. *J. Power Sources* **2012**, *208*, 67–73.

(74) Hu, Y.; Kong, W.; Li, H.; Huang, X.; Chen, L. *Electrochem. Commun.* **2004**, *6*, 126–131.

(75) Wang, X.; Naito, H.; Sone, Y.; Segami, G.; Kuwajima, S. *J. Electrochem. Soc.* **2005**, *152*, A1996–A2001.

(76) Chang, C.-C.; Hsu, S.-H.; Jung, Y.-F.; Yang, C.-H. *J. Power Sources* **2011**, *196*, 9605–9611.

(77) Burns, J. C.; Sinha, N. N.; Jain, G.; Ye, H.; VanElzen, C. M.; Lamanna, W. M.; Xiao, A.; Scott, E.; Choi, J.; Dahn, J. R. *J. Electrochem. Soc.* **2012**, *159*, A1095–A1104.

(78) Petibon, R.; Aiken, C. P.; Sinha, N. N.; Burns, J. C.; Ye, H.; VanElzen, C. M.; Jain, G.; Trussler, S.; Dahn, J. R. *J. Electrochem. Soc.* **2013**, *160*, A117–A124.

(79) Li, S. R.; Chen, C. H.; Xia, X.; Dahn, J. R. *J. Electrochem. Soc.* **2013**, *160*, A1524–A1528.

(80) Sloop, S. E.; Kerr, J. B.; Kinoshita, K. *J. Power Sources* **2003**, *119–121*, 330–337.

(81) Orazem, M. E.; Tribollet, B. *Electrochemical Impedance Spectroscopy*; John Wiley & Sons, 2011.

(82) Meyers, J. P.; Doyle, M.; Darling, R. M.; Newman, J. *J. Electrochem. Soc.* **2000**, *147*, 2930–2940.

(83) Levi, M. D.; Aurbach, D. *J. Power Sources* **2005**, *146*, 727–731.

(84) Hjelm, A.-K.; Lindbergh, G. *Electrochimica Acta* **2002**, *47*, 1747–1759.

(85) Gaberscek, M.; Moskon, J.; Erjavec, B.; Dominko, R.; Jamnik, J. *Electrochem. Solid-State Lett.* **2008**, *11*, A170–A174.

(86) Burns, J. C.; Krause, L. J.; Le, D.-B.; Jensen, L. D.; Smith, A. J.; Xiong, D.; Dahn, J. R. *J. Electrochem. Soc.* **2011**, *158*, A1417–A1422.

(87) Sinha, N. N.; Burns, J. C.; Sanderson, R. J.; Dahn, J. *J. Electrochem. Soc.* **2011**, *158*, A1400–A1403.

(88) Ogihara, N.; Kawauchi, S.; Okuda, C.; Itou, Y.; Takeuchi, Y.; Ukyo, Y. *J. Electrochem. Soc.* **2012**, *159*, A1034–A1039.

(89) Ota, H.; Sakata, Y.; Inoue, A.; Yamaguchi, S. *J. Electrochem. Soc.* **2004**, *151*, A1659–A1669.

(90) Atebamba, J.-M.; Moskon, J.; Pejovnik, S.; Gaberscek, M. *J. Electrochem. Soc.* **2010**, *157*, A1218–A1228.

(91) Lukács, Z. *J. Electroanal. Chem.* **1997**, *432*, 79–83.

(92) Macdonald, J. R. *J. Appl. Phys.* **1985**, *58*, 1971–1978.

(93) Accepted to JES (JES-13-1826); Burns, J. C.; Petibon, R.; Nelson, K. J.; Sinha, N. N.; Kassam A.[a]; Way, B. M.; and Dahn, J.R.**,** *Studies of the Effect of Varying Vinylene Carbonate (VC) Content in Lithium Ion Cells on Cycling Performance and Cell Impedance.*